



저작자표시-변경금지 2.0 대한민국

이용자는 아래의 조건을 따르는 경우에 한하여 자유롭게

- 이 저작물을 복제, 배포, 전송, 전시, 공연 및 방송할 수 있습니다.
- 이 저작물을 영리 목적으로 이용할 수 있습니다.

다음과 같은 조건을 따라야 합니다:



저작자표시. 귀하는 원저작자를 표시하여야 합니다.



변경금지. 귀하는 이 저작물을 개작, 변형 또는 가공할 수 없습니다.

- 귀하는, 이 저작물의 재이용이나 배포의 경우, 이 저작물에 적용된 이용허락조건을 명확하게 나타내어야 합니다.
- 저작권자로부터 별도의 허가를 받으면 이러한 조건들은 적용되지 않습니다.

저작권법에 따른 이용자의 권리는 위의 내용에 의하여 영향을 받지 않습니다.

이것은 [이용허락규약\(Legal Code\)](#)을 이해하기 쉽게 요약한 것입니다.

[Disclaimer](#)

**GENERAL
INTRODUCTION
AND
PURPOSE**

GENERAL INTRODUCTION

1. Introduction of the Spinal Cord

1.1. Spinal Cord

The spinal cord, connected to the brain, is the major nerve tract through the canal of the spinal column. The brain and spinal cord are referred to as the central nervous system (CNS), and the nerves linking from the spinal cord to the other parts of the body are termed the peripheral nervous system (PNS). The nerves, which carry information from the brain to muscles, are called motor neurons. The nerves, which carry information from the PNS back to the brain, are called sensory neurons. Sensory neurons carry information about skin temperature, touch, pain, and joint position to the brain (Bear et al., 2006; Watson et al., 2008).

In the case of humans, the spinal cord is divided into 31 pairs of spinal nerves (Fig. 1): 8 cervical, 12 thoracic, 5 lumbar, 5 sacral, and 1 coccygeal. Whereas, in mice and rats, there are 34 pairs: 8 cervical, 13 thoracic, 6 lumbar, 4 sacral, and 3 coccygeal. In the cross-section of a spinal cord, a butterfly-shaped gray matter can be seen surrounded by white matter (Fig. 2). Gray matter is mostly made up of the cell bodies of neurons and white matter is composed of nerve fibers embedded in neuroglial cells. The processes of neurons that comprise the surrounding white matter are assembled into pathways called fiber tracts (Bear et al., 2006; Watson et al., 2008).

1.2. Spinal Tracts

The nerves within the spinal cord are assembled into distinct bundles called the ascending and descending tracts. Ascending tracts are bundles of nerve fibers linking the spinal cord with the higher centers of the brain. In addition, they convey sensory information such as pain, temperature, position sense and touch from the soma/viscera to the supraspinal levels. Descending tracts are composed of motor fibers that carry information from the brain to the spinal cord (Watson et al., 2008; Rossignol and Frigon, 2011). Figure 2 shows the various fiber tracts in a cross-section of a spinal cord (Bear et al., 2006).

1.2.1. Ascending Tracts

The ascending sensory system consists of 3 distinct pathways: the anterolateral system (ALS), the dorsal column–medial lemniscal (DCML) pathway, and the somatosensory pathways to the cerebellum (Table 1). The tracts are located in the separated region of the spinal cord shown in the figure 2 (Bear et al., 2006; Patestas and Gartner, 2006).

1) The anterolateral system includes 3 main pathways including the spinothalamic tract important for sensing painful or thermal stimuli; the spinoreticular tract causing alertness and arousal in response to painful stimuli; and the spinotectal tracts positioning the eyes and head towards stimuli (Willis and Westlund, 1997).

2) The dorsal column–medial lemniscal pathway is responsible for transmitting fine touch, vibration and conscious proprioceptive information from the body to the cerebral cortex, as well as tactile pressure, barognosis, graphesthesia, stereognosis, recognition of texture, kinesthesia and two-point discrimination (O'Sullivan and Schmitz, 2007). It has 2 structures in which

sensation can travel: the dorsal columns of the spinal cord, and the medial lemniscus in the brainstem (Patestas and Gartner, 2006).

3) The somatosensory pathways to the cerebellum, which include the spinocerebellar as well as the cuneocerebellar tracts, relay primarily proprioceptive (including some pain and pressure) information (Patestas and Gartner, 2006).

1.2.2. Descending Tracts

The best known of these descending tracts is the corticospinal tract, which is a huge fiber bundle. Apart from the corticospinal tract, the ventromedial system is comprised of 4 tracts that contribute chiefly to postural control and certain reflex movements. The originating neurons of these tracts receive sensory information related to balance, body position, and visual environment (Watson et al., 2008).

1) Corticospinal tracts - All mammals possess corticospinal tracts; however, the location of the corticospinal tracts in the spinal cord varies considerably according to species. The corticospinal tracts originate from the premotor, primary motor and primary sensory cortex. In the lower medulla, about 90 percent of the tract fibers decussates and descends in the dorsolateral funiculus of the spinal cord. The corticospinal tracts are involved in skilled voluntary activity (Watson et al., 2008).

2) The rubrospinal tract - It is prominent in many vertebrates that use limbs or pectoral fins for locomotion (ten Donkelaar, 1976). As well as manipulating general locomotion, the rubrospinal tract in at least some mammalian species has a supportive role with corticospinal tracts regulating more skilled motor tasks (Whishaw et al., 1998).

3) The tectospinal tract - In mammals, the tectospinal tract arises from cells in the superior colliculus and projects to cervical spinal cord (Nyberg-Hansen, 1964; Nudo and Masterton, 1989), and is mainly involved in the control of head and neck movements. Most of the fibers crosses in the dorsal tegmental decussation and connect the predorsal bundle as they travel caudally (Harting, 1977; Redgrave et al., 1987; Dean et al., 1989).

4) The reticulospinal tracts - Reticulospinal tracts have roles in preparatory and movement-related activities, postural control, and modulation of some sensory and autonomic functions (Buford and Davidson, 2004; Deumans et al., 2005). It arises from the reticular formation nuclei in 2 major parts of the brainstem: the pons and the medulla oblongata. The reticular formation receives inputs from many sources and extends along the entire length of the brainstem, from the pons to the medulla (Peterson, 1979).

5) The vestibulospinal tracts - The main projections of the vestibular complex to the spinal cord are the lateral vestibulospinal tract, which arises in the lateral vestibular nucleus (Brodal et al., 1962), and the medial vestibulospinal tract, which arises in the medial and spinal vestibular nuclei (Brodal et al., 1962; Kneisley et al., 1978; Peterson et al., 1978). The vestibulospinal tracts are the major initiators of coordinated postural extensor activity in the limbs and trunk (Pompeiano, 1972).

2. Spinal Cord Injury

As the dictionary definition, spinal cord injury (SCI) is mentioned as any damage to the spinal cord that is caused by trauma instead of disease (Venes and Taber, 2009). Statistically, there are approximately 250,000 people who suffer from SCIs and about 11,000 new cases of SCIs each year from

accidents in the United States. The important thing is that most of the injured people (> 56%) are between the ages of 16 and 30, with the majority being males (Websites: Spinal Cord Injury Information Pages). Currently, there is no definitive cure for SCIs and the myriad mechanisms that contribute to this condition are still unclear.

2.1 Pathophysiology of SCI

After a traumatic SCI, several successive events occur in the spinal cord, including neuronal necrosis/apoptosis, axonal loss, demyelination, and inflammation (Schwab and Bartholdi, 1996). There are 3 phases that pathologically occur after SCI (Fig. 3) (Bareyre and Schwab, 2003).

1) The acute phase starts at the moment of injury and extends over the first few days. Mechanically injured lesions induce immediate damage to neuronal tracts in the spinal cord, and necrotic cell death occurs at the injury site (Bareyre and Schwab, 2003). Edema of the spinal cord progresses and metabolic instabilities involving intracellular Ca^{2+} accumulate and increased extracellular K^{+} concentrations occur (Schwab and Bartholdi, 1996).

2) The secondary phase starts from minutes to a few weeks after the injury. Though massive ischemic necrosis often occurs in the secondary phase, apoptosis dominates. In apoptosis, the chromosomal DNA inside cells becomes fragmented. Moreover, the production of free radicals increases, excitatory neurotransmitters are excessively released, and strong inflammatory responses transpire recruiting peripherally derived immune cells such as neutrophils, macrophages, and T cells (Liu et al., 1997; Hengartner, 2000). Simultaneously, the process of reactive gliosis is enhanced. Reactive gliosis is the proliferation and hypertrophy of astrocytes in and around the lesion site with an increase in

GFAP (Fitch and Silver, 1997; Fawcett, 1998). Reactive astrocytes form an astroglial scar, which acts as a physical and/or chemical barrier to axonal regeneration and releases inhibitory molecules (Fawcett, 1998).

3) In the chronic phase, ranging from days to years after SCI, channel and receptor functions are compromised, and scarring and demyelination with Wallerian degeneration occur (Bareyre and Schwab, 2003). All these processes results in permanent functional deficits. One of the causes is that adult CNS axons are capable of abortive sprouting which result in a failure to re-innervate their targets (Silver and Miller, 2004). It could be caused by improper formation of neuronal axon regeneration.

2.2 Immune Response of SCI

The representative resident cells of the spinal cord are microglia, astrocytes, and oligodendrocytes. Microglia is a kind of immune cell capable of phagocytosis in the CNS. It comprises approximately 10-20% of the total cells of the CNS. Astrocytes are the most abundant cell types in the CNS. The function of astrocytes are to support endothelial cells that build up the blood–brain barrier, providing nutrients to neurons, balancing extracellular ions, and forming astrogliosis in the brain and spinal cord following traumatic injuries (Dong and Benveniste, 2001; Farina et al., 2007). The main function of oligodendrocytes is the insulation of axons in the CNS. Traumatic injury to the body, such as spinal cord injury, causes demyelination of oligodendrocytes (Korn, 2008).

Microglia and astrocytes are the first cells to respond to traumatic injury (Bush et al., 1999; Bessis et al., 2007). Reactive microglia and astrocytes

secrete several chemokines and cytokines that recruit peripheral immune cells, such as macrophages, neutrophils and T cells (Bartholdi and Schwab, 1997).

Neutrophils are the first infiltrated cells of peripheral circulating leukocytes into the injured spinal cord after SCI (Carlson et al., 1998). Neutrophils adhere to the endothelium at 6-12 hour post-injury and within 24 hours, and they infiltrate into the lesion site to phagocytose the debris (Taoka et al., 1997; Guth et al., 1999). Upon neutrophil infiltration, chemokines and cytokines induce the neutrophils to generate their own cytokines, such as TNF- α , IL-1, IL-8 and TGF- β , as well as produce matrix metalloproteinase-9 (MMP-9) via the NF- κ B pathway (Cassatella, 1995; Noble et al., 2002). The mediators from neutrophils loosen the extracellular matrix to enhance the extravasation of leukocytes, stimulate leukocyte chemotaxis, activate glial cells, and enhance neuronal damage (Carlson et al., 1998).

After 2 dpi with maximal infiltration occurring 1 to 2 weeks later, monocyte derived macrophages start to infiltrate into the lesion site. Macrophages cause “bystander damage” by the cytotoxic products of activated phagocytes and induce the secondary demyelination of surviving nerve fibers. However, macrophages help clear apoptotic cellular debris at the lesion site of injuries (Blight, 1992; Stirling and Yong, 2009). From the injury, the activated macrophages become polarized resulting in cells with either pro- or anti-inflammatory properties (Fig. 4). M1 macrophages generally express iNOS and pro-inflammatory cytokines such as interleukin (IL)-1 β and TNF- α and produce large quantities of oxidative metabolites such as reactive oxygen intermediates (ROIs) and reactive nitrogen intermediates (RNIs). Whereas, M2 macrophages generally act as anti-inflammatory cells by expressing high levels of IL-10, TGF- β and arginase 1 and showing defective NF- κ B activation and down-

regulated expression of pro-inflammatory cytokines (Sica et al., 2008). A recent study characterized macrophage polarization in a contused mouse spinal cord and reported that most macrophages/microglia are M1 cells, with only a transient and small number showing M2 polarization (Kigerl et al., 2009).

2.3. Axon Regeneration of SCI

Axon regeneration is known as the re-growth or repair of neuronal axons. In most cases, once receiving traumatic injury, the spinal cord as a result has permanent functional impairment. Unlike PNS injuries, the CNS does not have widespread regeneration after injury. In addition, glial scar forms rapidly which contain many inhibitory molecules (Yiu and Zhigang, 2006).

2.3.1 Glial Scar and CSPG

The formation of glial scars is caused by injury in the central nervous system. In addition, nerve regeneration is significantly withdrawn where glial scars form, leading to functional impairment. After injury, several groups of molecules are secreted to promote the formation of glial scars by activated immune cells. Some representative molecules of these secretions are TGF- β , interleukins and cytokines (Giulian et al., 1988; Yong et al., 1991; Susarla et al., 2011). In addition, reactive astrocyte induced glial scars produce and release axon growth-inhibiting molecules known as chondroitin sulfate proteoglycans (CSPGs). Therefore, glial scars as well as CSPGs affect nerve regeneration resulting in failure (Yiu and Zhigang, 2006; Wang et al., 2008).

CSPGs are kinds of inhibitory extracellular matrix (ECM) molecules. In the developmental stage, expressed CSPGs provide a repulsive cue. In the adult CNS, CSPGs are linked with several extracellular matrixes, including

hyaluronan, tenascin-R, and N-CAM (Yamaguchi, 2000). Neurocan, brevican, versican, and aggrecan are grouped together as lecticans/hyalecticans; they have homologous N-terminal hyaluronan-binding domains. NG2 and phosphacan have distinct structures, separate from the lecticans/hyalecticans (Yamaguchi, 2000). NG2 has a transmembrane structure and little homology with other CSPGs (Nishiyama et al., 1991), and phosphacan is a receptor-type protein tyrosine phosphatase. After SCI, the concentration of phosphacan is slightly decreased initially at the lesion site. However, the expression of phosphacan significantly increases later at the site of glial scar formation (McKeon et al., 1999). Neurocan, brevican, phosphacan, and versican are produced by reactive astrocytes after SCI (Jones et al., 2003).

2.3.2 Matrix Metalloproteinase

Matrix metalloproteinases (MMPs) belong to a large family of zinc-dependent endopeptidases. Until now, at least 26 species of human MMPs have been elucidated (Table 2). Generally, MMPs have 4 distinct domains, which are the autoinhibitory N-terminal pro-domain, catalytic domain, hinge region, and C-terminal hemopexin-like domain. The membrane-type MMPs (MT-MMPs) contain an additional transmembrane domain for anchoring to the cell surface. Apart from these domains, MMP-2 and MMP-9 have a fibronectin type II repeat domain, which binds to collagens inserting into the catalytic domain (Parks et al., 2004; Verma and Hansch, 2007). MMPs are responsible for the tissue remodeling associated with various physiological and pathological processes and for the degradation of different kinds of extracellular matrix (ECM) like collagen, elastin, fibronectin, laminin, and proteoglycans (Page-McCaw et al., 2007). The functions of MMPs do more than simply break down

the extracellular matrix. MMPs affect bone formation and remodeling during development, homeostasis, and repair. In addition, MMPs are essential in sustaining homeostasis during environmental changes, such as wound formation and infection (Page-McCaw et al., 2007).

Inflammation is a process of consecutive cellular responses to injury and infection. The infiltrating immune cells to the wound site remove invaded microorganisms and the cell debris. Then, the repair of damaged tissues is processed. For each disease, there is the process in which different members of MMPs are upregulated (Parks, 1999). Some of the MMPs have a crucial role for wound healing. For example, the activity of MMP-1 is required for the repair of skin wounds by inducing of keratinocyte migration (Pilcher et al., 1997). In addition, MMP-2 and MMP-9 are upregulated during nerve degeneration and degrade the inhibitory CSPG (Ferguson and Muir, 2000). In the case of MMP-9, however, it functions to disrupt the blood–spinal cord barrier within the first 3 dpi (Noble et al., 2002). Whereas, according to a published paper from the same group, MMP-2 modulates wound healing by decreasing the glial scars of SCI. (Hsu et al., 2006).

메모 [DK1]: How about “the repair of damaged tissues proceeds” instead?

3. Toll-like Receptors

Toll-like receptors (TLRs) with a key role in the innate immune system are a type of pattern-recognition receptors (PRRs) and recognize pathogen-associated molecular patterns (PAMPs; infection and microbes) or danger-associated molecular patterns (DAMPs; injury and tissue damage) (Sims et al., 2010). The common structure of TLRs is a single, membrane-spanning, non-catalytic receptor that recognizes structurally conserved molecules derived from pathogens (Akira and Takeda, 2004). So far, 13 TLR family members have been

revealed in murine. Among the TLR family, TLR1, TLR2, TLR4, TLR5, and TLR6 located on cell surfaces are activated by microbial protein components from pathogens; TLR3, TLR7/TLR8 and TLR9 are located in endosomes and activated by viral dsRNA, ssRNA, DNA and bacterial CpG, respectively (Akira and Takeda, 2004). In innate immune cells, such as granulocytes, neutrophils, monocytes/macrophages, dendritic cells, B cells and T cells, activated TLRs trigger a myriad of intercellular signaling pathways. There are 2 representative signaling pathways of TLRs depending on which of the 2 adapter molecules (MyD88 and TRIF) are involved. MyD88 and TRIF each lead to a distinct profile of immune mediators. TLR4 mediates its actions through both the MyD88 and TRIF pathways; TLR3 signals only through TRIF, and all the other TLRs mediate through the MyD88 dependent pathway (Pandey and Agrawal, 2004; Takeda and Akira, 2004).

3.1. TLRs in CNS

The CNS is an immune privilege site with limited capacity for inflammation and regeneration. In addition, the CNS has a specialized innate immune system against infection or injury (McGavern and Kang, 2011). In the CNS, resident cells, such as microglia, astrocytes and oligodendrocytes, are involved in the innate immune system express different types of TLRs (Fig. 5) (Kielian, 2009; Hanke and Kielian, 2011).

Microglial cells express all known members of the TLR family except TLR10 (Jack et al, 2005). Microglia cells constitutively express TLR2 recognizing numerous molecules such as LTA, PGN and lipoproteins and TLR4 recognizing LPS (Aravalli et al., 2007). TLR3 responds to dsRNA and the synthetic TLR3 agonist, poly(I:C) and TMEV (Theiler's murine

encephalomyelitis virus), and also produces various cytokines including IFN- β , IL-1 β and IL-6 (Olson and Miller, 2004).

Astrocytes are the major glial cells in the CNS and also participate in inflammatory responses inducing several cytokines and chemokines via TLR activation (Jack et al., 2005). Astrocytes express several TLRs including TLR1, 2, 3, 4, 5 and 9 (Jack et al., 2005; Farina et al., 2007). In astrocytes, poly(I:C)-induced TLR3 expression is engaged in not only neuroprotective responses, typified by the expression of numerous growth factors and protective mediators but also pro-inflammatory responses (Carpentier et al., 2005; Bsibsi et al., 2006).

In comparison with astrocytes and microglia, the list of expressed TLRs in oligodendrocytes is even more limited. As shown in previous reports, only TLR2, TLR3 and TLR4 are expressed in oligodendrocytes (Lehnardt et al., 2002; Bsibsi et al., 2012). In highly purified oligodendrocyte cultures, the TLR2 agonist, zymosan, promoted survival, differentiation, and myelin-like membrane formation, whereas the TLR3 agonist, poly(I:C), was a potent inducer of apoptosis (Bsibsi et al., 2012). Moreover, the TLR4 agonist, LPS, induced oligodendrocyte cell death (Lehnardt et al., 2002).

However, in addition to the relevant innate immune system, neurons express some kinds of TLR family receptors, namely TLR2, TLR3, TLR4, and TLR8 (Prehau, et al., 2005; Ma et al., 2006; Mishra et al., 2006; Tang et al., 2007). Neuronal TLR2 and TLR4 affect the proapoptotic signaling pathway that may render them vulnerable to ischemic death (Tang et al., 2007). In TLR3-deficient embryos, there is a greater number of neurosphere formations compared to the wild-type mice (Lathia et al., 2008). In mouse cortical cultures, the TLR8 agonist, R848, inhibits neurite outgrowth and induces neuronal

apoptosis (Ma et al., 2006). However, not all the roles of TLRs in neurons have yet to be elucidated in physiological and pathological environments.

3.2. TLRs in the Spinal Cord

Traumatic SCI triggers several inflammatory processes in the spinal cord. First, resident microglia and astrocytes are activated and secrete various cytokines and chemokines. Then, peripheral immune cells such as neutrophils, macrophages, and other leukocytes infiltrate and exaggerate the lesion site of the accident. At this point, the involved immune cells express several kinds of TLRs in response to injury.

3.2.1 TLRs in SCI

After the SCI, TLRs initiate intracellular signaling by binding DAMP, which is released at sites of tissue injury (Zhang and Schluesener, 2006). The kinds of DAMP are heat-shock proteins (HSPs), necrotic cells, degradation products of the ECM, high mobility group box 1 (HMGB1) and mRNA (Taguchi et al., 1996; Basu et al., 2000; Ohashi et al., 2000; Li et al. 2001; Okamura et al., 2001; Asea et al., 2002; Johnson et al., 2002; Termeer et al., 2002; Chen et al., 2011). Reportedly related to SCI, the expression of TLR2 and TLR4 are increased at 3 dpi. TLR2 is expressed on astrocytes and CNS macrophages, while TLR4 is predominantly expressed on CNS macrophages. This report, also, suggested that TLR2 or TLR4 expression have effects on positively modulating functional recovery and reducing cytokine secretions and gliosis (Kigerl et al., 2007). In another report, significantly induced CCR1 and CCL3 (MIP-1a) at a lesion site from SCI participated in neuropathic pain and were co-labeled with TLR4 and GFAP (Knerlich-Lukoschus et al., 2011). This

report suggested the possibility that SCI-induced TLR4 expression in astrocytes plays potential integrative roles in pain.

3.2.2 TLRs in Regeneration

After injecting the TLR2 agonist, zymosan, directly into the eye, it activated macrophages and induced regeneration of retinal ganglion cell axons into the lesioned optic nerve or into peripheral nerve grafts (Leon et al., 2000; Yin et al., 2003). In addition, Wallerian degeneration, axonal regeneration, and recovery of locomotor functions after sciatic nerve lesion are significantly delayed in mice deficient in TLR signaling but accelerated after a single microinjection of either zymosan (TLR2) or LPS (TLR4) at the site of injury (Biovin et al., 2007). However, according to a recent report, after optic nerve injury, retinal ganglion cell survival and axon regeneration improved by repressing microglia activation in the TRIF knockout mice (Lin et al., 2012). Downstream of TLR3 and TLR4, activation of TRIF is essential for the MyD88-independent pathway. Until now, despite increasing reports for the role of TLRs in CSN injury, only a few studies have been done on the function of TLRs in axon degeneration.

Figure 1. Illustration of the spinal cord

The spinal cord is segmentally organized. There are 31 segments, defined by 31 pairs of nerves exiting the cord. These nerves are divided into 8 cervical, 12 thoracic, 5 lumbar, 5 sacral, and 1 coccygeal nerve in human.

(<http://www.daviddarling.info/encyclopedia/ETEmain.html>)

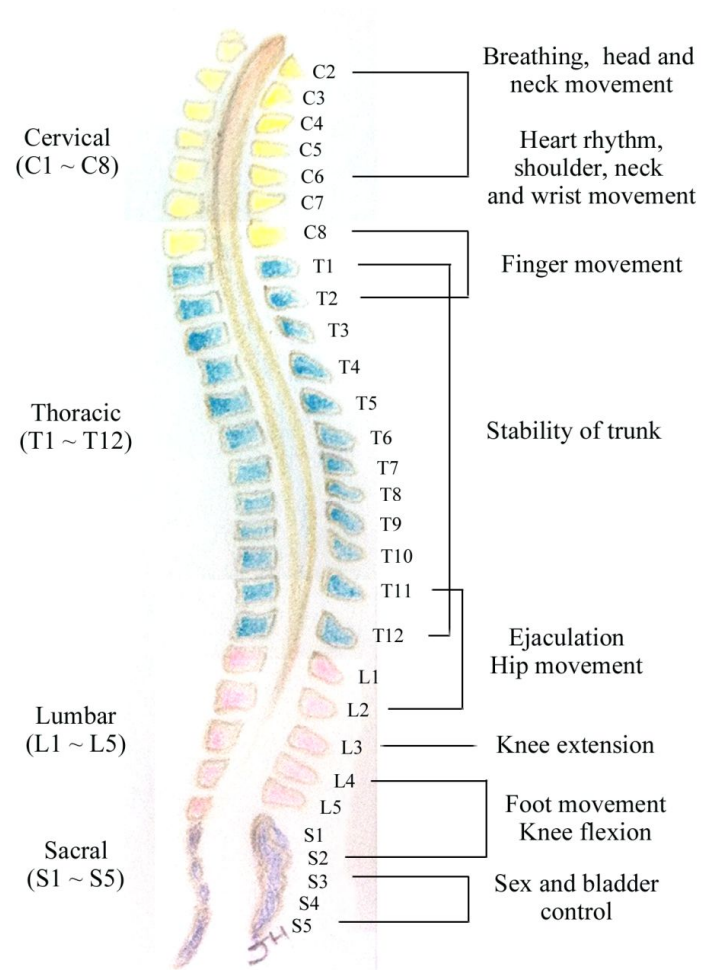


Figure 2. Ascending and Descending tracts in the spinal cord

A diagram of a transverse section of cervical spinal cord showing the position of the major ascending and descending tracts in a mammal (Bear et al., 2006)

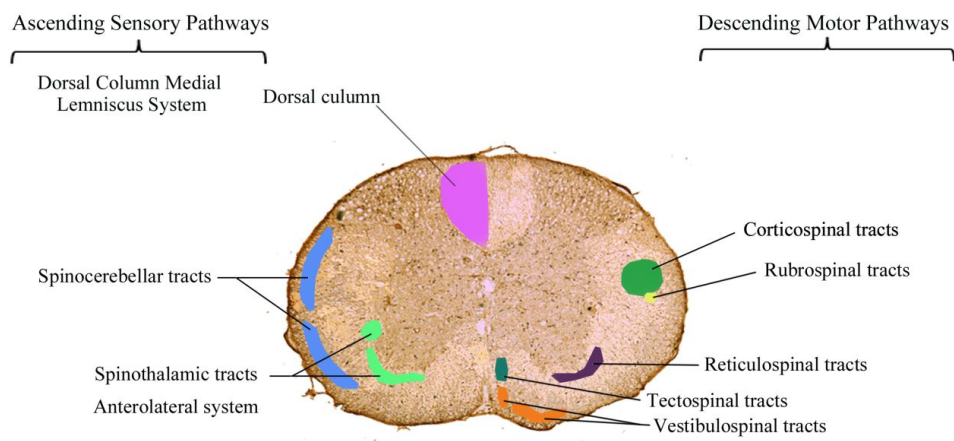


Figure 3. Pathophysiology and concomitant gene expression changes after SCI

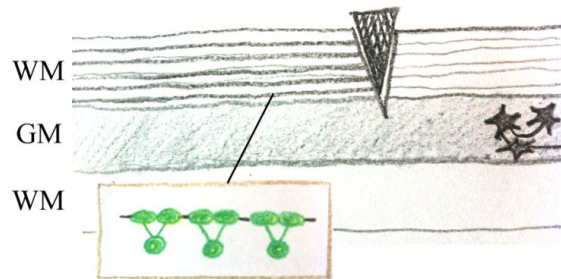
(a) During the acute early phase after injury, immediate damage to the axonal tracts occurring at the moment of the insult are followed by general metabolic disturbances involving Na^+ and K^+ channels, as reported by gene expression analysis data. Dysfunction of ATPases (Ca^{2+} and Na^+/K^+ ATPases) also contributes to the general failure of the spinal cord to function appropriately. (b) The secondary phase is characterized by accumulation of immune-system molecules within the injury site and the release of free radicals into the spinal cord. Accordingly, gene expression data highlight the upregulation of inducible nitric-oxide synthase (iNOS), IL-6 and IL-1 β . The downregulation of myelin proteins can be interpreted as an indication of demyelination. (c) In the chronic phase following the injury, demyelination accompanies Wallerian degeneration of the distal axons. At the same time, upregulation of growth-promoting factors and growth-associated molecules indicates a sustained effort of axonal regrowth. Increased glial fibrillary acidic protein (GFAP) expression highlights the formation of scar tissue around the lesion site.

(Bareyre and Schwab, 2003)

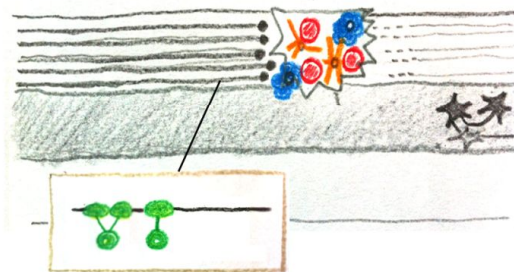
oligodendrocytes (light green); Schwann cells (dark green); macrophages (blue); neutrophils (red); astrocytes (orange); neurons (black).

LAMP, limbic-system-associated membrane protein; MCP, monocyte chemoattractant protein; NGFI-A, nerve-growth-factor-induced A; PDGF, platelet-derived growth factor; SNAP-25, 25 kDa synaptosomal-associated protein; VCAM, vascular cell adhesion molecule; VGF, inducible nerve growth factor; WM, white matter..

(a) Acute: from the impact to the first few days after SCI



(b) Secondary: within minutes to weeks after SCI



(c) Chronic: within days to years after SCI

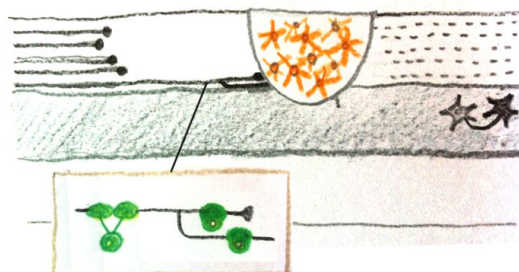


Figure 4. Key properties and functions of polarized macrophages

In the presence of interferon (IFN)- γ , lipopolysaccharide (LPS) and other microbial products, monocytes differentiate into M1 macrophages. In the presence of macrophage colony stimulating factor (CSF-1), interleukin (IL)-4, IL-13, IL-10 and immunocomplexes in association with either IL-1R- or TLR-ligands, monocytes differentiate into M2 macrophages. M1 and M2 subsets differ in terms of phenotype and functions. M1 cells have high microbicidal activity, immuno-stimulatory functions and tumor cytotoxicity. M2 cells have high scavenging ability, promote tissue repair and angiogenesis and favor tumor progression.

(Sica et al., 2008)

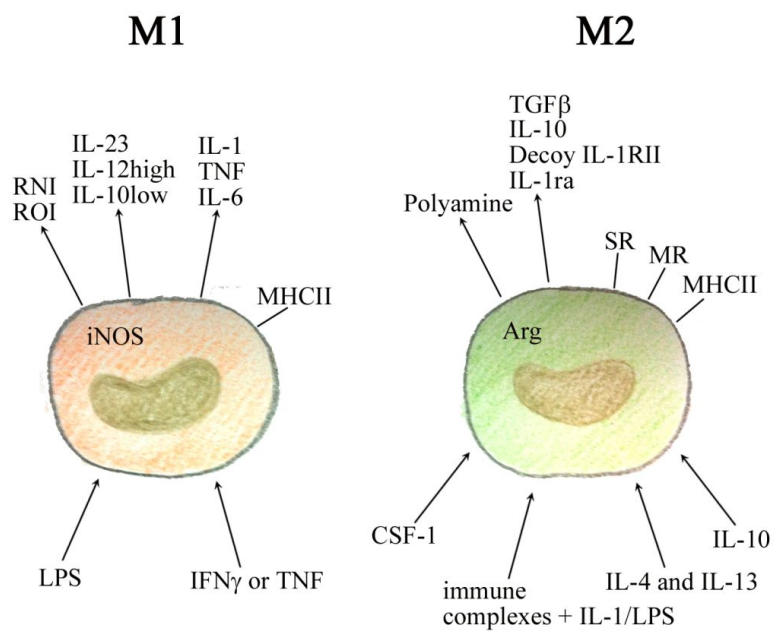
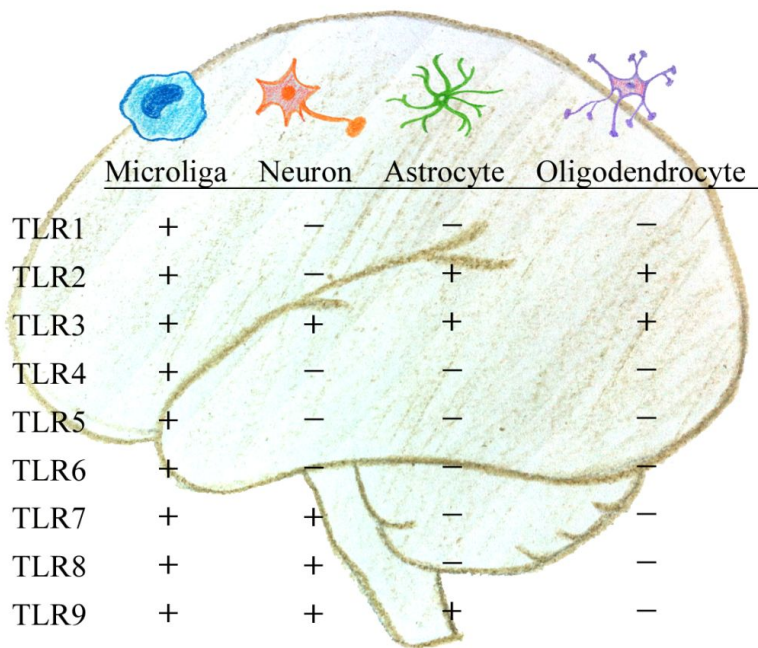


Figure 5. Expression of TLR family members in CNS cells

Microglia expresses all TLRs identified to date, whereas astrocytes, oligodendrocytes and neurons express a more limited TLR repertoire in comparison.

(Hanke and Kielian, 2011)



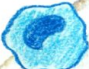


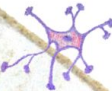
	 Microglia	 Neuron	 Astrocyte	 Oligodendrocyte
TLR1	+	—	—	—
TLR2	+	—	+	+
TLR3	+	+	+	+
TLR4	+	—	—	—
TLR5	+	—	—	—
TLR6	+	—	—	—
TLR7	+	+	—	—
TLR8	+	+	—	—
TLR9	+	+	+	—

Table 1. A general description of the anatomical and functional aspects of the ascending sensory pathways

Anatomical system	Anatomical tracts	Functional component(s)
Anterolateral (ALS)	Spinothalamic* Spinoreticular Spinomesencephalic Spinotectal Spinohypothalamic	Pain, temperature, nondiscriminative (crude) touch, pressure, and some proprioceptive sensation
Dorsal column–medial lemniscal (DCML)*	Fasciculus gracilis Fasciculus cuneatus	Discriminative (fine) touch, vibratory sense, position sense
Somatosensory to the cerebellum	Anterior spinocerebellar Posterior spinocerebellar Rostral spinocerebellar Cuneocerebellar	Primarily proprioceptive information (also some pain and pressure information)
*Indicates conscious level.		

(Patesta and Gartner, 2006)

Table 2. Classification of matrix metalloproteinase enzymes

No.	MMP No.	Class	Enzyme
1	MMP-1	Collagenases	Collagenase-1
2	MMP-8		Neutrophil collagenase
3	MMP-13		Collagenase-3
4	MMP-18		Collagenase-4
5	MMP-2	Gelatinases	Gelatinase-A
6	MMP-9		Gelatinases-B
7	MMP-3	Stromelysins	Stromelysin-1
8	MMP-10		Stromelysin-2
9	MMP-11		Stromelysin-3
10	MMP-27		Homology to stromelysin-2 (51.6%)
11	MMP-7	Matrilysins	Matrilysin (PUMP)
12	MMP-26		Matrilysin-2
13	MMP-14	MT1-MMP	MT1-MMP
14	MMP-15		MT2-MMP
15	MMP-16		MT3-MMP
16	MMP-17		MT4-MMP
17	MMP-24		MT5-MMP
18	MMP-25		MT6-MMP
19	MMP-12	Other enzymes	Macrophage metalloelastase
20	MMP-19		RASI 1
21	MMP-20		Enamelysin
22	MMP-21		MMP identified on chromosome 1
23	MMP-22		MMP identified on chromosome 1
24	MMP-23		From human ovary cDNA
25	MMP-28		Epilysin
26	MMP-29		Unnamed

(Verma and Hansch, 2007)

PURPOSE

Spinal cord injuries are caused by an accident, not a disease. More than 56% of these injuries occur between the ages of 16 and 30, and the injured people never fully recover from the serious trauma, leading to a poor QOL (quality of life). Currently, there is no definitive cure for SCI and the myriad of mechanisms that contribute to this condition are still unclear.

SCI provokes a series of inflammations. In the process of inflammation, several immune cells are engaged in these steps; however, the role of neutrophils and macrophages is still being debated. Therefore, the aims of this study were as follows.

1. The first aim of this study was to characterize the *in vivo* role of neutrophils and macrophages in the inflammation following SCI using myeloid cell type-specific IKK β -deficient (*ikk β ^{Amyle}*) mice.

There are many studies about the mechanism in the SCI; however, there are no definitive reports on TLR3 and SCI. In addition, the role of TLR3 in injury is quite controversially. Through this study, I tried to elucidate the role of TLR3 in SCI.

메모 [DK2]: Sorry, I had to guess the author's intent.

2. The second aim was to elucidate the *in vivo* role of TLR3 in functional recovery of SCI using TLR3 knockout mice.

In this research, I will address the specific aims set forth in the subsequent two chapters.

CHAPTER 1

**IKK- β -mediated myeloid cell activation
exacerbates inflammation and inhibits
recovery after spinal cord injury**

INTRODUCTION

Innate immune cells are actively involved in pathogenesis and recovery after spinal cord injury (SCI). In a rat SCI model, neutrophils infiltrate the primary lesion site within several hours, peak at 12-24 hour and disappear after several days (Taoka et al., 1997). Similarly, blood-derived monocytes/macrophages are detected in and around the lesion 2-3 days after injury and may persist for weeks (Popovich et al., 1997). Studies on the roles of these immune cells indicate that myeloid cells in the spinal cord produce putative neurotoxic mediators, such as reactive oxygen species (ROS), cytokines, and proteases, and thereby contribute to secondary damage after SCI (Bareyre and Schwab, 2003). The neurotoxic effects of neutrophils were originally suggested by studies that blocked cell adhesion molecules with antibodies (Hamada et al., 1996; Taoka et al., 1997). Administering anti-P-selectin or anti-ICAM-1 antibodies to SCI animal models reduced neutrophil infiltration into the spinal cord and attenuated tissue damage. Likewise, depleting blood monocytes by administering chlodronate liposomes improved recovery of functional activity after SCI, indicating that blood-derived macrophages contribute to tissue damage (Popovich et al., 1999).

Activated neutrophils and macrophages, on the other hand, express not only tissue-damaging molecules, but also produce neurotrophic and ROS-scavenging molecules known to be involved in wound repair and tissue healing in SCI (Liu et al., 2002; Bouhy et al., 2006). In addition, macrophages contribute to neuroregeneration by removing myelin debris, which inhibits neurite outgrowth (Stoll and Muller, 1999). Based on these findings, intralesional neutrophil/macrophage infiltration was argued to protect the spinal

cord from secondary damage and facilitate recovery after SCI. In support of this model, depletion of blood neutrophils by i.v. administration of anti-Ly6G antibody was found to amplify neurological deficit after SCI (Stirling et al., 2009). Activated macrophages can also be neuroprotective, as evidenced by a study in which implanting activated macrophages post-injury improved locomotive recovery (Bomstein et al., 2003). Such conflicting reports indicate that the *in vivo* roles of neutrophil/macrophage activation and infiltration in SCI are controversial and far from understood.

In this study, I revisited this question using IKK β conditional knockout mice (*ikk β ^{Amve}*), in which the *ikk β* gene has been specifically deleted from myeloid cells, including the majority of neutrophil and macrophage populations (Greten et al., 2004; Greten et al., 2007). IKK β is a protein kinase responsible for NF- κ B activation via various inflammatory stimuli (Rothwarf and Karin, 1999); NF- κ B is a key transcription factor responsible for the expressions of inflammatory genes and adhesion molecules (Barnes, and Karin, 1997). I reasoned that the *ikk β* deficiency would interfere with neutrophil/macrophage activation after SCI, allowing for the investigation of the *in vivo* role of IKK β /NF- κ B-mediated neutrophil and macrophage activation in SCI.

MATERIALS AND METHODS

Mice and spinal cord injuries

Myeloid cell type-specific IKK β -deficient (*ikk β ^{Δmye}*) mice were generated by crossing floxed-*ikk β* (*ikk β ^{F/F}*) mice and LysM-Cre knock-in mice expressing Cre under the control of the endogenous lysozyme M promoter, as described (Clausen et al., 1999; Li et al., 2003). While these mice do not exhibit any phenotypic signatures at physiological condition or developmental abnormalities, *ikk β* is deleted in more than 75% of neutrophil and 79% of macrophage population in these mice (Clausen et al., 1999; Hong et al., 2010). Adult male mice (8-10 weeks old) were anesthetized with sodium pentobarbital (30 mg/kg body weight, i.p.) and laminectomized between T8 and T10. The exposed spinal cord was subjected to lateral hemisection at the T9 level with mini-Vannas scissors under microscope visualization. To ensure a complete hemisection in each surgery, a needle (gage number 23) was injected from the dorsal median sulcus to the ventral wall of the vertebral canal and then moved laterally to the left lateral wall. Laminectomized mice without hemisection were used as controls. In case of crush injury, a laminectomy at the T9 level was performed with number 5 Dumont forceps ground down to a tip width of 0.5 mm. The forceps I used in this report were modified with a spacer so that at maximal closure a 1 mm space remained to make incomplete lesion (Faulkner et al., 2004). The spinal cord was compressed with the forceps laterally from both sides for 10 sec. All surgical and experimental procedures were reviewed and approved by the Institutional Animal Care and Use Committee (IACUC) at Seoul National University.

Immunohistochemistry

The mice were anesthetized with Avertin (2-2-2 tribromoethanol) and perfused with 0.1 M phosphate-buffered saline (PBS), followed by 4% paraformaldehyde in 0.1 M PBS. A 1-cm tissue block containing the injury site was collected, post-fixed in the same fixative overnight at 4°C, and cryoprotected in 30% sucrose in 0.1 M phosphate buffer. The spinal cord was cryo-cut to 16 µm in the horizontal and coronal plane and placed onto gelatin-coated glass slides. Sections were blocked in the blocking solution (5% normal goat serum, 5% FBS, 2% BSA, and 0.1% Triton X-100) for 1 hour at RT and incubated overnight at 4°C with mouse anti-NeuN (1:1000; Chemicon, Temecula, CA, USA) for neurons, rat anti-CD68 (1:500; Serotec Inc., Oxford, UK) for macrophages, rat anti-Gr-1 (1:1000; Invitrogen, Carlsbad, CA, USA) for neutrophils, anti-caspase-3 (1:200; Santa Cruz Biotechnology, Santa Cruz, CA, USA), mouse anti-iNOS (1:100; Santa Cruz Biotechnology), rabbit anti-Arginase 1 (1:100; Santa Cruz Biotechnology), goat anti-CXCL1 (1:10; R&D Systems, Minneapolis, MN, USA), rabbit anti-nitrotyrosine (1:500; Upstate, Temecula, CA, USA), or mouse anti-8-hydroxyguanosine (1:1000; Abcam, Cambridge, MA, USA) antibodies. After three washes in 0.1 M PBS plus 0.1% Triton X-100 for 10 min at RT, tissue sections were incubated with Cy3- or FITC-conjugated secondary antibodies (1:200; Jackson ImmunoResearch, West Grove, PA, USA) for 1 hour at RT. Sections were mounted with Vectashield (Vector Labs, Burlingame, CA, USA) and examined using a fluorescent microscope (LSM 5 PASCAL; Carl Zeiss, Munchen, Germany). For neuronal cell counting, pictures of 6 sections from each mouse were analyzed using Axiovision 4.8 image program (Carl Zeiss) for NeuN⁺ cells in a rectangular

area 500 μm caudal and rostral to injury site. For OHG⁺ cell counting, pictures of 2 sections from each mouse were analyzed in a rectangular area 300 μm caudal lesion to injury site.

Luxol Fast Blue (LFB) staining and lesion volume measurement

LFB staining was performed as reported (Brechtel et al., 2006) to calculate lesion volume. Briefly, longitudinal sections of injured spinal cord at 28 dpi were stained with 0.1% LFB (Sigma, St. Louise, MO, USA) in acidified 95% ethanol for overnight at 56°C. Differentiation and counterstaining were carried out by incubating sections in 0.05% lithium carbonate solution. Images of the stained sections were taken under the microscope (Axiovert200, Carl Zeiss) using a lens with a 2.5 X 10 (objective X eye piece), and then lesion size (x-y stage) was calculated using Axiovision 4.8 image program. The total lesion volume was calculated by summing their individual subvolumes, using Cavalieri method (Michel and Cruz-Orive, 1988; Oorschot, 1994). Individual subvolumes of lesion area were calculated by multiplying the longitudinal-sectional area (S) and the distance between sections (10 μm). Each measurement value was a mean of 3 animals and calculated by one-way ANOVA followed by Tukey's post-hoc test.

Terminal deoxynucleotidyl transferase dUTP nick end labeling (TUNEL) staining

Apoptotic cells were detected using an Apoptaq Plus Fluorescein *in situ* cell apoptosis detection kit (Chemicon) following the manufacturer's instructions. Briefly, spinal cord sections were blocked in blocking solution for 1 hour at RT and stained with anti-NeuN antibody for 1 hour at RT for

detection of neuronal cells. After washing in 0.1 M PBS, tissue slices were pre-hybridized in equilibration buffer for 5 min, followed by incubation with terminal deoxynucleotidyl transferase (TdT) enzyme for 2 hours at 37°C, then, stained with FITC-conjugated anti-digoxigenin antibody and Cy3-conjugated anti-rabbit IgG antibody (to detect mouse anti-NeuN) (Jackson ImmunoResearch) for 1 hour at RT. Sections were mounted and visualized as above.

Real-time RT-PCR

Total RNA from isolated spinal cord tissue and cells was extracted using Trizol (Invitrogen), and reverse transcribed using M-MLV Reverse Transcriptase (Invitrogen). Real-time PCR was performed using a 7500 Real-Time PCR system (Applied Biosystems, Foster City, CA, USA) as previously described (Li et al., 2003). Relative mRNA levels were calculated according to the $2^{-\Delta\Delta C_t}$ method (Livak and Schmittgen, 2001). All Ct values were normalized to GAPDH. All experiments were performed at least three times. The PCR primer sequences used in this study are listed in Table 3.

Behavioral tests

Hind limb motor function was assessed by open field locomotion using the Basso Mouse Scale (Basso et al., 1996; Basso et al., 2006). Before and after SCI, the locomotive activity of each mouse was graded on a 10-point scale (scores 0-9) designed to assess hind limb locomotion recovery by evaluating hind limb joint movements, stepping, trunk position and stability, forelimb-hind limb coordination, paw placement, and tail position. A score of 0 indicated no observable hind limb movement; a score of 9 represented normal locomotion. All behavioral tests were performed blind.

Neutrophil and monocyte isolations

After anesthetization, blood was collected by cardiac puncture and drained into 15 ml conical tubes containing 500 µl of acid citrate dextrose solution B (0.48% (w/v) citric acid, 1.32% (w/v) sodium citrate, 1.47% (w/v) glucose). Immediately after collection, whole blood was lysed in 10 ml of red blood cell (RBC) lysis buffer (0.15 M NH₄Cl, 10 mM KHCO₃, and 0.1 mM EDTA) for 20 min on ice to remove the RBCs. The solution was passed through 70-µm nylon mesh (BD Biosciences, Oxford, UK) and centrifuged for 5 min at 400 x g. The cell pellet was lysed again in 10 ml of RBC lysis buffer for 10 min on ice and resuspended in 30 ml of 0.1 M PBS before layering onto a discontinuous Percoll gradient solution (3 ml 80%, 3 ml 60% and 3 ml 50% Percoll) and centrifuging for 5 min at 400 x g. After high-speed centrifugation (2500 x g for 30 min at 4°C; Sorvall RC-5 C Plus), neutrophils were recovered from the 60%/80% Percoll interface, and monocytes were isolated from the 50%/60% interface. Cells were washed twice with 1 M PBS and incubated in DMEM containing 5% bovine serum.

Migration assay

Isolated neutrophil or monocyte cells (5×10^4 cells/well) were seeded onto a 5-µm pore-size Transwell plate (Costar, Corning, NY, USA) and incubated for 2 hours in culture medium, in the presence or absence of CXCL1 (100 ng/ml, Bio-Research Products, South Lancaster, MA, USA) or CCL2 (50 ng/ml, Bio-Research Products) in the lower chamber. Neutrophils or monocytes that had migrated into the lower chamber were counted under magnification.

***In situ* zymography**

In situ gelatinolytic activity was detected as described report (Frederiks and Mook, 2004). At 6 hour after SCI, spinal cords were isolated and immediately frozen with dry ice. Fresh cryostat sections (14 μ m) were subjected to post-fixing with ethanol and acetic acid (2:1) for 20 min and incubated with 10 μ g/ml fluorescein conjugated-DQ gelatin substrate (Invitrogen) for 3 hours. For neuron and neutrophil staining, sections were incubated with anti-NeuN and Gr-1 antibodies, respectively, followed by Cy3-conjugated secondary antibodies. Sections were mounted and visualized as described above.

Fluorescence activated cell sorting (FACS) assay

All procedures were performed on ice to minimize the *in vitro* expression of surface molecules (Forsyth and Levinsky, 1990). Spinal cord tissue (\pm 0.25 cm from the injury site) was dissected from injured spinal cord and cells were isolated by homogenization and filtration, and then cells were fixed with 1 ml 2% paraformaldehyde in 0.1 M PBS for 15 min. After three washes with 1 ml FACS buffer (0.1 M PBS, 2% FBS), cells were incubated with primary antibody for 1 hour, followed by washing. Cells were analyzed with a BD FACSCaliburTM flow cytometer and CellQuest software (Becton Dickinson, San Jose, CA, USA). To analyze CD11a, CD11b, and CD11c expression, PE-conjugated anti-CD11a (eBioscience, San Diego, CA, USA), FITC-conjugated anti-CD11b (BD Pharmingen, San Diego, CA, USA), and AlexaFluor 647-conjugated anti-CD11c (BioLegend, San Diego, CA, USA) antibodies were used, respectively. To analyze spinal cord-infiltrating leukocytes, cells were incubated in FITC-conjugated anti-CD11b (BD Pharmingen, San Diego, CA, USA) and PE-conjugated anti-CD45 (BD

Pharmingen) antibodies to analyze macrophages (CD11b⁺/CD45^{high}) and microglia (CD11b⁺/CD45^{low}) populations. Likewise, cells were incubated in FITC-conjugated anti-Gr-1 antibody (BioLegend, San Diego, CA, USA) and PE-conjugated anti-CD11a or Cy5.5-conjugated anti-CXCR2 (BioLegend) antibodies to analyze CD11a and CXCR2 expression levels in tissue-infiltrating neutrophils.

CXCL1 ELISA

Spinal cord tissues (\pm 0.25 cm to the injury site) were dissected from the spinal cord and proteins were extracted using tissue lysis buffer (137 mM NaCl, 20 mM Tris-HCl, 1% NP40, and protease inhibitor cocktail set III (Calbiochem, La Jolla, CA, USA)). The KC/CXCL1 in the tissue lysates was measured using ELISA kit (R&D Systems, Minneapolis, MN, USA) according to the manufacturer's instructions.

Statistical analysis

Data were presented as mean \pm SEM. Statistical analysis for real time PCR data and image analysis was performed using a one-way ANOVA analysis of variance for measurements, followed by independent *t* or Tukey's post hoc test for comparisons procedures. A $p < 0.05$ was considered to be statistically significant. Statistical analysis for motor behavioral tests was performed using two-way ANOVA analysis of variance for measurements, followed by Tukey's post hoc test ($p < 0.05$) for comparison procedures.

RESULTS

Attenuated myeloid cell infiltration in $ikk\beta^{Amye}$ mice after SCI

To study the *in vivo* role of IKK β -mediated myeloid cell activation in SCI, I used a well-characterized SCI model, spinal cord hemisection at the T9 level (Dong et al., 2003; Li et al., 2007) using wild-type ($ikk\beta^{+/+}$) and myeloid cell-specific IKK β deficient ($ikk\beta^{Amye}$) mice. Neutrophils in the injured spinal cord tissue were counted by flow cytometry. Six hours after SCI, Gr-1⁺ neutrophils were detected in $ikk\beta^{+/+}$ mice spinal cord tissue, with numbers further increasing at 24 hour (3.0% of total counted cells at 6 hour and 5.6% at 24 hour) (Fig. 1A and B). In comparison, the neutrophil number in $ikk\beta^{Amye}$ mice spinal cord tissue was significantly less, 52% and 59% lower than in $ikk\beta^{+/+}$ mice at 6 and 24 hour, respectively (Fig. 1A and B). No Gr-1⁺ cells were detected in spinal cords of sham-operated mice of either genotype (data not shown). To more confirm the difference of infiltrations of neutrophils into the lesion sites, I analyzed using with immunohistochemistry. Six hours after SCI, Gr-1⁺ neutrophils were detected in and around the lesion area of $ikk\beta^{+/+}$ mice, with numbers further increasing by 24 hours (Fig. 1C, left panels). In comparison, in $ikk\beta^{Amye}$ mice, the number of Gr-1⁺ neutrophils at the lesion was significantly reduced being 50% and 60% lower than the number of $ikk\beta^{+/+}$ mice at 6 and 24 hour, respectively (Figs. 1C and D). Neutrophil infiltration in $ikk\beta^{Amye}$ mice was similarly reduced in another SCI model, spinal cord crush injury (Fig. 1E).

Macrophages infiltrated the lesion site at a considerably later time point following SCI. By flow cytometry, CD11b⁺/CD45^{high} macrophages (Greter et al., 2005) in the injured spinal cord increased to 2.6% at 5 days post-injury (dpi) in *ikkβ*^{+/+} mice (Fig. 2A and B), and only increased to 1.2% in *ikkβ*^{Δmye} mice. The proportion of CD11b⁺/CD45^{low} cells, which represent resident microglia (Greter et al., 2005), did not change significantly after SCI in either *ikkβ*^{+/+} or *ikkβ*^{Δmye} mice. It has been reported that macrophages exert different effects on spinal cord injury depending on their activation type (M1 vs. M2) (Sica et al., 2008). To characterize the type of the tissue-infiltrating macrophages, I immunostained macrophages for iNOS and Arginase 1, an M1 and M2 macrophage marker, respectively. CD68⁺ macrophages in both *ikkβ*^{+/+} and *ikkβ*^{Δmye} mice expressed iNOS but not Arginase 1 (Fig. 2C and D) at 5 dpi, indicating that these macrophages are mostly M1 macrophages. Taken together, these data show that deleting *ikkβ* from myeloid cells reduced neutrophil/macrophage infiltration into the spinal cord after SCI.

SCI-induced neutrophil chemoattractants are reduced in *ikkβ*^{Δmye} mice

To test whether the reduced neutrophil infiltration in *ikkβ*^{Δmye} mice was due to innate characteristics of IKKβ-deficient neutrophils, I isolated neutrophils from both *ikkβ*^{+/+} and *ikkβ*^{Δmye} mice and assessed the expression of CD11a and CXCR2, an adhesion molecule and a chemokine receptor involved in neutrophil extravasation and migration (Green et al., 2006). CD11a and CXCR2 expression in blood neutrophils from *ikkβ*^{Δmye} mice were comparable to

ikkβ^{+/+} mice both at mRNA (Fig. 3A). Also the protein level of CD11a, CD11b, CD11c and CXCR2 were not significantly different in *ikkβ^{+/+}* or *ikkβ^{Δmye}* blood leukocytes (Fig. 3B). CD11b and CD11c are adhesion molecules preferentially expressed on myeloid cells. Likewise, CD11a and CXCR2 expression in tissue-infiltrating neutrophils after SCI were not altered in *ikkβ^{Δmye}* mice (Fig. 3C).

I also tested the migratory activities of neutrophils from *ikkβ^{+/+}* and *ikkβ^{Δmye}* mice by incubating cells in media containing CXCL1, a chemokine specific for neutrophil attraction using Transwell plates (Fig. 4A). Neutrophils from *ikkβ^{Δmye}* mice migrated more than cells from *ikkβ^{+/+}* mice (547±15 vs. 357±13). These data suggest that the reduced neutrophil infiltration in *ikkβ^{Δmye}* mice was not due to an altered migratory capacity of neutrophils in the blood after *ikkβ* deletion.

I tested whether *ikkβ^{Δmye}* mice had altered expression of neutrophil-attracting chemokine in the injured spinal cord (Fig. 4B). At 4 hour after SCI, CXCL1 mRNA levels increased by 364-fold in the injured tissue of *ikkβ^{+/+}* mice and declined slightly to 286-fold at 8 hour. However, in *ikkβ^{Δmye}* mice, CXCL1 mRNA only increased 134-fold at 4 hour and 88-fold at 8 hour. Similarly, CXCL1 protein expression was reduced in *ikkβ^{Δmye}* mice by more than 80% (153±82 vs. 26±12) at 1 dpi (Fig. 4C). These data suggest that reduced expression of neutrophil-attracting chemokines in the injured spinal cord of *ikkβ^{Δmye}* mice may, in part, account for low neutrophil infiltration in the lesion site.

CXCL1 is reportedly expressed in spinal cord-infiltrating neutrophils after SCI (Kobayashi, 2008). I also detected CXCL1 expression in Gr1⁺ neutrophils in injured spinal cords (Fig. 4D). To test whether induction of these

genes in neutrophils depends on IKK β expression, I stimulated neutrophils with LPS, and compared CXCL1 expression *in vitro*. In neutrophils from *ikk β ^{+/+}* mice, LPS stimulation increased CXCL1 transcript levels by 192-fold, whereas the inductions were almost completely abrogated in cells from *ikk β ^{Δ mye}* mice (Fig. 4E). Taken together, these data suggest a possibility that the first neutrophils to arrive at the SCI lesion are less activated in *ikk β ^{Δ mye}* than in *ikk β ^{+/+}* mice, resulting in reduced chemokine expression. This might further attenuate neutrophil recruitment to the lesion at later time points.

I also assessed monocyte migration in *ikk β ^{+/+}* and *ikk β ^{Δ mye}* mice. Migration of *ikk β ^{Δ mye}* monocytes stimulated by CCL2 was not significantly different from *ikk β ^{+/+}* monocytes (Fig. 4F). Yet, CCL2, 3, and 4 expressions in the injured spinal cord were almost completely blocked in *ikk β ^{Δ mye}* mice (Fig. 4G). These data once again suggest that reduced myeloid cell infiltration in *ikk β ^{Δ mye}* mice is not due to reduced migratory activity of the IKK β -deficient cells, but is more likely due to the reduced expression of chemoattractants in lesions of the *ikk β ^{Δ mye}* mice.

Compromise of SCI-induced neuronal cell death and behavioral deficit in *ikk β ^{Δ mye}* mice

To address the effects of myeloid cell activation and infiltration on SCI, I measured lesion volume in the spinal cords of *ikk β ^{+/+}* and *ikk β ^{Δ mye}* mice after hemisection injury (Fig. 5A). The lesion volume in *ikk β ^{Δ mye}* mice spinal cord was 30% less than *ikk β ^{+/+}* mice at 28 dpi. I then examined neurons in the coronal and longitudinal sections of injured spinal cords by immunohistochemistry using anti-NeuN antibody. Five days after SCI, there

were 44% fewer NeuN⁺ neurons in the region ipsilateral to the lesion site in *ikkβ^{+/+}* mice than in sham-operated mice (Fig. 5C). However, in *ikkβ^{Δmye}* mice, more NeuN⁺ neurons were detected in the injured spinal cord (Fig. 5B). In *ikkβ^{Δmye}* mice, there were 26% more NeuN⁺ neurons per unit area rostral (-500 μm) to the lesion site than in *ikkβ^{+/+}* mice (44 vs. 33) (Fig. 5C). Similarly, I found an increase in NeuN⁺ cells in the longitudinal sections (±500 μm to the lesion site) of injured spinal cords in *ikkβ^{Δmye}* mice (Fig. 5D). Compared to *ikkβ^{Δmye}* mice, the number of NeuN⁺ neurons in *ikkβ^{+/+}* mice was 49% (25 vs. 48) at the rostral site and 54% (17 vs. 37) at the caudal site (Fig. 5E). Neuronal cell death in *ikkβ^{Δmye}* mice was also compromised after spinal cord crush injury (Fig. 5F). These data demonstrate that IKKβ-mediated myeloid cell activation and infiltration in injured spinal cords contribute to neuronal cell death after SCI.

To characterize the nature of cell death after SCI, I measured apoptotic cells in the lesion area by TUNEL staining (Fig. 6A). One day after SCI, TUNEL-positive apoptotic cells were detected close to the lesion site in *ikkβ^{+/+}* mice, co-localizing with NeuN⁺ neurons (Fig. 6A, white arrows), shown magnified in figure 6B. In addition, active caspase-3 expression co-localized to NeuN⁺ neurons at 1 dpi (Fig. 6D, white arrows). Thus neurons in the lesion underwent apoptosis one day after spinal hemisection injury in *ikkβ^{+/+}* mice. In *ikkβ^{Δmye}* mice, however, few TUNEL⁺ or caspase-3⁺ neurons were detected at the lesion (Fig. 6A, lower panels, and D, right panel, and 6C). Since I did not detect any obvious macrophage infiltration into the lesion site within 1 dpi, IKKβ-mediated neutrophil activation was likely involved in neuronal apoptosis

at 1 dpi. This might eventually have resulted in the reduced number of neurons in *ikkβ^{+/+}* mice compared to *ikkβ^{Δmye}* mice at the later time point.

To test whether the reduced cell death in *ikkβ^{Δmye}* mice affects functional recovery from SCI, I determined the BMS scores (Basso et al., 2006) of injured mice (Fig. 7). Up to three days after injury, no difference in motor function was observed between *ikkβ^{+/+}* and *ikkβ^{Δmye}* mice. After seven days, the average BMS score of *ikkβ^{Δmye}* mice was higher than *ikkβ^{+/+}* mice, showing that lack of myeloid IKKβ improved recovery after SCI.

Reduced ROS and reactive nitrogen species (RNS) production after SCI in *ikkβ^{Δmye}* mice

To identify the mechanisms underlying differences in the rates of neuronal apoptosis, I measured neurotoxic gene expression in the injured spinal cord tissue. Previous studies suggest that neuronal cell death is induced by proinflammatory cytokines and ROS generated by neutrophils (Owaga et al., 2008; Zemans and Arndt, 2009). Therefore, I measured the mRNA expression of IL-6, IL-1β, and TNF-α in injured spinal cords of *ikkβ^{+/+}* and *ikkβ^{Δmye}* mice. Four hours after injury, when neutrophils begin to infiltrate the injured tissue, IL-6, IL-1β, and TNF-α mRNAs increased by 85-, 160- and 21-fold, respectively, in *ikkβ^{+/+}* mice (Fig. 8A). However, in *ikkβ^{Δmye}* mice, the mRNAs levels increased by only 18-, 43-, and 3-fold, respectively. Similarly, inductions of iNOS, which is involved in RNS production, and COX-2, which is involved in ROS generation, were attenuated in *ikkβ^{Δmye}* mice compared to *ikkβ^{+/+}* (2-fold vs. 5-fold for iNOS expression at 8 hour; 4-fold vs. 13-fold for COX-2 expression at 4 hour) (Fig. 8B and C). Nitric oxide (NO) and peroxides

generated by iNOS and COX-2 may cause neuronal cell death via nitrotyrosylation and DNA damage (Virdis et al., 2005; Zayachkivska et al., 2008). To examine whether protein nitrotyrosylation and DNA damage were involved in SCI-induced neuronal death, I measured the levels of nitrotyrosylated proteins and 8-hydroxy-guanine (8-OHG) incorporation into DNA in the spinal cord by immunostaining. After injury, nitrotyrosine and 8-OHG-immunoreactive cells were detected in the lesion areas of *ikkβ^{+/+}* mice (Fig. 8D and E, left panels). The number of immunoreactive cells and the staining intensities were lower in *ikkβ^{Δmye}* mice (Fig. 8D and E, right panels). Nitric oxide activates neuronal matrix metalloproteinase-9 (MMP-9) through nitrotyrosylation, leading to neuronal apoptosis (Gu et al., 2002).

To test if SCI-induced NO production and subsequent tyrosine nitrosylation leads to neuronal MMP-9 activation, I measured the MMP-9 activity in the injured spinal cord by *in situ* zymography (Fig. 9A). In *ikkβ^{+/+}* mice, gelatinolytic activity was detected in many cells near the lesion site, which mostly co-localized with NeuN⁺ neurons, but not with Gr-1⁺ neutrophils (Figs. 9A and B). However, the injured spinal cord of *ikkβ^{Δmye}* mice showed significantly reduced gelatinase-active neuronal cells (Fig. 9A, lower panels). I also measured MMP-9 mRNA in the spinal cord. MMP-9 transcripts were upregulated by 10-fold at 8 hour post-injury in *ikkβ^{+/+}* spinal cords, with little or no induction in *ikkβ^{Δmye}* mice (Fig. 9C). These data show that increased MMP-9 expression in injured *ikkβ^{+/+}* mice might contribute to the enhanced MMP-9 activity observed in these mice. Taken together, these data imply that, in *ikkβ^{Δmye}* mice, reduced RNS and ROS production and MMP-9 activation might, at least in part, account for the reduced neuronal apoptosis after SCI in these mice.

Figure 1. Neutrophil infiltration was reduced in *ikkβ^{Δmye}* mice

(A) To quantify neutrophils, spinal cord cells were analyzed by flow cytometry at 24 hour post-injury. Representative data from three independent experiments are shown. (B) The percentage of Gr-1⁺ neutrophils at 6 hour and 24 hour post-injury were shown in a graph. The data are mean ± SEM of three independent experiments (**p*<0.5). (C) Gr-1⁺ neutrophil infiltration was detected at 6 hour and peaked at 24 hour post-injury in the spinal cord of *ikkβ^{+/+}* mice. Spinal cord-infiltrating neutrophils were reduced in *ikkβ^{Δmye}* mice. Scale bar, 50 μm. (D) Stained sections were counted for Gr-1⁺ cells. Results are given as mean ± SEM of values from six slides from three animals (**p*<0.05). (E) Crush injury was applied to the spinal cord of *ikkβ^{+/+}* and *ikkβ^{Δmye}* mice. Neutrophils infiltrating crush-injured spinal cord tissue were immunostained with anti-Gr-1 antibodies at 24 hour post-injury. Scale bar, 50 μm.

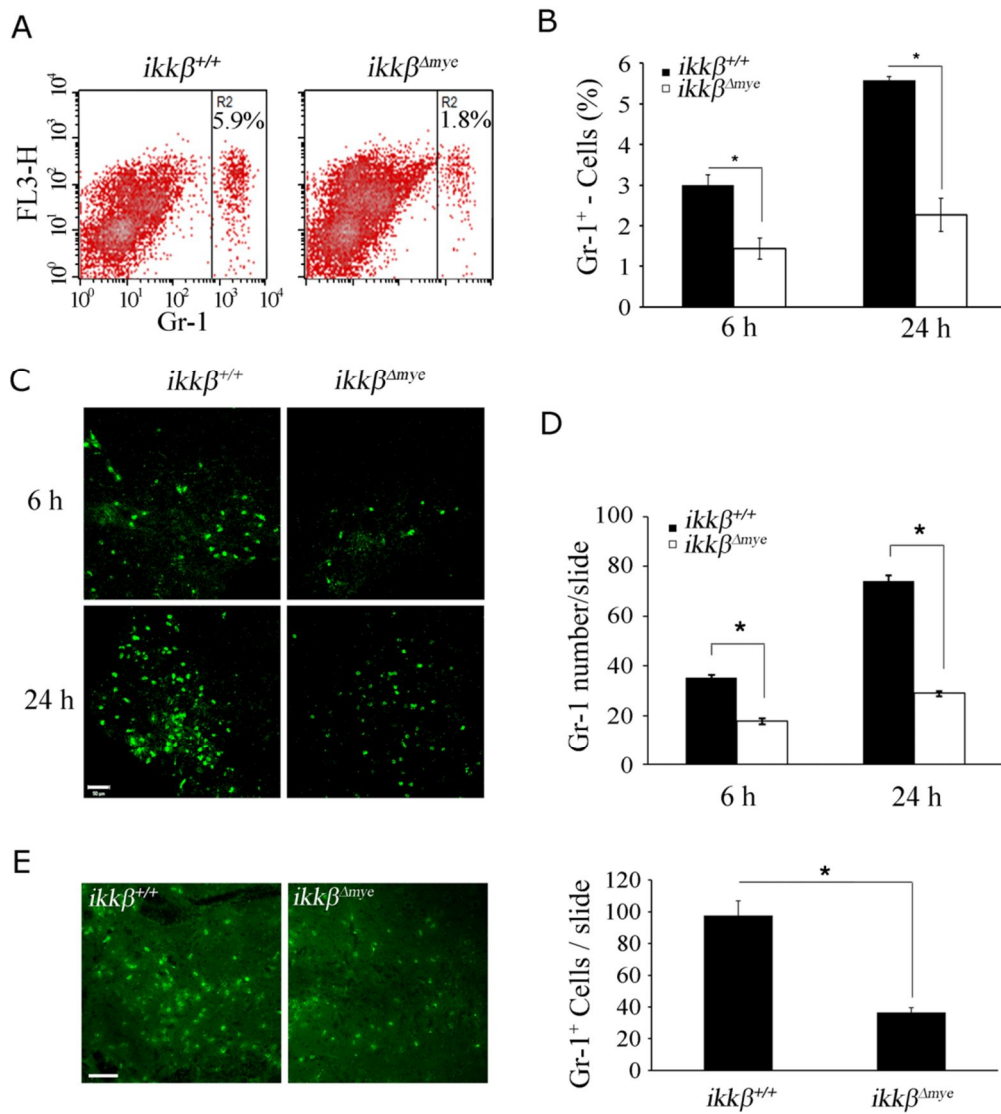


Figure 2. Macrophage infiltration was reduced in $ikk\beta^{Amye}$ mice

(A) The $CD11b^+/CD45^{high}$ macrophage population (R3 gate) was increased in the injured spinal cords of $ikk\beta^{+/+}$ mice at 5 dpi, while the increase was significantly lower in $ikk\beta^{Amye}$ mice. $CD11b^+/CD45^{low}$ microglia populations (R4 gate) were not significantly increased. Representative data from three independent experiments are shown, and the mean \pm SEM of three independent experiments are shown (B) (* $p < 0.05$). (C, D) $CD68^+$ (red) macrophages in the injured spinal cord sections (5 dpi) were co-stained for iNOS (green), marker of M1 macrophages (C), or Arginase 1 (Arg) marker of M2 macrophages (D). A representative figure from three independent experiments is shown. Scale bar 20 μm .

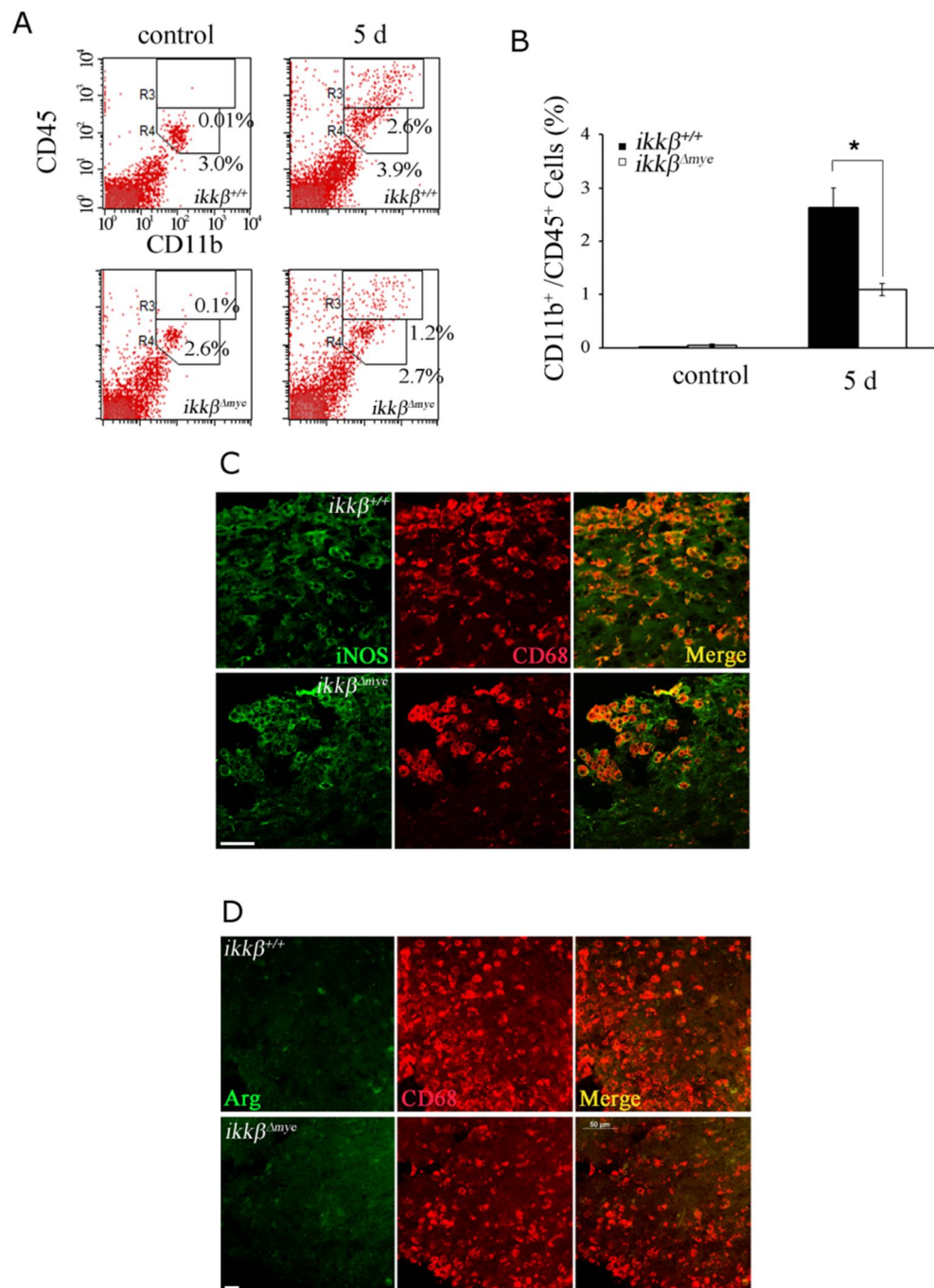
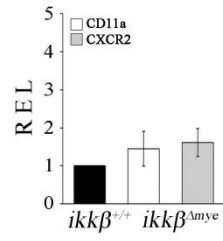


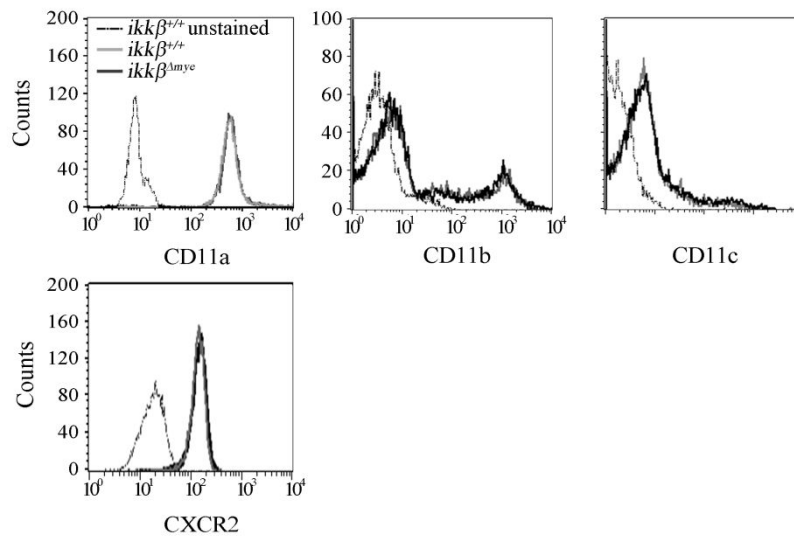
Figure 3. SCI-induced chemokine receptor and integrin of neutrophils expression did not differ

(A) Total RNA was prepared from neutrophils isolated from *ikkβ^{+/+}* and *ikkβ^{Δmye}* mice blood. CD11a and CXCR2 mRNA levels were measured by real-time RT-PCR (left graph). The relative gene expression levels (REL) in *ikkβ^{Δmye}* neutrophils compared to *ikkβ^{+/+}* neutrophils are presented (n=3). (B) CD11a, CD11b, CD11c and CXCR2 levels in *ikkβ^{+/+}* and *ikkβ^{Δmye}* neutrophils were measured by flow cytometry (right histograms). Representative data from three independent experiments are shown. (C) CD11a and CXCR2 expressions in Gr-1⁺ neutrophils of injured-spinal cord tissue were analyzed by flow cytometry. Representative data from three independent experiments are shown.

A



B



C

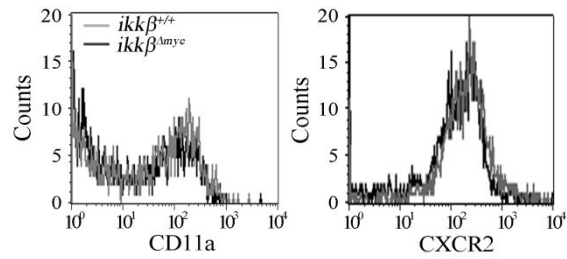
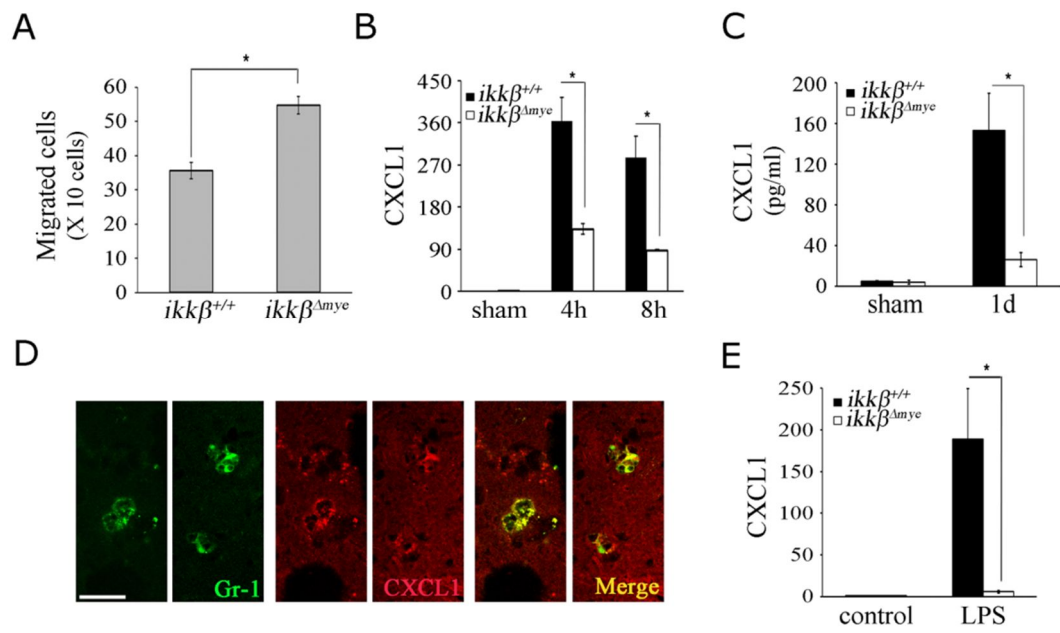


Figure 4. SCI-induced neutrophil-attracting chemokine expression was reduced in *ikkβ^{Δmye}* mice

(A) Neutrophils isolated from *ikkβ^{+/+}* and *ikkβ^{Δmye}* mice blood were used for migration assays. Neutrophils that migrated into the lower chamber of Transwell were counted by light microscopy. More *ikkβ^{Δmye}* neutrophils migrated than *ikkβ^{+/+}* neutrophils (**p*<0.05). (B) CXCL1 mRNA level in the injured spinal cord of *ikkβ^{Δmye}* mice was reduced at 4 and 8 hour compared to *ikkβ^{+/+}* mice. CXCL1 mRNA expression was assayed using real-time RT-PCR. The data are mean ± SEM of three independent experiments (**p*<0.05). (C) CXCL1 expression levels in the injured spinal cord tissues at 1 dpi were measured by ELISA. The data are mean ± SEM of three independent experiments (**p*<0.5). (D) To test CXCL1 expression from tissue-infiltrating neutrophils, spinal cord tissue sections of *ikkβ^{+/+}* mice at 1 dpi were immunostained with anti-Gr-1 antibody (green) and anti-CXCL1 antibody (red). A representative figure from three independent experiments is shown and the results were similar. Scale bar, 20 μm. (E) Isolated neutrophils from blood were stimulated with LPS (50 ng/ml) for 3 hours, and CXCL1 expression was measured by real-time RT-PCR. Means ± SEM of three independent experiments are shown (**p*<0.5).

(Continued)



(F) Monocytes isolated from $ikk\beta^{+/+}$ and $ikk\beta^{Amye}$ mice were used for migration assays. No significant difference was detected between cells from $ikk\beta^{+/+}$ vs. $ikk\beta^{Amye}$ mice. (G) CCL2, 3 and 4 expressions in the injured spinal cords of $ikk\beta^{+/+}$ and $ikk\beta^{Amye}$ mice were measured by real-time RT-PCR. The data are mean \pm SEM of three independent experiments (* $p < 0.05$).

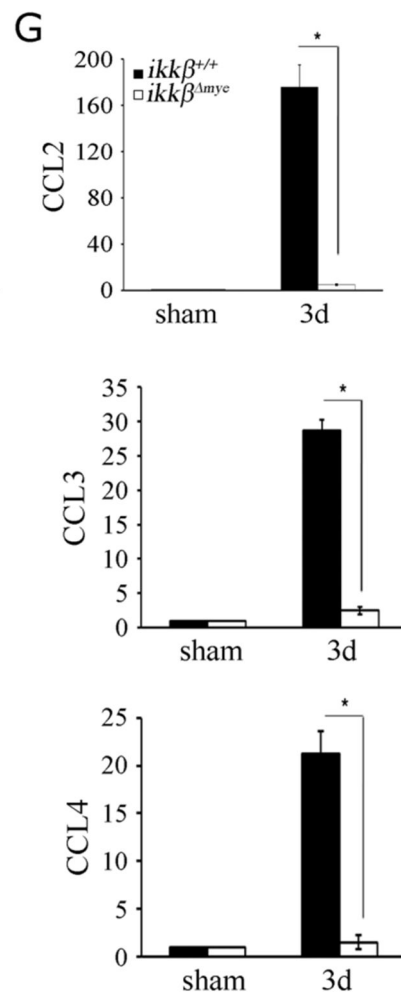
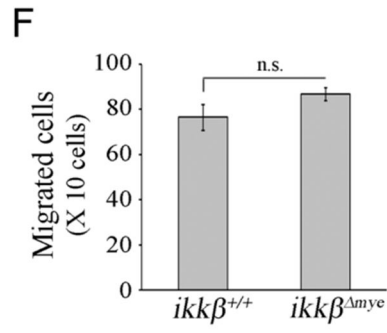
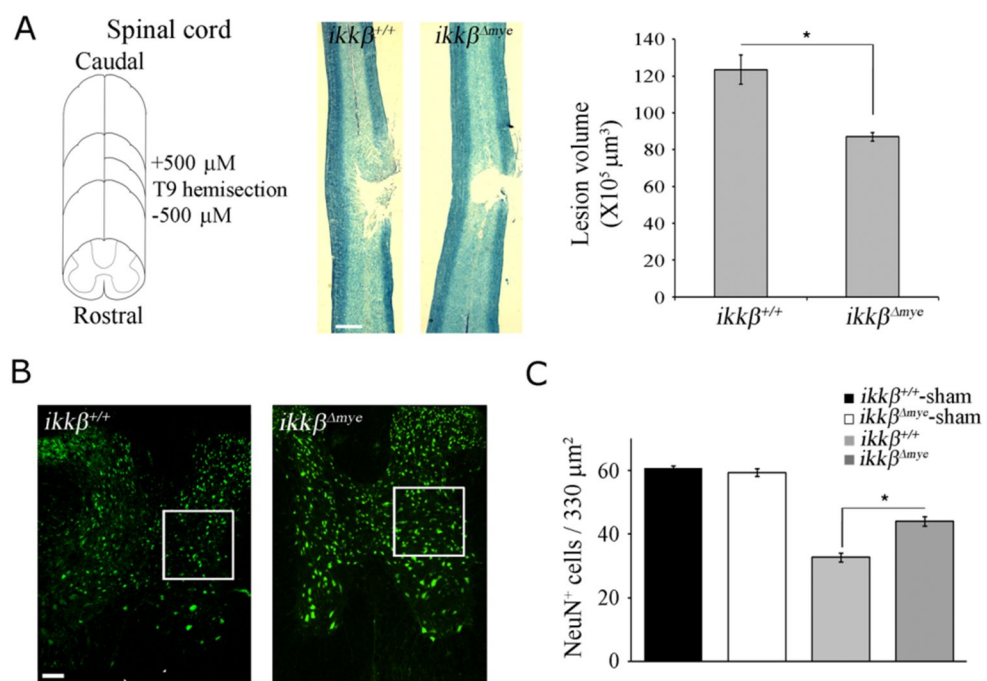


Figure 5. SCI-induced neuronal cell death was attenuated in *ikkβ^{Δmye}* mice

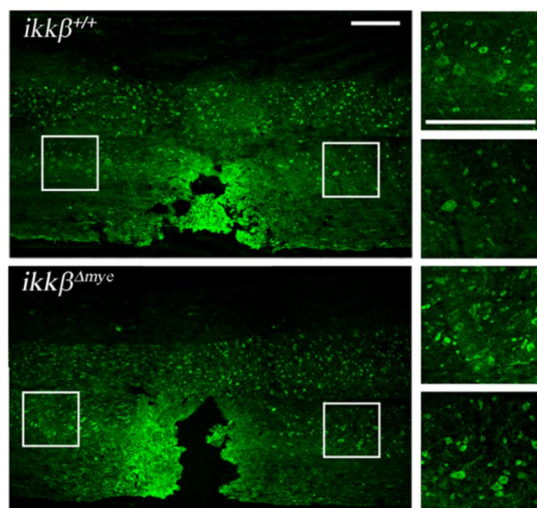
(A) At 28 dpi, coronal and longitudinal sections were prepared from tissue within 500 μm of the lesion in SCI-induced or sham-operated mice. Spinal cord sections were stained with LFB. Scale bar, 250 μm. Total lesion volume was calculated from 68 sections per animal (n=3) (**p*<0.5). (B) Neurons in coronal sections were detected by immunohistochemistry using anti-NeuN antibodies. Scale bar, 50 μm. A representative picture of a coronal section at -500 μm in the ipsilateral region shows NeuN⁺-signal elevated in *ikkβ^{Δmye}* mice compared to *ikkβ^{+/+}* mice. (C) NeuN⁺ cells in the 330 μm² white rectangle area (ipsi-region) -500 μm from the lesion site in the spinal cord of sham-operated *ikkβ^{+/+}* mice (*ikkβ^{+/+}*-sham), sham-operated *ikkβ^{Δmye}* mice (*ikkβ^{Δmye}*-sham), SCI-injured *ikkβ^{+/+}* mice (*ikkβ^{+/+}*), and SCI-injured *ikkβ^{Δmye}* mice (*ikkβ^{Δmye}*) were quantified. Six slides from three animals were counted, and the means ± SEM are presented (**p*<0.5).

(Continued)

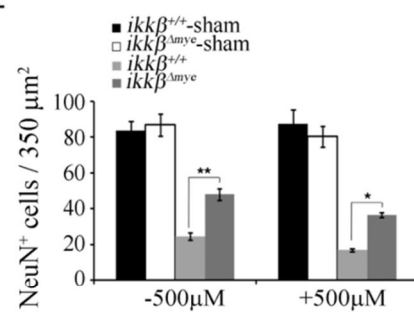


(D) Neurons in the spinal cord longitudinal sections were detected by immunohistochemistry using anti-NeuN antibody. Scale bar, 100 μm . A representative image shows increased NeuN⁺-cells in *ikk β ^{Δ mye}* mice. (E) NeuN⁺ cells in the 350 μm^2 white rectangle area ± 500 μm from the lesion site in the spinal cord of *ikk β ^{+/+}*-sham, *ikk β ^{Δ mye}*-sham, *ikk β ^{+/+}*, and *ikk β ^{Δ mye}* mice were quantified. Eight slides from four animals were counted, and the means \pm SEM are presented (* $p < 0.005$, ** $p < 0.05$). (F) Neuronal damage was assessed by immunostaining longitudinal sections of the injured spinal cord at 5 dpi using anti-NeuN antibody. Scale bar, 50 μm .

D



E



F

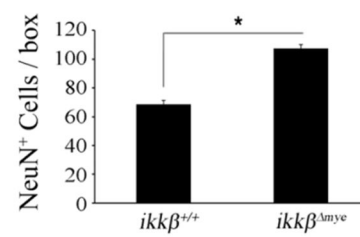
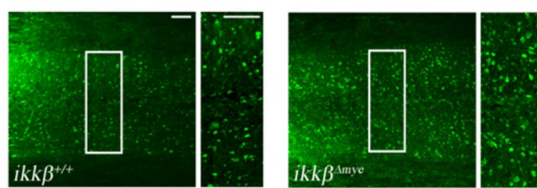


Figure 6. Apoptotic neuronal cell death was reduced in *ikkβ^{Δmye}* mice

(A) Spinal cord sections prepared 1 dpi were used for TUNEL (green) staining, and the same sections were used for anti-NeuN (red) immunostaining. DNA fragmentation in neurons was detected at the lesion boundary of *ikkβ^{+/+}* mice. Scale bar, 50 μm. Arrows indicate areas that are magnified at the right. A representative figure from three independent experiments is shown and the results were similar. Scale bar, 20 μm (B). (C) All TUNEL⁺ and NeuN⁺ cells in each section were counted and shown in a graph. Means ± SEM of three independent experiments are shown (**p*<0.005). (D) Spinal cord sections prepared 1 dpi were immunostained for active caspase-3 (red) and NeuN⁺ (green). Immunoreactivity of active caspase-3 was detected in NeuN⁺ cells in the sections of *ikkβ^{+/+}* mice. A representative figure from three independent experiments is shown and the results were similar. Scale bar, 20 μm.

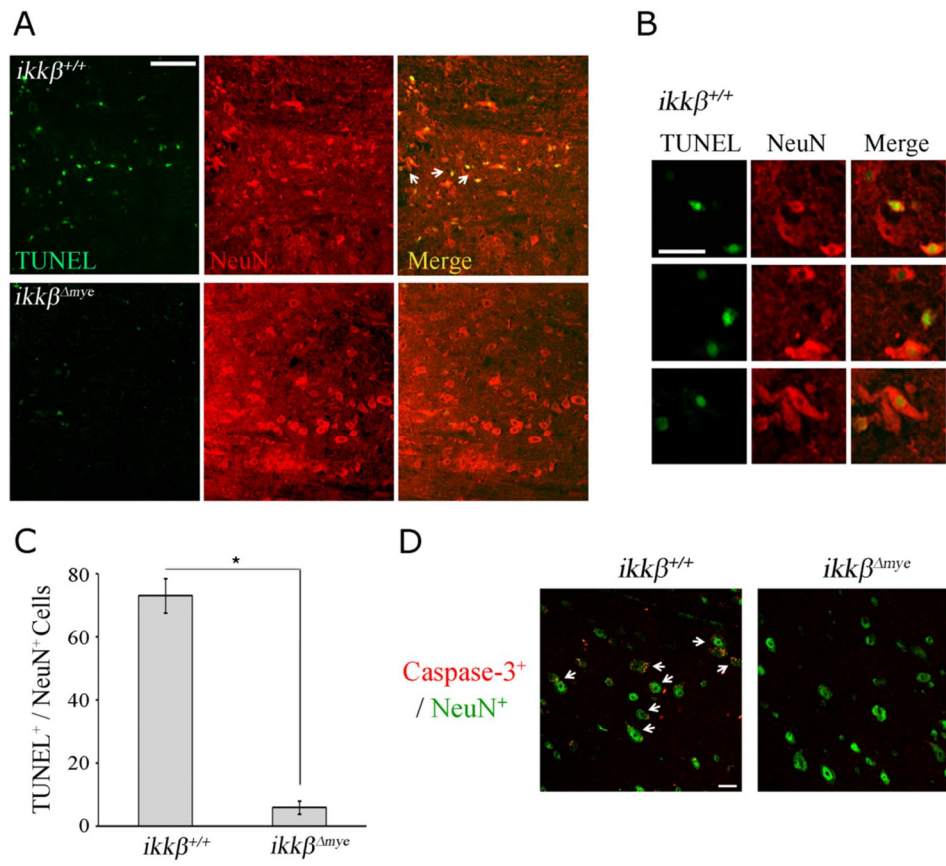


Figure 7. Improved functional recovery after SCI in $ikk\beta^{\Delta mye}$ mice

BMS tests were carried out in an open field over 28 days after SCI in $ikk\beta^{+/+}$ (n=5) and $ikk\beta^{\Delta mye}$ mice (n=6). $ikk\beta^{+/+}$ and $ikk\beta^{\Delta mye}$ mice exhibited initial impairments in hind limb locomotive performance followed by gradual recovery. The BMS scores of $ikk\beta^{\Delta mye}$ mice 7 dpi were significantly higher compared to the scores of $ikk\beta^{+/+}$ mice (* $p<0.05$, ** $p<0.01$, two-way ANOVA followed by Tukey's post-hoc test).

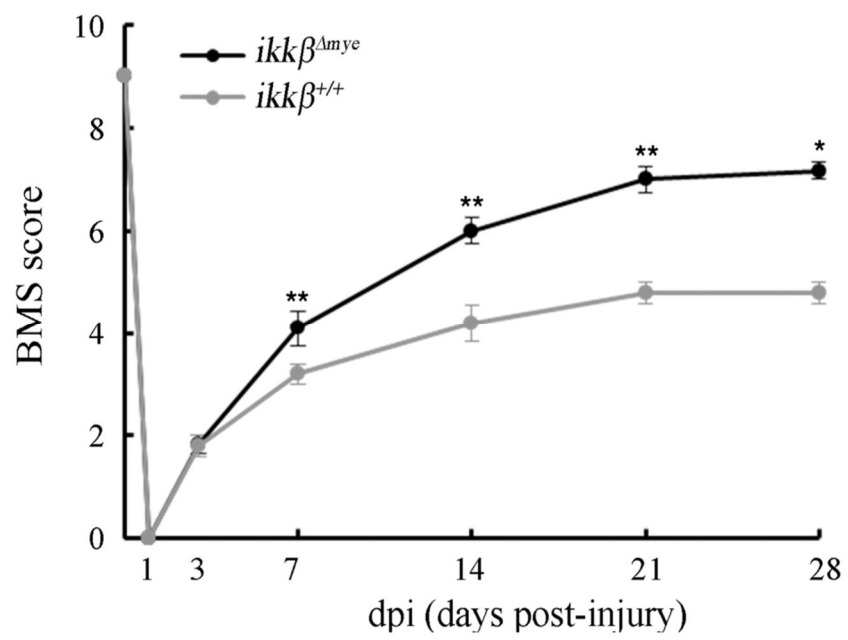


Figure 8. Expression of SCI-induced proinflammatory cytokines, iNOS and COX-2 was attenuated in *ikkβ^{Δmye}* mice

(A) Spinal cords of sham-operated and SCI-injured *ikkβ^{+/+}* and *ikkβ^{Δmye}* mice were isolated at 4 and 8 hour post-injury. Real-time RT-PCR measured IL-6, IL-1β, and TNF-α levels. Means ± SEM of three independent experiments are shown (**p*<0.05, ***p*<0.01). mRNA levels of iNOS (B) and COX-2 (C) in the spinal cord at different time points after SCI, as measured by real-time RT-PCR (**p*<0.05, ***p*<0.01). (D) Tyrosine nitrosylated-proteins in the injured spinal cords of *ikkβ^{+/+}* and *ikkβ^{Δmye}* mice were detected by immunostaining using anti-nitrotyrosine antibodies. Nitrotyrosine immunoreactivity was detected in cells surrounding the lesion site at 1 dpi in *ikkβ^{+/+}* mice. A representative figure from three independent experiments is shown and the results were similar. Scale bar, 20 μm. NT⁺ cells in each section were counted and shown in a graph. Means ± SEM of three independent experiments are shown (**p*<0.05). (E) DNA-damaged cells in the injured spinal cord were detected by immunostaining with anti-8-OHG antibodies. A representative figure from three independent experiments is shown and the results were similar. Scale bar, 50 μm. OHG⁺ cells in the 52250 μm² white rectangle area 300 μm caudal from the lesion site in the spinal cord were quantified. Six slides from three animals were counted, and the means ± SEM are presented (**p*<0.05). DNA-damaged cells increased in *ikkβ^{+/+}* mice at 1 dpi. Anti-nitrotyrosine and anti-8-OHG immunoreactivities were both significantly reduced in *ikkβ^{Δmye}* mice (D, E).

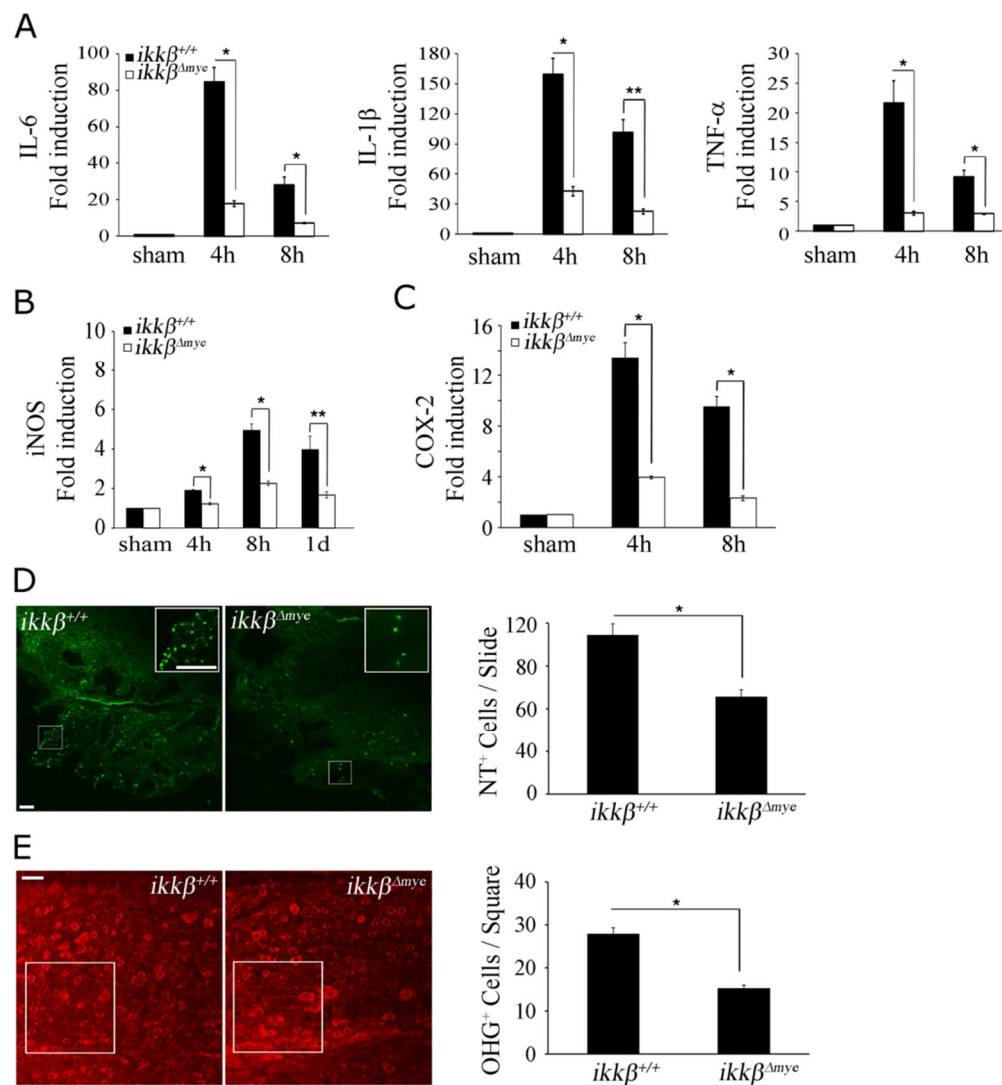


Figure 9. Localization of gelatinolytic activity in neurons and MMP expression after SCI

(A) Cryostat tissue sections at 6 hour post-SCI were used for *in situ* zymography (ISZ) and NeuN immunostaining. The number of cells with gelatinolytic activity was lower in $ikk\beta^{\Delta mye}$ mice (lower panels) than $ikk\beta^{+/+}$ mice (upper panels). A representative figure from three independent experiments is shown and the results were similar. Scale bar, 20 μ m. Gelatinolytic activity co-localized with NeuN⁺ neurons (A) but not Gr-1⁺ neutrophils (B). (C) MMP-9 mRNA was induced in the spinal cords of $ikk\beta^{+/+}$, but not $ikk\beta^{\Delta mye}$ mice. Real-time RT-PCR of MMP-9 from injured spinal cord tissue at 4 and 8 hour after injury. The data are means \pm SEM of three independent experiments (* p <0.05, ** p <0.05).

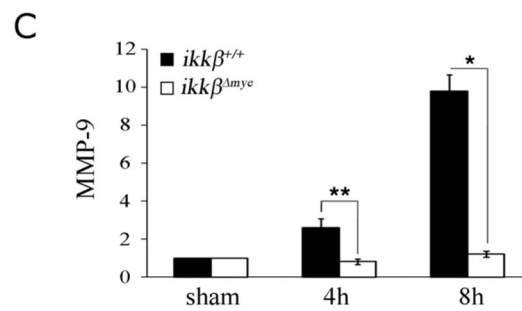
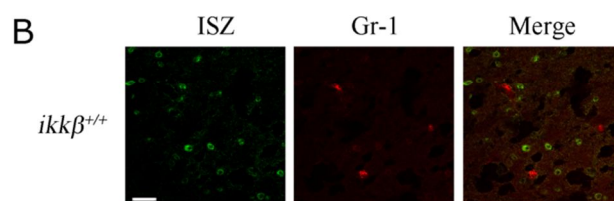
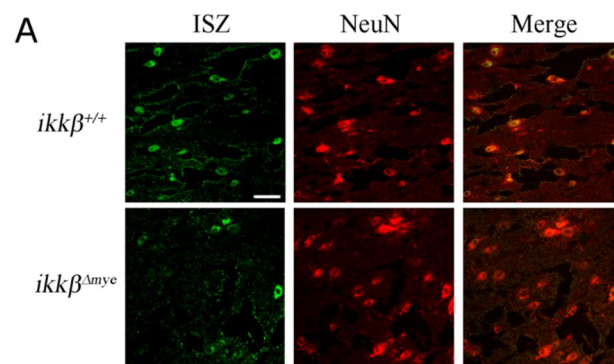


Table 3. The mouse primer sequences used for real-time RT-PCR

Genes	Forward primers	Reverse primers	GenBank No.
GAPDH	5'-AGG TCA TCC CAG AGC TGA ACG-3'	5'-CAC CCT GTT GCT GTA GCC GTA T-3'	NM_008084
IL-6	5'-GCC CTT CAG GAA CAG CTA TG-3'	5'-CAG AAT TGC CAT TGC ACA AC-3'	NM_012589
IL-1 β	5'-TTG TGG CTG TGG AGA AGC TGT-3'	5'-AAC GTC ACA CAC CAG CAG GTT-3'	NM_008361
TNF- α	5'-AGC AAA CCA CCA AGT GGA GGA-3'	5'-GCT GGC ACC ACT AGT TGG TTG T-3'	NM_013693
iNOS	5'-TCT GTG CCT TTG CTC ATG ACA-3'	5'-TGC TTC GAA CAT CGA ACG TC-3'	NM_012611
COX-2	5'- CAG TAT CAG AAC CGC ATT GCC-3'	5'- GAG CAA GTC CGT GTT CAA GGA-3'	U03389
CXCL1	5'-CCG AAG TCA TAG CCA CAC TCA A-3'	5'-GCA GTC TGT CTT CTT TCT CCG TTA C-3'	NM_008176
CXCL2	5'-AGA CAG AAG TCA TAG CCA CTC TCA AG-3'	5'-CCT CCT TTC CAG GTC AGT TAG C-3'	NM_009140
CXCR1	5'-CCG TCA TGG ATG TCT ACG TG-3'	5'- CAG CAG CAG GAT ACC ACT GA -3'	AY749637.1
CXCR2	5'-GGT GGG GAG TTC GTG TAG AA-3'	5'-CGA GGT GCT AGG ATT TGA GC-3'	BC051677.1
CD11a	5'-AGA TCG AGT CCG GAC CCA CAG-3'	5'-GGC AGT GAT AGA GGC CTC-3'	NM_008400.2
CCL2	5'-TCA GCC AGA TGC AGT TAA CG-3'	5'-GAT CCT CTT GTA GCT CTC CAG C-3'	BC05507
CCL3	5'- ACT GCC TGC TGC TTC TCC TAC A -3'	5'- AGG AAAATG ACA CCT GGC TGG-3'	BC111443
CCL4	5'-TCC CAC TTC CTG CTG TTT CTC T-3'	5'-GAA TAC CAC AGC TGG CTT GGA-3'	NM_013652.2
MMP-9	5'-TGT ACG GAC CCG AAG C-3'	5'-CCG TCC TTA TCG TAG TCA G-3'	NM_013599

DISCUSSION

In this study, I tested the *in vivo* role of IKK β activation in neutrophils responding to SCI. Previously, conflicting results suggested both beneficial and detrimental roles of neutrophil activation and infiltration after SCI. My results showing that ablating IKK β reduced morphological and behavioral deficits after SCI are consistent with previous studies that suggest a detrimental role for neutrophils in SCI secondary damage. My study is distinct from a recent study that used a Ly6G/Gr-1 antibody to deplete blood neutrophils (Stirling et al., 2009). In that study, Gr-1⁺ cells consisting of mainly, but not exclusively, neutrophils were depleted from the circulatory system. In contrast, *ikk β ^{Amye}* mice did not lose blood neutrophils (data not shown), and only IKK/NF- κ B-mediated responses were compromised. Although it is speculative, neutrophils in a resting state might possibly have a neuroprotective role, so depleting the total neutrophil population worsens the neurological outcome after SCI. In contrast, my system specifically addressed the *in vivo* role of neutrophil activation after SCI and demonstrated that neutrophil activation and infiltration to injured spinal cords at an early time point contributed to SCI secondary damage.

In *ikk β ^{Amye}* mice, the IKK β gene was deleted not only in neutrophils but also in a majority of monocytes/macrophages. Therefore, the phenotype observed in these mice cannot be attributed solely to IKK β deficiency in neutrophils. In this study, however, leukocytes infiltrating the lesion at early time points were mostly neutrophils, and I did not detect any macrophage infiltration within 1 dpi. Neuronal apoptosis was clear at 1 dpi in *ikk β ^{+/+}* but not

ikkβ^{Amve} mice. These findings argue that the early effects on neuronal apoptosis were most likely due to neutrophil activation and infiltration, not macrophages. Therefore, I deduced that IKKβ-dependent neutrophil activation contributed to neuronal damage at early time points. Macrophage infiltration was also reduced in *ikkβ^{Amve}* mice at later time points. Therefore, the relative improvement in behavioral recovery observed in *ikkβ^{Amve}* mice cannot be totally attributed to inhibiting neutrophil activation and infiltration. Rather, it might be the result of combined neutrophil and macrophage activation. Thus far, I have not been able to dissect the relative contributions of each cell type to behavioral deficits. In addition, an approximately 50% reduction in neuronal cell number was observed in the injured spinal cords of *ikkβ^{Amve}* mice compared to sham-operated mice, as measured by NeuN-immunostaining, but very few TUNEL-positive cells were detected in *ikkβ^{Amve}* mice at 1 dpi. These data imply that neuronal cells also underwent non-apoptotic cell death in these mice, and this cell death was not much affected by neutrophil infiltration and activation.

To elucidate the molecular mechanisms underlying the reduced neutrophil and macrophage infiltrations in *ikkβ^{Amve}* mice, I tested the innate migratory activities of neutrophils and monocytes from *ikkβ^{Amve}* mice. My data showed that IKKβ deficiency did not alter the migratory activities of these cells. Therefore, neutrophil- and macrophage-recruitment are more likely impaired in *ikkβ^{Amve}* mice due to defective production of neutrophil- and macrophage-attracting chemokines after SCI. Indeed I found that SCI-induced CXCL1 expression is severely compromised in *ikkβ^{Amve}* mice and LPS-mediated CXCL1 expression *in vitro* was eliminated in *ikkβ^{Amve}* neutrophils. Based on these data, I speculated that neutrophils that initially infiltrated the spinal cord

of injured $ikk\beta^{Amye}$ mice did not express CXCL1, so they did not further augment neutrophil infiltration. This might explain the observed differences in post-SCI neutrophil infiltration rate between $ikk\beta^{+/+}$ and $ikk\beta^{Amye}$ mice.

I also found that the expression levels of proinflammatory cytokines (IL-1 β , IL-6, and TNF- α), iNOS, COX-2, and MMP-9 were lower in the injured spinal cords of $ikk\beta^{Amye}$ mice than in $ikk\beta^{+/+}$ mice. All of these proinflammatory cytokines are implicated in neuronal apoptosis (Liu et al., 2008). NO and prostaglandin E (PGE), which are produced by iNOS and COX-2, respectively, induce neuronal apoptosis by nitrotyrosylation of proteins or DNA damage (Tuna et al., 2001; Nguyen et al., 2007). I found reduced nitrotyrosylation and DNA damage in the injured spinal cords of $ikk\beta^{Amye}$ mice compared to $ikk\beta^{+/+}$ mice. In addition, neuronal gelatinase activation was attenuated in $ikk\beta^{Amye}$ mice, probably because of the combined effects of reduced MMP-9 expression and MMP-9 nitrotyrosylation. MMP-9 activation is a key event in neuronal apoptosis (Yu et al., 2008), although the underlying molecular mechanisms are not completely understood. My data imply that reduced proinflammatory cytokines, NO and PGE in $ikk\beta^{Amye}$ mice might contribute to reduced neuronal apoptosis at 1 dpi. Again, since IKK β is deficient only in neutrophils and macrophages, and only neutrophils infiltrate at 1 dpi, the differences in the above genes are likely in neutrophils. This is supported by *in vitro* studies using neutrophils cultured from $ikk\beta^{+/+}$ and $ikk\beta^{Amye}$ mice. Of note, I found that LPS-induced inflammatory gene expression was completely blocked in $ikk\beta^{Amye}$ neutrophils, although expression of these genes was only partially reduced *in vivo*. This implies that cells other than the tissue-infiltrating neutrophils express these genes in the spinal cord after SCI,

although I did not demonstrate this experimentally.

In conclusion, the results of my study demonstrate that IKK β -dependent neutrophil activation and infiltration in the injured spinal cord potentiated inflammation and neuronal damage and impeded functional recovery after SCI.

CHAPTER 2

**Toll-like receptor 3 signaling inhibits
astrocyte MMP-2 activation and recovery
from spinal cord injury**

INTRODUCTION

Spinal cord injury (SCI) causes neuronal damage, consecutive inflammatory processes, and glial scar formation. Once the spinal cord is injured, the damaged axons begin to sprout and attempt to extend across the lesion site. However, the glial scar hinders these axonal extensions and regenerations (Yiu and Zhigang, 2006). The glial scar is comprised mostly of reactive astrocytes, which become hypertrophic and intensely increase the expression of glial fibrillary acidic protein (GFAP), the major protein constituent of glial intermediate filaments (Fitch and Silver, 2008). During the process of gliosis in glial scar formation, reactive astrocytes express and secrete chondroitin sulfate proteoglycans (CSPGs), such as neurocan, versican, aggrecan, brevican and phosphacan, in and around the lesion site (Stallcup and Beasly, 1987; McKeon et al., 1999; Jones et al., 2003; Buss et al., 2009). Generally, CSPGs play a repulsive role in axon guidance and act as a barrier that inhibits the regeneration of damaged neuronal axons. However, according to a recent report (Rolls et al., 2008), CSPGs do not always have a detrimental role. Within 2 days post-injury (dpi), CSPGs modulate microglia/macrophage activation and limit the spread of damage by creating a physical barrier. Therefore, CSPG degradation is an important aspect of axon regeneration at later time points after SCI.

Matrix metalloproteinases (MMPs) are well known as secreted or membrane-bounded mammalian zinc endopeptidases that can degrade the extracellular matrix and other extracellular proteins (Sternlicht and Werb, 2001; Wells et al., 2003; Agrawal et al., 2008). In the injured spinal cord, MMP-9 and MMP-2 are up-regulated. After SCI, MMP-9 activity maximizes in 12-24 hours

while MMP-2 activity increases after 5 days in the injured spinal cord. (de Castro et al., 2000). MMP-9 plays a key role in abnormal vascular permeability and inflammation within the first 3 dpi (Noble et al., 2002). Likewise, MMP-9 and MMP-2 are capable of degrading and inactivating CSPGs (Zuo et al., 1998; Ferguson and Muir, 2000). Moreover, MMP-2 is preferentially expressed during reactive gliosis and modulates wound healing after SCI (Hsu et al., 2006).

It has been suggested that toll-like receptor 3 (TLR3) plays a key role in the innate immune system and is a major mediator of inflammation in response to dsRNA from viral infections and cellular damage (Sen and Sarkar, 2005). Although TLR3 is expressed in several cell types, the actual roles of TLR3 are still unclear in viral or cellular inflammatory circumstances (Bsibsi et al., 2006; Cameron et al., 2007; Murray et al., 2008). According to previous reports, TLR3 triggers antiviral defenses against infection and neuroprotective responses that release anti-inflammatory cytokines (Bsibsi et al., 2006; Negishi et al., 2008). On the other hand, TLR3 has a deleterious role during hypoxia-induced acute lung injury and West-Nile virus infection (Wang et al., 2004; Murray et al., 2008). Recently, it has been reported that TLR3-induced microglia activation contributes to neuropathic pain after nerve injury (Mei et al., 2011). However, there have been no reports on the role of TLR3 in SCI. In the present study, the *in vivo* role of TLR3 involved in the inflammatory responses after SCI was elucidated using TLR3 knockout mice.

MATERIALS AND METHODS

Mice and spinal cord injury

TLR3 knockout mice on a C57BL/6 background provided by Dr. Flavell (Alexopoulou et al., 2001) and the wild-type (C57BL/6) mice purchased from Koatech (Pyeongtaek, Korea) were housed at $23 \pm 2^{\circ}\text{C}$ with a 12 hour light-dark cycle and fed food and water *ad libitum*. All surgical and experimental procedures were reviewed and approved by the Institutional Animal Care and /Use Committee (IACUC) at Seoul National University. Adult male mice (8-10 weeks old) were anesthetized with sodium pentobarbital (30 mg/kg body weight, i.p.) and laminectomized between T8 and T10. The exposed spinal cord was subjected to crush injury at the T9 level with number 5 Dumont forceps ground down to a tip width of 0.5 mm. The forceps I used in this report were modified with a spacer so that at maximal closure a 1 mm space remained to make incomplete lesion (Faulkner et al., 2004). The spinal cord was compressed with the forceps laterally from both sides for 10 sec. Laminectomized mice without compression were used as controls.

Behavioral tests

Hind limb motor function was assessed by open field locomotion using the Basso Mouse Scale (Basso et al., 1996; Basso et al., 2006). Before and after SCI, the locomotive activity of each mouse was graded on a 10-point scale (scores 0-9) designed to assess hind limb locomotion recovery by evaluating hind limb joint movements, stepping, trunk position and stability, forelimb-hind

limb coordination, paw placement, and tail position. A score of 0 indicated no observable hind limb movement; a score of 9 represented normal locomotion.

Cresyl violet staining/Luxol Fast Blue (LFB) staining and volume measurement

Cresyl violet (ICN Biomedicals, Aurora, OH, USA) staining (0.5% in ddH₂O) for 15 min was performed on a series of longitudinal sections of injured spinal cord at 35 dpi. And then differentiation carried out by incubating sections in 70% EtOH. LFB staining was performed as reported (Brechtel et al., 2006). Briefly, longitudinal sections of injured spinal cord at 5 dpi and 35 dpi were stained with 0.1% LFB (Sigma, St. Louise, MO, USA) in acidified 95% ethanol for overnight at 56°C. Differentiation and counterstaining were carried out by incubating sections in 0.05% lithium carbonate solution.

Images of the stained sections were taken under the microscope (Axiovert200, Carl Zeiss, Munich, Germany) using a lens with a 2.5 X 10 (objective X eye piece), and then lesion size (x-y stage) was calculated using Axiovision 4.8 image program. The total lesion volume was calculated by summing their individual subvolumes using Cavalieri method (Michel and Cruz-Orive, 1988; Oorschot, 1994). Individual subvolumes of lesion area were calculated by multiplying the longitudinal-sectional area (S) and the distance between sections (10 µm). Each measurement value was calculated by one-way ANOVA followed by Tukey's post-hoc test.

Immunohistochemistry

The mice were anesthetized with Avertin (2-2-2 tribromoethanol) and perfused with 0.1 M phosphate-buffered saline (PBS), followed by 4%

paraformaldehyde in 0.1 M PBS. A 1-cm tissue block containing the injury site was collected, post-fixed in the same fixative overnight at 4°C, and cryoprotected in 30% sucrose in 0.1 M phosphate buffer. The spinal cord was cryo-cut to 16 µm in the horizontal and coronal plane and was placed onto gelatin-coated glass slides. Sections were blocked in the blocking solution (5% normal goat serum, 5% FBS, 2% BSA, and 0.1% Triton X-100) for 1 hour at RT and incubated overnight at 4°C with mouse anti-NF200 (1:500; Chemicon, Temecula, CA, USA), rabbit anti-TLR3 (1:100; IMGENEX, San Diego, CA, USA), rabbit anti-MMP-2 (1:500; Millipore, Temecula, CA, USA), rabbit anti-GFAP (1:1000; DAKO, Glostrup, Denmark) for astrocytes, mouse anti-adenomatous polyposis coli (APC, 1:100; Oncogene Science, Cambridge, MA, USA) for mature oligodendrocytes, mouse anti-CS-56 (1:200; Sigma) for CSPGs. After three washes in 0.1 M PBS plus 0.1% Triton X-100 for 10 min at RT, tissue sections were incubated with Cy3- or FITC-conjugated secondary antibodies (1:200; Jackson ImmunoResearch, West Grove, PA, USA) for 1 hour at RT. Sections were mounted with Vectashield (Vector Labs, Burlingame, CA, USA) and examined using a fluorescent microscope (LSM 5 PASCAL; Carl Zeiss).

Biotinylated dextran amine injection and tissue processing

To trace the corticospinal tract, the biotinylated dextran amine (BDA; Molecular Probes, Eugene, OR, USA; 10% solution in dissolved in 0.1 M PBS) tracer was injected into the right sensorimotor cortex. Mice (8-12 week-old male, 22-25 g) were anesthetized by sodium pentobarbital (30 mg/kg, body weight, i.p.), placed on a stereotaxic apparatus (myNeuroLab, St. Louis, MO, USA), and injected with 0.4 µl BDA at the speed of 0.1 µl/min into the left

cortex (stereotaxic coordinates in mm with reference to bregma: AP 1.0/1.5, 0.5/1.5, -0.5/1.5, -1.0/1.5, all at a depth of 0.5 mm into cortex) using a 30-G needle. After 5 min, the needle was removed in three intermediate steps for 3 min to minimize backflow. The incision was cleaned with the saline and sutured. Mice were kept for an additional 2 weeks before being killed. Mice deeply anesthetized with the sodium pentobarbital were perfused intracardially with the saline followed by cold 4% PFA in 0.1 M phosphate buffer at the indicated time after the surgery. The spinal cord were isolated, post-fixed overnight in the same fixative at 4°C, rinsed twice with PBS and placed in 30% sucrose in PBS for 2 days at 4°C. The spinal cords were then frozen and cryo-cut to 16 μ m in serial longitudinal sections on a cryostat (CM3050S, Leica, Solms, Germany). BDA immunostaining of tissue sections were carried out with fluorescently labeled Cy3-streptavidin (1:200; Jackson ImmunoResearch). Sections were mounted with Vectashield (Vector Labs) and examined using a fluorescent microscope (LSM 5 PASCAL; Carl Zeiss).

Primary astrocyte cell cultures

Primary murine microglial cultures were obtained from 1 to 3 day-old TLR3 knockout and C57BL/6 mice, as previously described (Giulian and Baker, 1986). Briefly, the cerebral cortices were dissected, carefully stripped of the meninges of brain, and triturated into single cells using a syringe with 18-G needle. The digested fraction was pelleted and resuspended in culture media [Dulbecco's modified Eagle's medium (JBI, Daejeon, Korea) supplemented with 10% fetal bovine serum (JBI) and 1% penicillin/streptomycin (Gibco, Grand Island, NY, USA)] and plated in 75-cm² T-flasks. Cultures were maintained in a 5% CO₂ incubator at 37°C and the media were changed every 1 week with

DMEM containing 5% FBS. After 2 weeks, to remove microglia, mixed glia were incubated with 60 mM L-Leucine methylether (L-LME; Sigma) for 90 min (Hamby et al., 1986), And then the media were freshly changed and the cells were stabilized for overnight in the 5% CO₂ incubator at 37°C. For harvesting more pure astrocytes, the cells were trypsinized with 0.25% trypsin for 5 min and detached by pipetting and then were left in the 5% CO₂ incubator for 30 min. Floating astrocytes were collected with the media and then seeded on 6-well plates for the experiments.

Real-time PCR

Total RNA from the isolated spinal cord tissue and the cells was extracted using Trizol (Invitrogen, Carlsbad, CA, USA) and reverse transcribed using M-MLV Reverse Transcriptase (Invitrogen). Real-time PCR was performed using a 7500 Real-Time PCR system (Applied Biosystems, Foster City, CA, USA) as previously described (Li et al., 2003). Relative mRNA levels were calculated according to the $2^{-\Delta\Delta C_t}$ method (Livak and Schmittgen, 2001). All ΔC_t values were normalized to GAPDH. All experiments were performed at least three times. The PCR primer sequences used in this study are listed in Table 4.

Gelatin gel zymography

To detect the gelatinolytic activity of MMP, the samples were evaluated by gelatin zymography. Spinal cord tissues (0.5 cm) were homogenized in a lysis buffer (50 mM Tris-HCl (pH 8.0), 150 mM NaCl, 1% NP40, 0.5% deoxycholate, 0.1 % sodium dodecyl sulfate (SDS) and proteinase

inhibitors (1 mM PMSF, 1 μ g/ml apolipoprotein and 10 μ g/ml leupeptin)). And then the tissue homogenates were incubated for 20 min at 4°C, and centrifuged at 25,000 \times g for 30 min at 4°C. The protein level of the supernatant was determined using the BCA assay (Pierce, Rockford, IL, USA). Under the nonreducing conditions, 50 μ g samples were subjected to the SDS–polyacrylamide gel electrophoresis (PAGE) in 10% acrylamide gels containing 0.1 mg/ml gelatin (gelatin monomer; Serva Feinbiochemica GmbH & Co., Heidelberg, Germany). After electrophoresis, the gels were washed in 2.5% Triton X-100 for 30 min at RT to remove all trace of SDS and washed in the developing buffer (50 mM Tris–HCl (pH 8.5), 5 mM CaCl₂, 0.2 M NaCl, and 0.02% Brij 35) for 30 min at RT. And then the gels were exchanged with the new developing buffer and incubated for 24 hours at 37°C. Following incubation, the gels were stained with 0.5% Coomassie brilliant blue R-250 (Sigma) for 24 hours and destained until the clear bands were appeared. Gelatin digestion was identified as a clear lytic zone against a blue background.

***In vitro* MMP assay**

The mixture of 40 μ g spinal cord tissue and 3 μ g recombinant CSPG (Millipore) with the developing buffer was incubated for 4 hours at 37°C. The reaction was stopped with 2X SDS sample buffer (60 mM Tris–Cl (pH 6.8), 2% SDS, 10% glycerol, 5% β -mercaptoethanol and 0.01% bromophenol blue) and boiled for 3 min. The reaction samples were electrophoresed on 10% SDS–PAGE and underwent the western blotting. Degraded CSPGs after the reaction were detected with anti-CS-56 antibody.

To inhibit the activity of MMP-2, the MMP-2 inhibitor I (Calbiochem, La Jolla, CA, USA) was used. Before adding the tissue sample, CSPGs were

mixed with the MMP-2 inhibitor I. As a loading control, β -actin was analyzed by western blot.

Fluorescence activated cell sorting (FACS) assay

All procedures were performed on ice to minimize the *in vitro* expression of surface molecules (Forsyth and Levinsky, 1990). Spinal cord tissue (± 0.25 cm from the injury site) was dissected from the injured spinal cord and placed immediately in ice-cold FACS buffer (0.1 M PBS (pH 7.4) and 2% FBS). The cells were isolated by homogenization and filtration, and then the cells were fixed with 1 ml 2% paraformaldehyde in 0.1 M PBS for 15 min. After three washes with 1 ml FACS buffer, the cells were incubated with primary antibody for 1 hour, followed by washing. The cells were analyzed with a BD FACSCaliburTM flow cytometer (Becton Dickinson, San Jose, CA, USA) and CellQuest software. To analyze spinal cord-infiltrating leukocytes, the cells were incubated in FITC-conjugated anti-Gr-1 antibodies (BioLegend, San Diego, CA, USA) and Cy5.5-conjugated anti-CXCR2 antibodies (BioLegend) in 2,500 gates of infiltrated neutrophils by 1 dpi. Infiltrated macrophages (CD11b⁺-FITC (BD Pharmingen, San Diego, CA, USA)/CD45^{high}-PE (BD Pharmingen)) or microglia (CD11b⁺-FITC/CD45^{low}-PE) were analyzed at 5 dpi.

Statistical analysis

Data were presented as mean \pm SEM. Statistical analysis for real time PCR data, gel zymography and image analysis were performed using a one-way ANOVA analysis of variance for measurements, followed by independent *t* or Tukey's post hoc test for comparisons procedures. A *p* < 0.05 was considered to

be statistically significant. Statistical analysis for motor behavioral tests was performed using two-way ANOVA analysis of variance for measurements, followed by Tukey's post hoc test ($p < 0.05$) for comparison procedures.

RESULTS

Functional recovery is enhanced in TLR3 knockout mice after SCI

To investigate whether TLR3 signaling is involved in the behavioral recovery after SCI, the Basso Mouse Scale (BMS) test was performed for 35 dpi (Fig. 1) using the TLR3 knockout mice. Up to 7 dpi, no difference in motor function was observed between the wild-type and TLR3 knockout mice. After 14 dpi, the average BMS score of the TLR3 knockout mice was higher than the wild-type mice. The behavioral score of the wild-type mice over 28 dpi began to plateau below the BMS score of 2.0, whereas the recovery of the TLR3 knockout mice continuously increased up to the score of 4.2. In addition, the TLR3 knockout mice could support their weight using their hind limbs while the wild-type mice could not support their weight. These behavioral results suggested that TLR3 signaling has a negative effect on behavioral recovery after SCI. Next, I examined the lesion volume and axon demyelination of injured spinal cord from the mice that had undergone the BMS test (Fig. 2). The lesion volume was assessed by cresyl violet and the extent of axon demyelination was measured by LFB staining. The lesion volume in TLR3 knockout mice was 38% less than that in the wild-type mice at 35 dpi (Fig. 2A and B). Consistent with the data on the lesion volume, the extent of axon demyelination was significantly attenuated in the TLR3 knockout mice compared to the wild-type mice (36.4% vs. 64.5%). At 5 dpi, however, axon demyelination was not different between the wild-type and TLR3 knockout

mice (Fig. 2C and D). These data suggest that the TLR3 deficiency not only ameliorates functional recovery but also decreases lesion volume and axon demyelination.

Neuronal axon regeneration is enhanced in TLR3 knockout mice after SCI

From the results of the above mentioned data, TLR3 could have effects on SCI-induced axon loss and/or axon regeneration which occurs at some later time rather than during or right after SCI. Then, to confirm whether the deficiency of TLR3 is associated with axon loss and/or axon regeneration, immunohistochemistry against NF200 and biotinylated dextran amines (BDA), an anterograde tracer, were used (Fig. 3). The dot signals of anti-NF200 staining apart from the 600 μ m caudal to the injury site were verified. As shown in figure 3A and B, the rectangular area within the region passing by vestibulospinal tract was counted (Yune et al., 2007). The NF200 positive-dot signals were significantly more numerous in the TLR3 knockout mice than in the wild-type mice (299.3 vs. 223.5). However, when compared to the intact spinal cord, the NF200 positive signals were considerably reduced (intact tissue: 375.5). At 5 dpi, the NF200 positive signals were indistinguishable in the wild-type and TLR3 knockout mice. Next, whether any axons in the corticospinal tract (CST), which is representatively involved in fine motor function, are spared after SCI was confirmed. Regenerated axons in the CST were evaluated by an anterograde tracer, BDA, with injection into the sensorimotor cortex at 10 dpi (Fig. 3C). In wild-type mice, no BDA signals passing through the lesion site could be detected. However, BDA positive signals, appearing as thin lines

shown in the enlarged rectangular figures, were detected in the caudal part over the lesion site of the TLR3 knockout mice. Moreover, if spinal cord surgery and BDA injection were implemented at the same time, no BDA-stained signal in the caudal part over the lesion site in both groups could be detected (data not shown). Taken together, these findings suggest that the TLR3 deficiency effects on enhancing axon regeneration and attenuating axon loss after SCI.

TLR3 is expressed in astrocytes and oligodendrocytes after SCI

To determine the changes in TLR3 expression levels after SCI, the TLR3 mRNA transcript levels were assessed in the injured spinal cord at various time points in wild-type and TLR3 knockout mice. TLR3 expression continuously increased by 17-fold until 1 dpi and then decreased at 5 dpi in the wild-type mice (Fig. 4A). However, the expression level did not change in the TLR3 knockout mice.

Generally, TLR3 is a major mediator in the immune response to viral infections and cellular damage (Sen and Sarkar, 2005). Thus, whether TLR3 is associated with inflammation due to injury was tested. It was confirmed by flow cytometry that the infiltration and activation of neutrophils at 1 dpi and of monocytes/macrophages at 5 dpi were no differences between wild-type and TLR3 knockout mice (Fig. 4B and C). Next, based on my lab report that TLR3 is expressed in astrocytes of the septum and hippocampus after injecting poly(I:C) (Park et al., 2007), immunostaining was performed with anti-TLR3 antibody and anti-GFAP antibody for astrocytes or anti-adenomatous polyposis coli (APC) antibody for oligodendrocytes in injured spinal cord tissue at 5 dpi. As shown in figure 4D, TLR3 was expressed in astrocytes which were detected in the white matter (b) and gray matter (a) surrounding the area of the lesion. In

addition, TLR3 was expressed in oligodendrocytes, which were detected in the white matter on the margin of the lesion site (c). These data show that TLR3 is induced and expressed in astrocytes and oligodendrocytes after SCI.

Astrocyte activation and CSPGs production due to SCI are reduced in TLR3 knockout mice

During the process of scar formation after CNS injury, activated astrocytes upregulate the production of chondroitin sulfate proteoglycans (CSPGs), which are neurite-outgrowth inhibitory molecules (Yiu and Zhigang, 2006). Therefore, whether TLR3 affects the level of CSPGs was investigated next. First, the level of astrocyte activation was determined in the wild-type and TLR3 knockout mice by immunostaining with anti-GFAP antibody at 14 dpi, which was when time differences started appearing between the groups in the BMS scores (Fig. 5A). Activated GFAP⁺-astrocytes were mainly detected in the wound periphery and were enlarged in the white rectangular area of the rostral part of the injury site. GFAP⁺-astrocytes were decreased in the TLR3 knockout mice compared to the wild-type mice at 14 dpi. Next, the levels of CSPGs were determined at 35 dpi, the last day of the BMS test (Fig. 5B). CSPGs were identified by immunostaining using the anti-CS-56 antibody. Unlike GFAP signal, CS-56-positive CSPGs immunoreactivity (IR) was detected at the center of the injured lesion. CSPG IR intensity was decreased by 15.7% in the TLR3 knockout mice compared to the wild-type mice. These results suggest that TLR3 deficiency reduces the scar formation by reactive astrocyte and the deposition of CSPGs in the injured spinal cord.

Among the CSPG family members, aggrecan, neurocan, versican and phosphacan are expressed and released from astrocytes (Jones et al., 2003;

Afshari et al., 2010). Whether the transcript levels of these 4 members were altered between the wild-type and TLR3 knockout mice after SCI was determined (Fig. 5C). Neurocan and versican transcripts were increased at 1 dpi and 5 dpi in the wild-type mice, while aggrecan and phosphacan transcripts were not significantly different from those of the laminectomized spinal cord. However, the change in transcripts for the 4 members had a similar pattern after SCI between the wild-type and TLR3 knockout mice (2.65 vs. 2.66 at 1 dpi and 2.32 vs. 2.48 at 5 dpi for neurocan; 2.41 vs. 2.84 at 1 dpi and 4.77 vs. 4.81 at 5 dpi for versican). These data show that the lack of TLR3 has no relevant effect on the transcription process of CSPGs after SCI.

SCI-mediated MMP-2 expression and activation were increased in TLR3 knockout mice

Since the level of CSPG transcripts did not differ between the two groups, the change in expression and activity of CSPG-degrading enzymes after SCI between wild-type and TLR3 knockout mice was determined next. As reported, MMP-2 and MMP-9 are endogenous proteolytic enzymes that can degrade CSPGs and contribute to the growth properties of degenerated nerves (Zuo et al., 1998; Ferguson and Muir, 2000). The mRNA expression levels of MMP-2 and MMP-9 from the injured spinal cord were measured using RT-PCR (Fig. 6A). At 5 dpi, MMP-2 expression level was increased slightly by 2.2-fold in the wild-type mice; however, the transcripts were significantly increased by 4.9-fold in the TLR3 knockout mice. Whereas, induction of the MMP-9 expression began at 4 hour (5.7 vs. 5.3; WT vs. KO) and reached maximum expression at 8 hour (11.13 vs. 11.38). Contrary to the MMP-2 mRNA, the MMP-9 transcript level had no significant difference between the

wild-type and TLR3 knockout mice. Further, the pro- and active forms of MMP-2 and MMP-9 in the injured spinal cord were verified using gelatin zymography (Fig. 6B). The pro-form of MMP-9 was significantly increased at 1 dpi but decreased further at 5 dpi and 10 dpi. The level of MMP-9 protein, similar to the data for previous mRNA levels, showed no difference between the wild-type and TLR3 knockout mice for each time point. On the other hand, the pro- and active forms of MMP-2 were observed at very low levels at 1 dpi but had more increased levels at 5 dpi in the TLR3 knockout mice than that of the wild-type mice. Taken together, these data suggest that TLR3 deficiency has an effect on increasing the expression of MMP-2, which could play a role in degrading CSPGs in the injured spinal cord.

CSPGs are degraded by MMP-2 in astrocytes

To confirm whether CSPGs are degraded by MMP-2 in the injured spinal cord, an *in vitro* assay with recombinant CSPGs and tissue from an injured spinal cord was carried out (Fig. 6C). Since the molecular weight of the CSPGs is high, non-degraded CSPGs could not be detected on the blot. After incubation with recombinant CSPGs and uninjured-spinal cord tissue lysate, no degraded CSPG bands could be detected. However, CSPG degradation bands increased after the incubation with injured-spinal cord tissue lysate in which MMP-2 was upregulated. Moreover, using the injured-spinal cord lysate of the TLR3 knockout mice, CSPG degradation was more increased compared to that of the wild-type mice. Further, to show that MMP-2 is responsible for the CSPG degradation, samples were treated with an inhibitor for MMP-2. The inhibition of MMP-2 significantly reduced the CSPG degradation. These results indicate that MMP-2 induced after SCI degrades CSPGs, which is attenuated in

the TLR3 knockout mice. Next, the kinds of cells that express MMP-2 in the injured spinal cord were investigated with immunostaining (Fig. 6D). MMP-2-positive signals were detected in GFAP⁺-cells on the lesion periphery at 10 dpi in the TLR3 knockout mice demonstrating that MMP-2 is upregulated in astrocytes after SCI.

TLR3 signaling inhibits MMP-2 expression in astrocytes

To determine whether MMP-2 expression is affected by TLR3 directly, an *in vitro* assay was done by inducing MMP-2 expression in cultured astrocytes. According to a previous study (Overall et al., 1991), MMP-2 expression was induced by transforming growth factor-beta 1 (TGF- β 1) in human fibroblast. After traumatic SCI, TGF- β 1 expression was increased in the injured spinal cord (Fig. 7A) implicating TGF- β 1 as an activator of MMP-2 expression in the injured spinal cord. In this regards, whether MMP-2 expression is induced in cultured astrocytes by TGF- β 1 was tested. TGF- β 1 stimulation for 6 hours increased the MMP-2 transcript levels in the wild-type mice as expected. Interestingly, the induction of MMP-2 was more significantly increased in the TLR3 knockout mice (4.4-fold vs. 8.0-fold) (Fig. 7B). Therefore, whether MMP-2 expression is affected by TLR3 stimulation with polyinosine-polycytidylic acid (poly(I:C)), in cultured astrocytes from the wild-type mice was investigated (Fig. 7C and D). The MMP-2 transcript level was diminished by stimulation with poly(I:C) by 40%. In addition, TGF- β 1-induced MMP-2 expression was reduced after treatment with poly(I:C) in cultured astrocytes from wild-type mice (4.3-fold vs 2.7-fold; a decrease of 23.5%). Taken together, these results suggest that TLR3 signaling directly inhibits MMP-2 expression in astrocytes.

Figure 1. Improved functional recovery after SCI in TLR3 knockout mice

BMS tests were carried out in an open field over 35 dpi in wild-type mice (n=5) and TLR3 knockout mice (n=5). Wild-type and TLR3 knockout mice exhibited initial impairments by 7 dpi in hind limb locomotive performance followed by gradual recovery. The BMS scores of the TLR3 knockout mice at 14 dpi were significantly higher compared to the scores of the wild-type mice (* $p < 0.05$, two-way ANOVA followed by Tukey's post-hoc test).

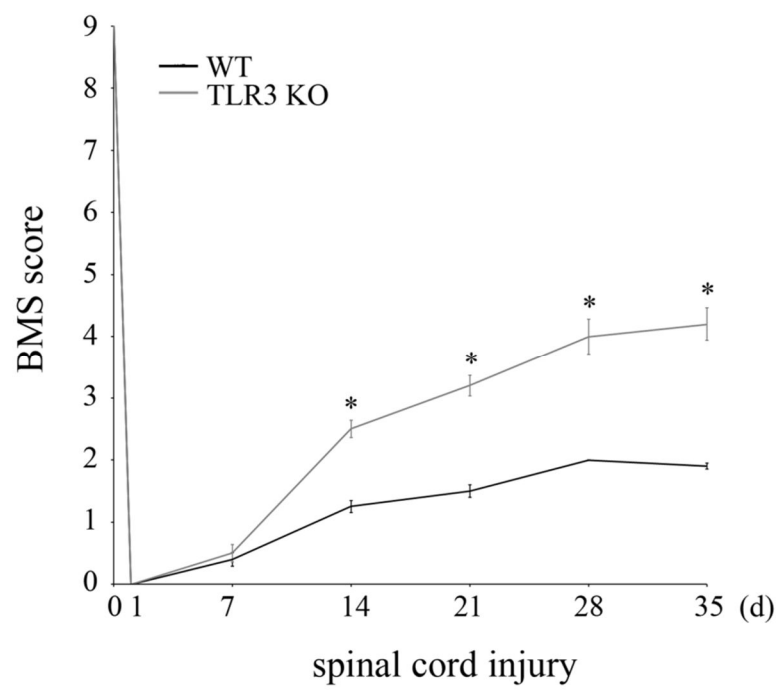


Figure 2. Reduction of lesion volume and axon demyelination in TLR3 knockout mice following SCI

Wild-type and TLR3 knockout mice were subjected to SCI, and the spinal cord was longitudinal sectioned and stained with cresyl violet (A) and Luxol fast blue (C) staining. Scale bar, 250 μm . (B) Lesion volumes of the injured spinal cord at 35 dpi in six sections from four separate series per animal ($n=3$) were calculated and the average volume (μm^3) was assessed by multiplying the total thickness. Data are expressed as the mean \pm SEM. ($*p<0.05$). (D) The axon demyelination area was calculated for the injured spinal cord at 5 dpi and 35 dpi from seven sections per animal ($n=3$). The axon demyelination area was calculated using the average (μm^2) of the area at regular intervals (240 μm). Data are expressed as the mean \pm SEM. ($*p<0.05$).

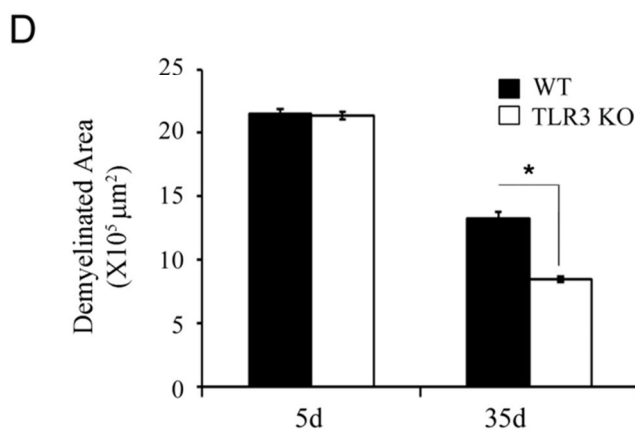
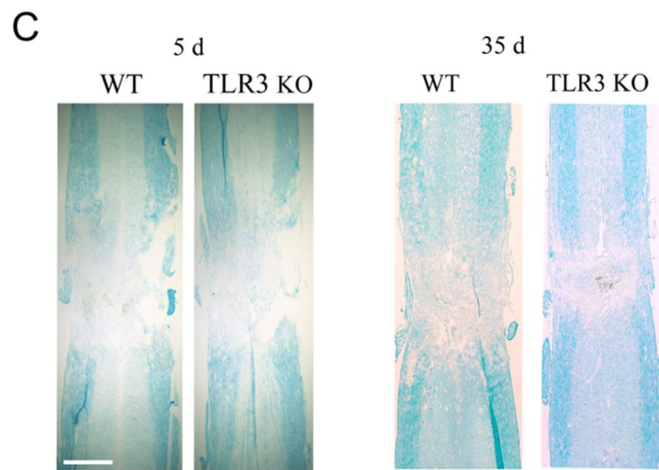
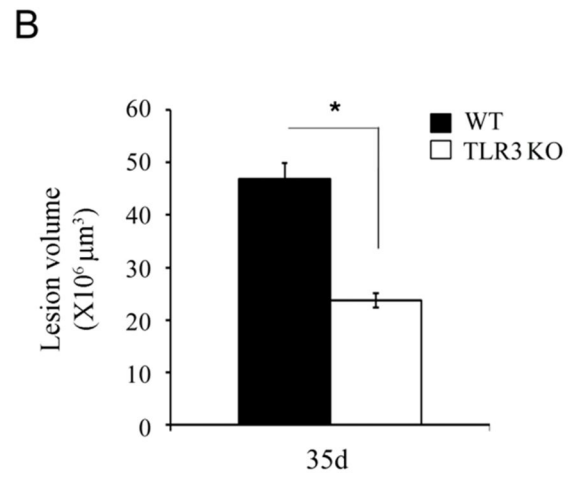
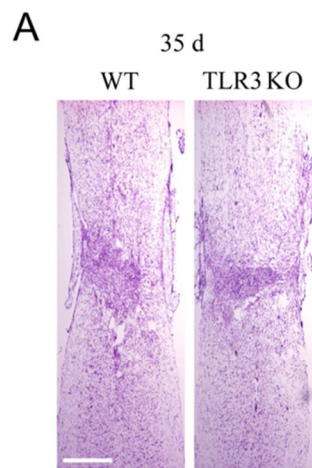
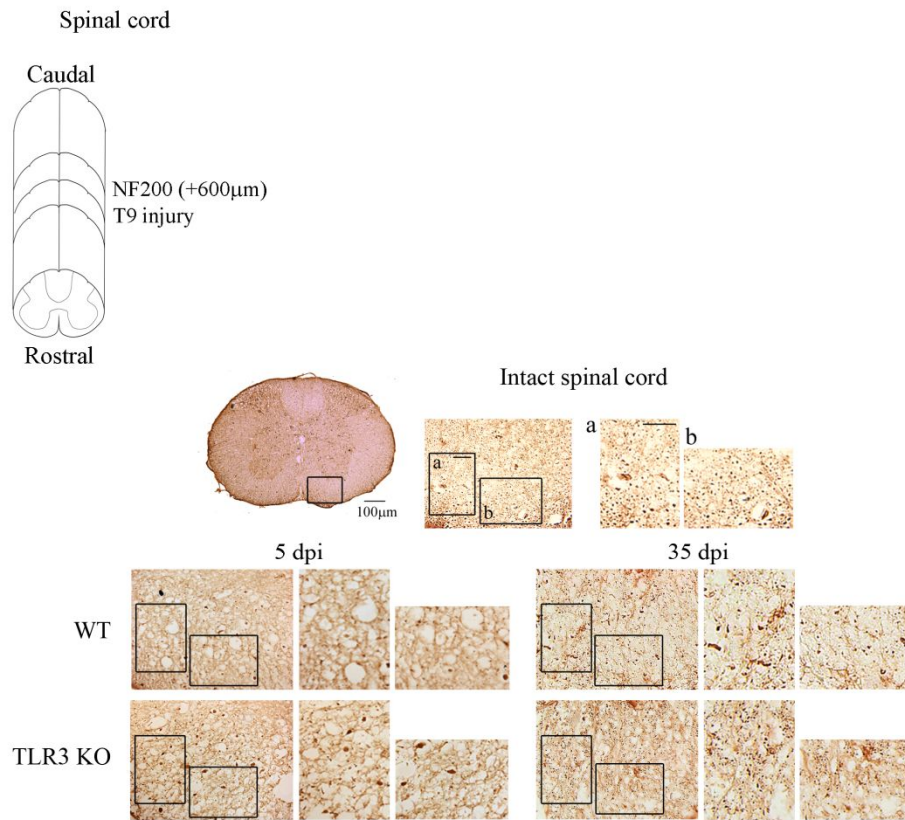


Figure 3. Reduction in axonal loss and enhancement in regeneration in TLR3 knockout mice

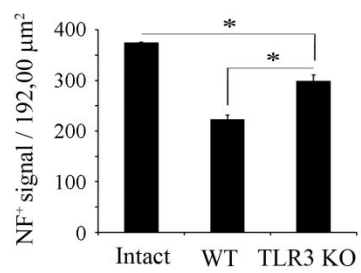
(A) Neuronal axon in coronal sections was detected by immunohistochemistry using anti-NF200 antibody. Black rectangle shows the vestibulospinal tract in the ventral part of the spinal cord. Scale bar, 100 μm . In the enlarged black rectangular area, NF200⁺-signals in two small black rectangles (a, b; Scale bar, 50 μm) were counted. Representative pictures in the 600 μm caudal region from the injury show a reduced NF200⁺-signal in 5 dpi and 35 dpi tissues compared to intact tissue. At 35 dpi, the NF200⁺-signal was increased in the TLR3 knockout mice compared to the wild-type mice. (B) Axon numbers were assessed as the average of the NF200⁺-signals in the two black rectangles from two animals (each 192,000 μm^2). Data are expressed as the mean \pm SEM. (* $p < 0.5$).

(Continued)

A



B



(C) Injected BDA into the sensorimotor cortex at 10 dpi was traced along the corticospinal fibers. BDA signal was detected 14 days after injection in the rostral part of the cross section. Scale bar, 100 μ m. In TLR3 knockout mice, BDA signals extended past the lesion site. However, any BDA signals could not be detected in the caudal part of the wild-type mice. Enlarged images show the extended tract in the TLR3 knockout mice. A representative figure from two independent experiments is shown and the results were similar. Scale bar, 100 μ m.

C

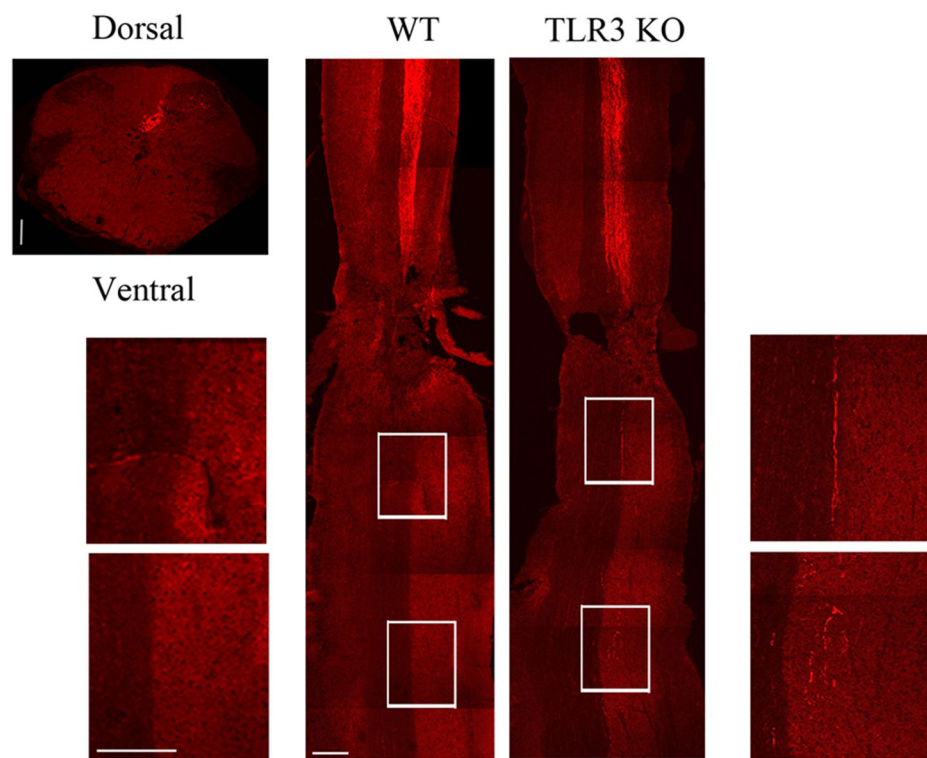
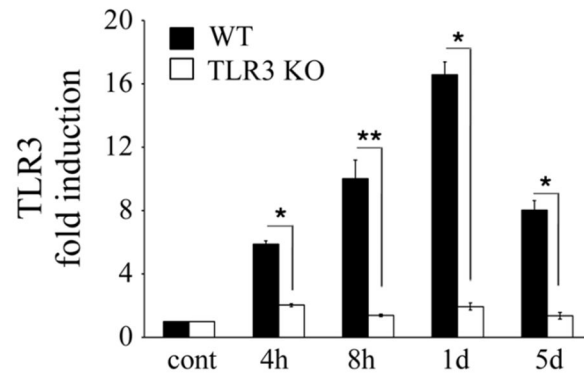


Figure 4. TLR3 expression in astrocytes and oligodendrocytes after SCI

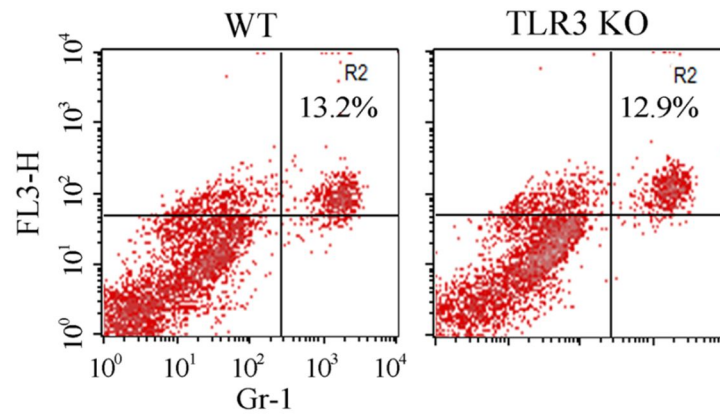
(A) The TLR3 mRNA level in the injured spinal cord of wild-type mice was increased at 4 hour and peaked at 1 day after the injury. The TLR3 mRNA expression was assayed using real-time RT-PCR. The data are the mean \pm SEM of three independent experiments (* p <0.05, ** p <0.05). (B) To quantify neutrophils, spinal cord cells were analyzed by flow cytometry at 1 dpi. Representative data from three independent experiments are shown. The Gr-1⁺ neutrophil population (R2 gate) did not differ at 1 dpi in the spinal cord of wild-type and TLR3 knockout mice. (C) The CD11b⁺/CD45^{high} macrophage population (R3 gate) and CD11b⁺/CD45^{low} microglia populations (R4 gate) were increased in the injured spinal cords of the wild-type mice at 5 dpi; however, the increase did not represent a difference between the two groups. Representative data from three independent experiments are shown.

(Continued)

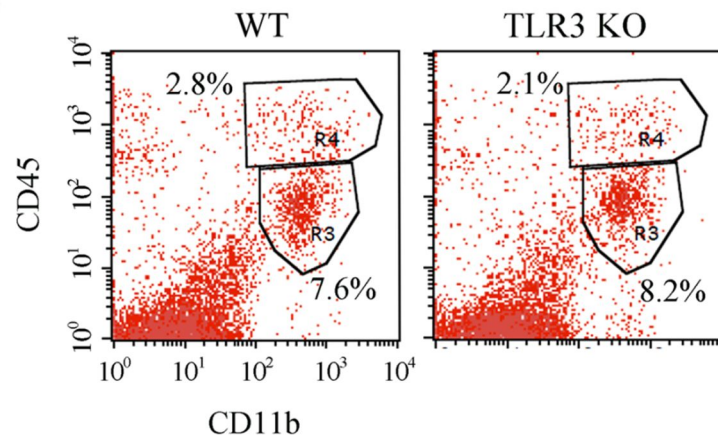
A



B



C



(D) TLR3 is expressed in astrocytes and oligodendrocytes at 5 dpi. TLR3 and GFAP are co-localized in the gray matter (a) and white matter (b) around the injury site. In the case of APC, a marker of mature oligodendrocytes, TLR3 was co-stained in the white matter margin (c) of the injury site. Scale bars, 20 μ m. Representative data from two independent experiments are shown.

D

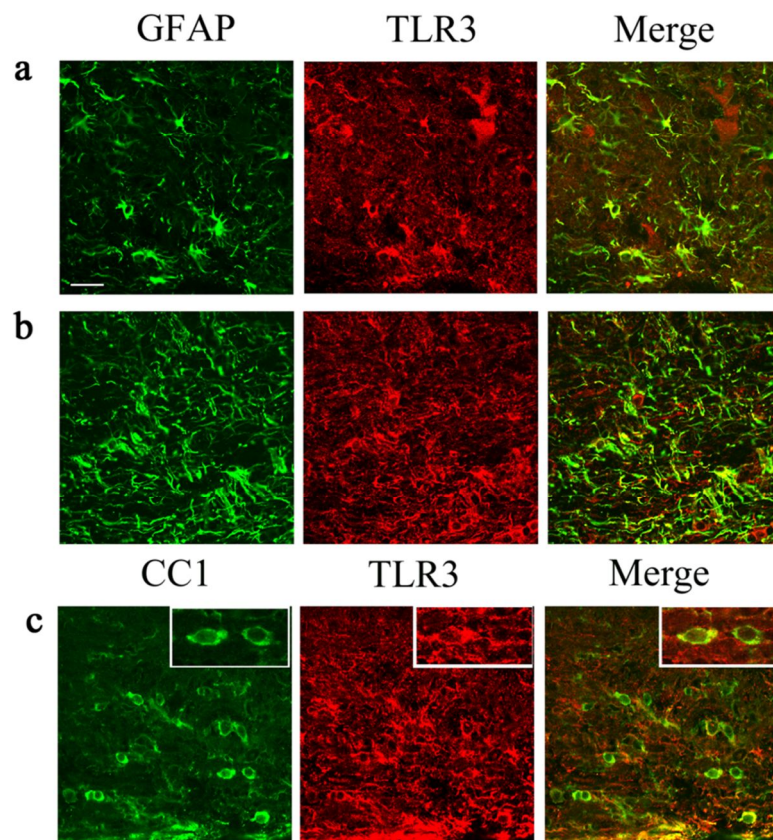
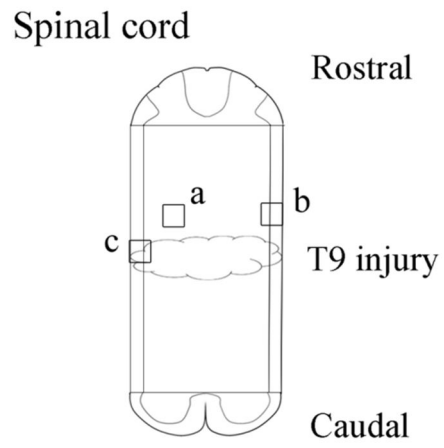


Figure 5. Astrocyte activation and CSPG deposition were diminished in TLR3 knockout mice

(A) At 14 dpi, longitudinal sections prepared from spinal cord tissue were used for anti-GFAP immunostaining. Activated astrocytes were decreased in the boundary of the lesion in the TLR3 knockout mice compared to the wild-type mice. White squares are magnified at the bottom. Scale bar, 100 μ m. A representative figure from three independent experiments is shown. (B) CSPG accumulation in the core of the lesion was detected using anti-CS-56 antibody. In the longitudinal sections at 35 dpi, CSPG accumulation was diminished in the TLR3 knockout mice compared to the wild-type mice. Scale bar, 100 μ m. A representative figure from three independent experiments is shown. (C) CSPG transcripts in the injured spinal cord were measured by real-time RT-PCR. The mRNA levels of the CSPGs (neurocan, versican, aggrecan, and phosphacan) did not differ between the two groups after SCI. The fold induction values from three independent experiments are shown, and the mean \pm SEM of three independent experiments are shown (* p <0.5, ** p <0.05, *** p <0.005).

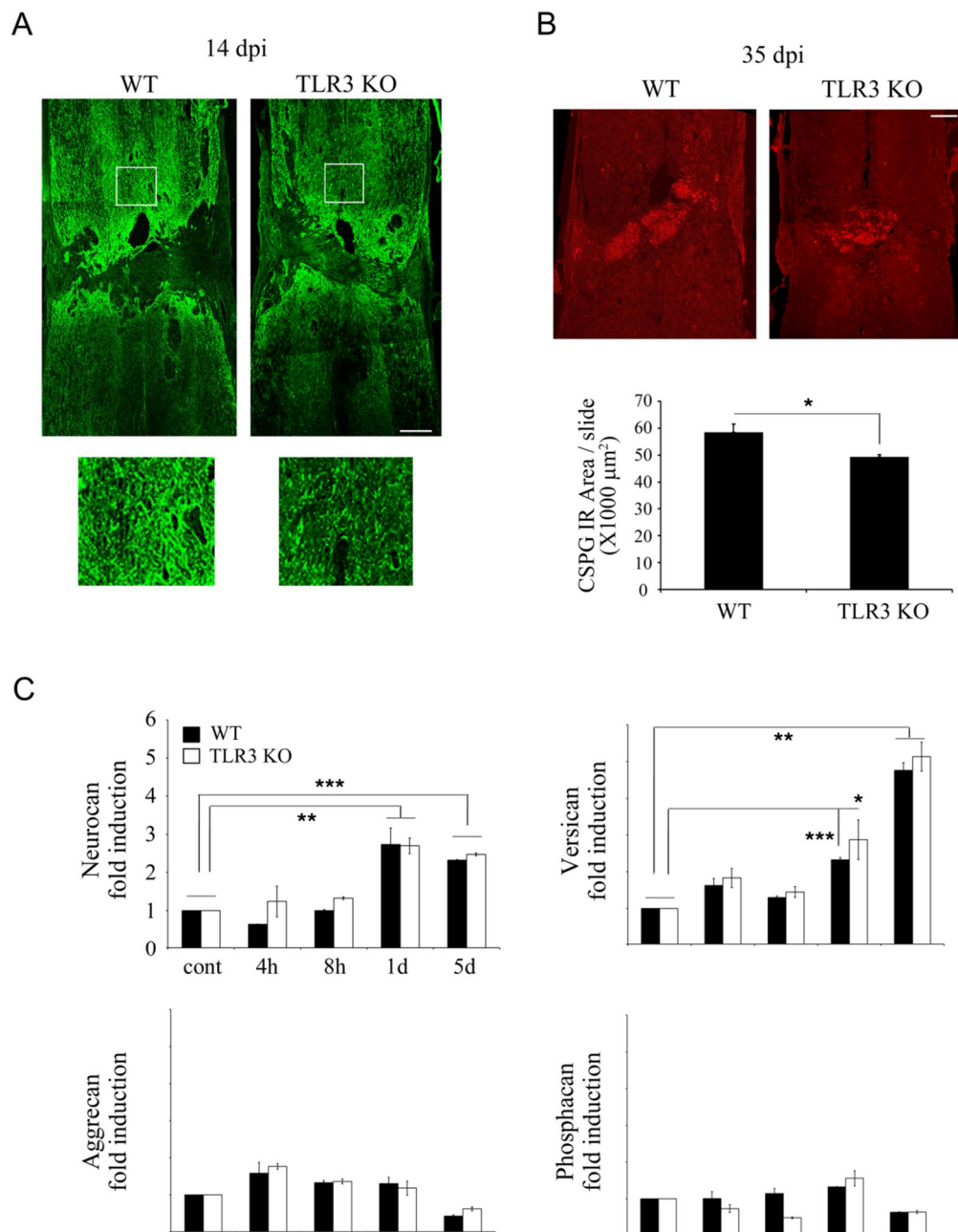


Figure 6. CSPG degradation by expressed MMP-2 activation enhanced by TLR3 deficiency

(A) MMP-2 mRNA level at 5 dpi was significantly increased in the TLR3 knockout mice compared to the wild-type mice. The MMP-9 mRNA level in the injured spinal cord was significantly increased at 8 hour but the transcripts level did not change due to TLR3 deficiency. MMP-2 and MMP-9 mRNA expression was assayed using real-time RT-PCR. The data are the mean \pm SEM of three independent experiments (** $p < 0.005$, * $p < 0.05$). (B) The activity of MMP-2 and MMP-9 was assayed by gelatin gel-zymography. A comparison of the gelatinase activities representing proMMP-9, proMMP-2 and activated MMP-2 is shown. At 5 dpi, the pro and active forms of MMP-2 were increased in the TLR3 knockout mice. Representative data from three independent experiments are shown. (C) Assay with injured spinal cord tissue and recombinant CSPGs was performed for 4 hours at 37°C followed by western blot using anti-CS-56 antibody. CSPGs degradation was increased by adding the tissue of the TLR3 knockout mice and the increased level of degraded CSPGs was reduced by MMP-2 inhibitor. Representative data from three independent experiments are shown. (D) At 10 dpi, spinal cord sections were used for MMP-2 and GFAP co-staining. Expressed MMP-2 localized in the astrocytes in the periphery of the injured lesion. Representative data from three independent experiments are shown. Scale bars, 20 μ m.

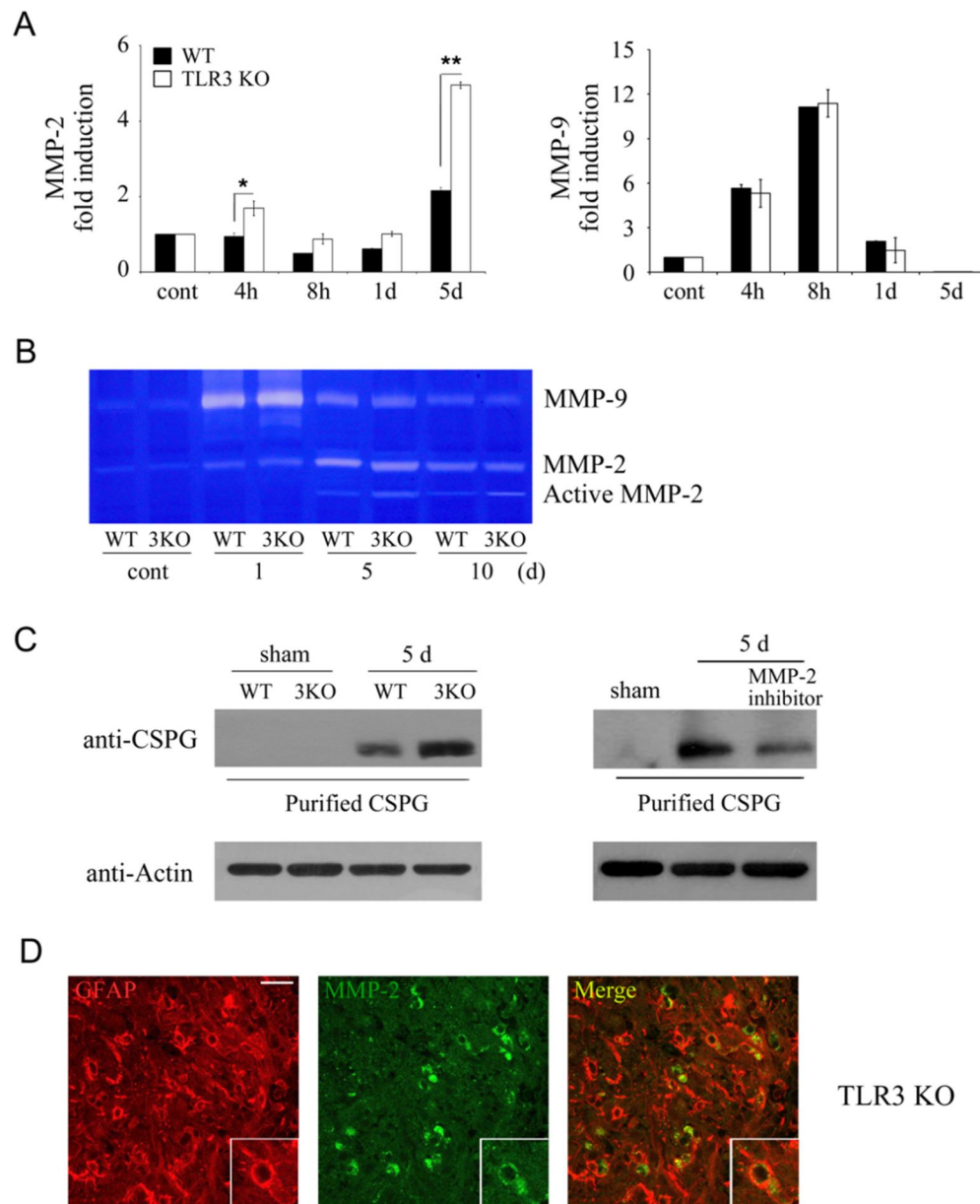


Figure 7. MMP-2 expression and activation in astrocytes via direct TLR3 signaling

(A) TGF- β 1 transcript level in the injured spinal cord of wild-type mice started to increase at 8 hour and increased by 3.8 times at 5 day after the injury. TGF- β 1 mRNA expression was assayed using real-time RT-PCR. The data are the mean \pm SEM of three independent experiments (* p <0.5, ** p <0.05). (B) To test MMP-2 mRNA expression, cultured astrocytes from wild-type and TLR3 knockout mice were treated by TGF- β 1, and MMP-2 expression was measured by real time PCR. The means \pm SEM of three independent experiments are shown (* p <0.5). (C) MMP-2 mRNA level was assayed by real-time RT-PCR and the mRNA level was reduced by stimulation with poly(I:C), a TLR3 ligand, for 3 hours in cultured astrocytes from wild-type mice. The means \pm SEM of three independent experiments are shown (* p <0.05). (D) TGF- β 1-induced MMP-2 mRNA expression in cultured astrocytes from wild-type mice was reduced by stimulation of poly(I:C) for 6 hours. It was performed using real-time RT-PCR. The means \pm SEM of three independent experiments are shown (* p <0.5).

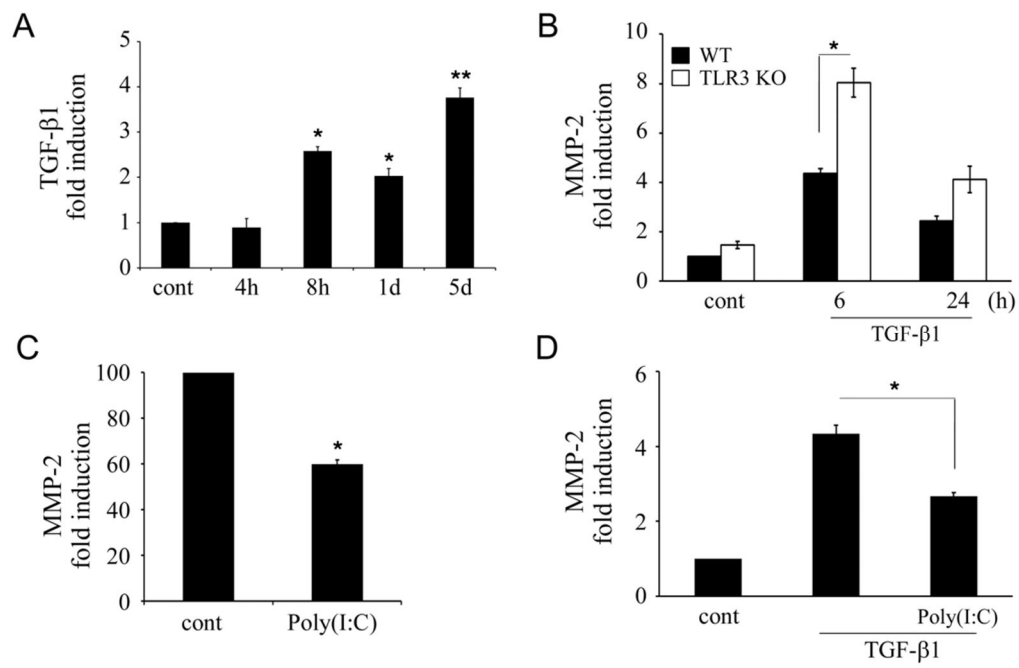


Table 4. The mouse primer sequences used for real-time RT-PCR

Genes	Forward primers	Reverse primers	GenBank No.
GAPDH	5'-AGG TCA TCC CAG AGC TGA ACG-3'	5'-CAC CCT GTT GCT GTA GCC GTA T-3'	NM_008084
TLR3	5'-GGA TCA ACC AGA CCC ACA CT-3'	5'-CAG GAG CAT ACT GGT GCT GA-3'	NM_126166.4
Neurocan	5'-GAG AGA GAT TGC AGG CGC CGA GCT G-3'	5'- CTC GGT GCT GGG AGA ATC CTT CAT C-3'	NM_007789.3
Versican	5'-TGC GAG GCT GGC GAC TGT TG-3'	5'-AGC TCT GTC AGG TAC CAT GTG TGG-3'	NM_001081249.1
Aggrecan	5'-ACG CCC CGG GAA GGT TGC TA-3'	5'-GGA GGT TGC CCC CGC AGT TG-3'	NM_007424.2
Phosphacan	5'-TTG GCT CCT ACT ATC AAC ATC CTC C-3'	5'-AGC TCA TCC CTC TCA GCA GCT GAA G-3'	NM_001081306.1
MMP-2	5'- AGA CAG AAG TCA TAG CCA CTC TCA AG -3'	5'-CCT CCT TTC CAG GTC AGT TAG C-3'	NM_009140
MMP-9	5'-TGT ACG GAC CCG AAG C-3'	5'-CCG TCC TTA TCG TAG TCA G-3'	NM_013599
TGF- β 1	5'-TCG CTA CCC GGC GTT CCT CA-3'	5'-GCC AGC AGG TCC GAG GGA GA-3'	NM_011577.1

DISCUSSION

For the first time, the *in vivo* role of TLR3 signaling in the injured spinal cord was demonstrated here. Until now, there has been no report elucidating the role of TLR3 after SCI. In my attempt to find the role of TLR3 in the injured spinal cord, the BMS data show that TLR3 has negative effects on functional recovery after SCI. Interestingly, the behavioral data show that the BMS scores of the TLR3 knockout mice were higher than that of the wild-type mice after 14 dpi, whereas the scores were not different between the two groups until 7 dpi. Moreover, at 35 dpi, the last day of the behavioral test, the lesion volume and axon demyelination of the injured spinal cord were diminished in the TLR3 knockout mice compared to the wild-type mice; however, the degree of axon demyelination was similar in both groups at 5 dpi. These data suggest that the effects of TLR3 deficiency not only improve functional recovery but also decrease lesion volume and axon demyelination not immediately but over time after SCI.

Functional recovery of the hind limb might be relevant to the remaining or regenerated axonal numbers in the injured spinal cord. Thus, I observed existing axonal tracts after SCI, such as the VST and the CST, which control limb and trunk coordination and voluntary movements, respectively. Similarly to the pattern of behavior data, both of the VST and CST remained the same in the two groups at the early time points, whereas more increased in the TLR3 knockout mice than in the wild-type mice at the delayed time points. These data show that TLR3 deficiency improves functional recovery through beneficial effects on the process of axon regeneration after SCI.

According to a previous report, TLR 2 and 4 promote nerve regeneration through the immune response leading to the clearance of myelin debris after SCI (Boivin et al., 2007). Generally, the immune response starts with the infiltration and activation of neutrophils and monocytes/macrophages within a few days after SCI (Barton, 2008). My FACS data also show that the infiltration of neutrophils and monocytes/macrophages was increased at 1 dpi and 5 dpi, respectively, but the infiltration of cells in the wild-type mice did not differ from those of the TLR3 knockout mice. This data verify that TLR3 is not involved in the action of immune cells after SCI. However, my immunohistochemistry data reveal that TLR3 was expressed in the astrocytes and oligodendrocytes of the injured spinal cord. Furthermore, SCI-induced astrocyte activation was diminished in the TLR3 knockout mice compared to the wild-type mice. Reactive astrocytes are the major components of a glial scar, a molecular barrier to axon regeneration (Rolls et al., 2008), and upregulate CSPG expression in the injury site (Jones et al., 2003). CSPGs have also an inhibitory effect on neural growth and regeneration (Bradbury et al., 2002). In this study, the CSPG deposition was increased in the wild-type mice at 35 dpi, whereas the increased CSPG deposition was attenuated in the TLR3 knockout mice. These data could explain that the enhanced axon regeneration in the TLR3 knockout mice is caused by the reduced deposition of CSPGs.

Based on above the results, there are two possible explanations for the reduced deposition of CSPGs in the TLR3 knockout mice when compared to the wild-type mice. One is the difference in the CSPG expression between two groups after SCI. The other is the expression and activation of endogenous enzymes such as MMP-2 and MMP-9, which degrade the expressed CSPGs in the injured spinal cord (Rolls et al., 2008). My data show that TLR3 deficiency

did not modify the transcript level of CSPGs after SCI in both groups. Therefore, the expression and activity of MMP-2 and MMP-9 in the injured spinal cord were investigated. Interestingly, I found that the expression and activity of MMP-2 were more increased in the TLR3 knockout mice than the wild-type mice at 5 dpi, but neither expression nor activity of MMP-9 was altered at 1 dpi in both groups. As suggested before, MMP-2 degrades and inactivates the neurite-inhibiting CSPG in the peripheral nerve injury model (Zuo et al., 1998). Also, my *in vitro* data verify that MMP-2 in the injured spinal cord degraded the recombinant CSPGs. Especially, at 5 dpi, more enhanced expression and activity of MMP-2 in the TLR3 knockout mice are meaningful, because, within 2 dpi, CSPGs inhibit the spread of damage from inflammatory cells (Rolls et al., 2008). Furthermore, my *in vitro* data show that recombinant CSPG degradation by MMP-2 was more increased in the TLR3 knockout mice than in the wild-type mice. These data support the idea that the enhanced MMP-2 expression and activity in the TLR3 knockout mice reduce CSPG deposition through degradation in the injured spinal cord.

Finally, the relationship between MMP-2 and TLR3 after SCI remains to be elucidated. I established an *in vitro* astrocyte culture system based on my *in vivo* data that MMP-2 was expressed in astrocytes after SCI. As reported, MMP-2 expression is induced by TGF- β 1 in human fibroblast (Overall et al., 1991) and the expression of TGF- β 1 was increased after SCI (Buss et al., 2008) as shown in this study. Consistent with the *in vivo* result, the expression and activity of MMP-2 were more enhanced by treatment with TGF- β 1 in the cultured astrocytes from the TLR3 knockout mice than in those from the wild-type mice. Furthermore, no-induced or TGF- β 1-induced MMP-2 expression

and activity were decreased by treatment with poly(I:C). These data suggest that MMP-2 expression is directly down-regulated by TLR3 in astrocytes.

In conclusion, these results in the present study reveal that, after SCI, TLR3 has a detrimental role in functional recovery and axon regeneration by down-regulating the expression and activity of MMP-2, which degrades inhibitory CSPGs.

SUMMARY

This thesis elucidated the deleterious role of neutrophils and macrophages at the early time points and the effects of astrocytic TLR3 at the late time points after SCI. Inflammatory responses after physical injury exaggerated the damage in the injured spinal cord, yet the specific function of inflammatory cells involved in the inflammatory response after SCI is not completely understood. In this regard, my aim was to elucidate the role of neutrophils and macrophages in spinal cord injury using *ikkβ^{Δmye}* mice in which the *ikkβ* gene is specifically deleted in the myeloid cells. Particularly, the activation and infiltration of neutrophils and macrophages of *ikkβ^{Δmye}* mice were only blocked without losing these cells in the blood. After hemisection SCI, the activation and infiltration of neutrophils and macrophages were attenuated at the lesion site of *ikkβ^{Δmye}* mice. The cause of attenuation is due to the reduced chemoattractant expression in infiltrated neutrophils and macrophages, but not due to the chemokine receptor expression and migration capacity of the neutrophils and macrophages. Especially, in *ikkβ^{Δmye}* mice, the decline of neutrophil activation and infiltration within 1 dpi significantly reduced apoptotic neuronal cell death through the lowered expression level of proinflammatory cytokines, ROS/RNS-producing proteins and MMP-9 than *ikkβ^{+/+}* mice. In conclusion, IKKβ deficiency in neutrophils and macrophages reduces inflammation, neuronal apoptosis in the injured spinal cord, and improves functional recovery after SCI.

It is well-known that TLRs in innate immune cell function as receptors detect tissue damage thereby triggering inflammatory responses. In an attempt

to investigate the signaling mechanisms leading to inflammatory cell activation after SCI, I characterized the role of TLR3 in SCI. To determine the effect of TLR3 in SCI, the mouse model of crushed SCI was established in the TLR3 knockout and wild-type mice. As shown in chapter 1, the inflammatory response from SCI arose during the early time points after injury. However, after 14 dpi, functional recovery in the TLR3 knockout mice was improved compared to the wild-type mice. Moreover, the lesion volume and axonal loss were significantly reduced in the TLR3 knockout mice compared to the wild-type mice at the later time points after SCI. In addition, the VST and CST were more enhanced at the later time points in the TLR3 knockout mice than in the wild-type mice. However, at 5 dpi, axonal loss and VST axon were not different between the two groups. At this point, I confirmed that neutrophils and macrophages did not express TLR3 after SCI. While, TLR3 expression was detected in astrocytes and oligodendrocytes after injury. In addition, astrocyte activation was reduced in the TLR3 knockout mice compared to the wild-type mice at 14 dpi. The expression level of CSPGs remained the same in both groups, whereas CSPG production was reduced in the lesion site of the TLR3 knockout mice at 35 dpi. Thus, I examined the expression and activity of MMP-2, a CSPG-degrading enzyme. MMP-2 expression and activity were increased in the TLR3 knockout mice compared to the wild-type mice at 5 dpi. In addition, *in vitro* assay showed that the expressed MMP-2 could degrade recombinant CSPGs and the inhibition of MMP-2 reduced that CSPG degradation. In conclusion, TLR3 has a detrimental role in SCI by inhibiting astrocytic MMP-2 expression, which results in the impairment of axon growth and functional recovery.

REFERENCES

Books and Journals

- Afshari FT, Kwok JC, White L, Fawcett JW (2010) Schwann cell migration is integrin-dependent and inhibited by astrocyte-produced aggrecan. *Glia*. 58: 857-869.
- Agrawal SM, Lau L, Yong VW (2008) MMPs in the central nervous system: where the good guys go bad. *Semin Cell Dev Biol*. 19:42-51.
- Akira S, Takeda K (2004) Toll-like receptor signalling. *Nat Rev Immunol*. 4: 499-511.
- Alexopoulou L, Holt AC, Medzhitov R, Flavell RA (2001) Recognition of double-stranded RNA and activation of NF-kappaB by Toll-like receptor 3. *Nature*. 413:732-738.
- Aravalli RN, Peterson PK, Lokensgard JR (2007) Toll-like receptors in defense and damage of the central nervous system. *J Neuroimmune Pharmacol*. 2: 297-312.
- Asea A, Rehli M, Kabingu E, Boch JA, Bare O, Auron PE, Stevenson MA, Calderwood SK (2002) Novel signal transduction pathway utilized by extracellular HSP70: role of toll-like receptor (TLR) 2 and TLR4. *J Biol Chem*. 277: 15028-15034.
- Bareyre FM, Schwab ME (2003) Inflammation, degeneration and regeneration in the injured spinal cord: insights from DNA microarrays. *Trends Neurosci*. 26:555-563.
- Barnes PJ, Karin M (1997) Nuclear factor-kappaB: a pivotal transcription factor in chronic inflammatory diseases. *N Engl J Med*. 336:1066-1071.

- Bartholdi D, Schwab ME, (1997) Expression of pro-inflammatory cytokine and chemokine mRNA upon experimental spinal cord injury in mouse: an in situ hybridization study. *Eur J Neurosci.* 9:1422-1438.
- Barton GM (2008) A calculated response: control of inflammation by the innate immune system. *J Clin Invest.* 118:413-420.
- Basso DM, Beattie MS, Bresnahan JC, Anderson DK, Faden AI, Gruner JA, Holford TR, Hsu CY, Noble LJ, Nockels R, Perot PL, Salzman SK, Young W (1996) MASCIS evaluation of open field locomotor scores: effects of experience and teamwork on reliability. Multicenter Animal Spinal Cord Injury Study. *J Neurotrauma.* 13:343-359.
- Basso DM, Fisher LC, Anderson AJ, Jakeman LB, McTigue DM, Popovich PG (2006) Basso Mouse Scale for locomotion detects differences in recovery after spinal cord injury in five common mouse strains. *J Neurotrauma.* 23: 35-659.
- Basu S, Binder RJ, Suto R, Anderson KM, Srivastava PK (2000) Necrotic but not apoptotic cell death releases heat shock proteins, which deliver a partial maturation signal to dendritic cells and activate the NF-kappa B pathway. *Int Immunol.* 12: 1539-1546.
- Bear MF, Connors BW, Paradiso MA (2007) *Neuroscience: exploring the brain*, 3rd Edn. Lippincott Williams & Wilkins, Philadelphia, PA.
- Bessis A, Bechade C, Bernard D, Roumier A (2007) Microglial control of neuronal death and synaptic properties. *Glia.* 55:233-238.
- Boivin A, Pineau I, Barrette B, Filali M, Vallieres N, Rivest S, Lacroix S (2007) Toll-like receptor signaling is critical for Wallerian degeneration and functional recovery after peripheral nerve injury. *J Neurosci* 27:12565-12576.

- Blight AR (1992) Macrophages and inflammatory damage in spinal cord injury. *J Neurotrauma*. 9 Suppl 1:S83-91.
- Bomstein Y, Marder JB, Vitner K, Smirnov I, Lisaey G, Butovsky O, Fulga V, Yoles E (2003) Features of skin-coincubated macrophages that promote recovery from spinal cord injury. *J Neuroimmunol*. 142:10-16.
- Bouhy D, Malgrange B, Multon S, Poirrier AL, Scholtes F, Schoenen J, Franzen R (2006) Delayed GM-CSF treatment stimulates axonal regeneration and functional recovery in paraplegic rats via an increased BDNF expression by endogenous macrophages. *FASEB J*. 20:1239-1241.
- Bradbury EJ, Moon LD, Popat RJ, King VR, Bennett GS, Patel PN, Fawcett JW, McMahon SB (2002) Chondroitinase ABC promotes functional recovery after spinal cord injury. *Nature*. 416:636-640.
- Brechtel K, Tura A, Abdibzadeh M, Hirsch S, Conrad S, Schwab JM (2006) Intrinsic locomotor outcome in dorsal transection of rat spinal cord: predictive value of minimal incision depth. *Spinal Cord*. 44:605-613.
- Brodal A; Pompeiano O, Walberg F (1962) *The Vestibular Nuclei and Their Connections*. C. C. Thomas Springfield III.
- Bsibsi M, Nomden A, van Noort JM, Baron W (2012) Toll-like receptors 2 and 3 agonists differentially affect oligodendrocyte survival, differentiation, and myelin membrane formation. *J Neurosci Res*. 90:388-398.
- Bsibsi M, Persoon-Deen C, Verwer RW, Meeuwsen S, Ravid R, Van Noort JM (2006) Toll-like receptor 3 on adult human astrocytes triggers production of neuroprotective mediators. *Glia*. 53:688-695.
- Buford JA, Davidson AG (2004) Movement-related and preparatory activity in the reticulospinal system of the monkey. *Exp Brain Res*. 159:284 –300.

- Bush TG, Puvanachandra N, Horner CH, Polito A, Ostenfeld T, Svendsen CN, Mucke L, Johnson MH, Sofroniew MV (1999) Leukocyte infiltration, neuronal degeneration, and neurite outgrowth after ablation of scar-forming, reactive astrocytes in adult transgenic mice. *Neuron*. 23:297-308.
- Buss A, Pech K, Kakulas BA, Martin D, Schoenen J, Noth J, Brook GA (2008) TGF-beta1 and TGF-beta2 expression after traumatic human spinal cord injury. *Spinal Cord*. 46:364-371.
- Buss A, Pech K, Kakulas BA, Martin D, Schoenen J, Noth J, Brook GA (2009) NG2 and phosphacan are present in the astroglial scar after human traumatic spinal cord injury. *BMC Neurol*. 9:32-46.
- Cameron JS, Alexopoulou L, Sloane JA, DiBernardo AB, Ma Y, Kosaras B, Flavell R, Strittmatter SM, Volpe J, Sidman R, Vartanian T (2007) Toll-like receptor 3 is a potent negative regulator of axonal growth in mammals. *J Neurosci*. 27:13033-13041.
- Carlson SL, Parrish ME, Springer JE, Doty K, Dossett L (1998) Acute inflammatory response in spinal cord following impact injury. *Exp Neurol*. 151:77-88.
- Carpentier PA, Begolka WS, Olson JK, Elhofy A, Karpus WJ, Miller SD (2005) Differential activation of astrocytes by innate and adaptive immune stimuli. *Glia*. 49:360-374.
- Cassatella MA (1995) The production of cytokines by polymorphonuclear neutrophils. *Immunol Today*. 16:21-26.
- Cavassani KA, Ishii M, Wen H, Schaller MA, Lincoln PM, Lukacs NW, Hogaboam CM, Kunkel SL (2008) TLR3 is an endogenous sensor of

- tissue necrosis during acute inflammatory events. *J Exp Med.* 205: 2609-2621.
- Chen KB, Uchida K, Nakajima H, Yayama T, Hirai T, Rodriguez Guerrero A, Kobayashi S, Ma WY, Liu SY, Zhu P, Baba H (2011) High-mobility group box-1 and its receptors contribute to proinflammatory response in the acute phase of spinal cord injury in rats. *Spine (Phila Pa 1976).* 36: 2122-2129.
- Clausen BE, Burkhardt C, Reith W, Renkawitz R, Forster I (1999) Conditional gene targeting in macrophages and granulocytes using LysMcre mice. *Transgenic Res.* 8:265-277.
- Dafny N (1997) *Anatomy of the Spinal Cord: Neuroscience Online*, UIHealth, The University of Texas Medical School at Houston, Houston, TX.
- Dean DD, Muniz OE, Howell DS (1989) Association of collagenase and tissue inhibitor of metalloproteinases (TIMP) with hypertrophic cell enlargement in the growth plate. *Matrix* 9:366-375.
- de Castro RC Jr, Burns CL, McAdoo DJ, Romanic AM (2000) Metalloproteinase increases in the injured rat spinal cord. *Neuroreport.* 11:3551-3554.
- Deumens R, Koopmans GC, Joosten EA (2005) Regeneration of descending axon tracts after spinal cord injury. *Prog Neurobiol.* 77:57-89
- Dong Y, Benveniste EN (2001) Immune function of astrocytes. *Glia* 36:180-190.
- Dong H, Fazzaro A, Xiang C, Korsmeyer SJ, Jacquin MF, McDonald JW (2003) Enhanced oligodendrocyte survival after spinal cord injury in Bax-deficient mice and mice with delayed Wallerian degeneration. *J Neurosci.* 23:8682-8691.

- Farina C, Aloisi F, Meinl E (2007) Astrocytes are active players in cerebral innate immunity. *Trends Immunol* 28:138-145.
- Faulkner JR, Herrmann JE, Woo MJ, Tansey KE, Doan NB, Sofroniew MV (2004) Reactive astrocytes protect tissue and preserve function after spinal cord injury. *J Neurosci*. 24:2143-2155.
- Fawcett JW (1998) Spinal cord repair: From experimental models to human application. *Spinal Cord* 36:811–817.
- Ferguson TA, Muir D (2000) MMP-2 and MMP-9 increase the neurite-promoting potential of schwann cell basal laminae and are upregulated in degenerated nerve. *Mol Cell Neurosci*. 16:157-167.
- Fitch MT, Silver J (2008) CNS injury, glial scars, and inflammation: Inhibitory extracellular matrices and regeneration failure. *Exp Neurol*. 209:294-301.
- Forsyth KD, Levinsky RJ (1990) Preparative procedures of cooling and re-warming increase leukocyte integrin expression and function on neutrophils. *J Immunol Methods*. 128: 159-163.
- Frederiks WM, Mook OR (2004) Metabolic mapping of proteinase activity with emphasis on in situ zymography of gelatinases: review and protocols. *J Histochem Cytochem*. 52:711-722.
- Giulian D, Baker TJ (1986) Characterization of ameboid microglia isolated from developing mammalian brain. *J Neurosci*. 6:2163-2178.
- Giulian D, Woodward J, Young DG, Krebs JF, Lachman LB (1988) Interleukin-1 injected into mammalian brain stimulates astrogliosis and neovascularization. *J Neurosci*. 8:2485–2490.

- Green CE, Schaff UY, Sarantos MR, Lum AF, Staunton DE, Simon SI (2006) Dynamic shifts in LFA-1 affinity regulate neutrophil rolling, arrest, and transmigration on inflamed endothelium. *Blood*. 107:2101-2111.
- Greten FR, Arkan MC, Bollrath J, Hsu LC, Goode J, Miething C, Goktuna SI, Neuenhahn M, Fierer J, Paxian S, Van Rooijen N, Xu Y, O'Cain T, Jaffee BB, Busch DH, Duyster J, Schmid RM, Eckmann L, Karin M (2007) NF-kappaB is a negative regulator of IL-1beta secretion as revealed by genetic and pharmacological inhibition of IKKbeta. *Cell*. 130: 918-931.
- Greten FR, Eckmann L, Greten TF, Park JM, Li ZW, Egan LJ, Kagnoff MF, Karin M (2004) IKKbeta links inflammation and tumorigenesis in a mouse model of colitis-associated cancer. *Cell* 118:285-296.
- Greter M, Heppner FL, Lemos MP, Odermatt BM, Goebels N, Laufer T, Noelle RJ, Becher B (2005) Dendritic cells permit immune invasion of the CNS in an animal model of multiple sclerosis. *Nat Med*. 11:328-334.
- Gu WL, Fu SL, Wang YX, Li Y, Wang XF, Xu XM, Lu PH (2007) Expression and regulation of versican in neural precursor cells and their lineages. *Acta Pharmacol Sin*. 28:1519-1530.
- Gu Z, Kaul M, Yan B, Kridel SJ, Cui J, Strongin A, Smith JW, Liddington RC, Lipton SA (2002) S-nitrosylation of matrix metalloproteinases: signaling pathway to neuronal cell death. *Science*. 297:1186-1190.
- Guth L, Zhang Z, Steward O (1999) The unique histopathological responses of the injured spinal cord. Implications for neuroprotective therapy. *Ann N Y Acad Sci*. 890:366-384.
- Hamada Y, Ikata T, Katoh S, Nakauchi K, Niwa M, Kawai Y, Fukuzawa K (1996) Involvement of an intercellular adhesion molecule 1-dependent

- pathway in the pathogenesis of secondary changes after spinal cord injury in rats. *J Neurochem.* 66:1525-1531.
- Hamby ME, Uliasz TF, Hewett SJ, Hewett JA (2006) Characterization of an improved procedure for the removal of microglia from confluent monolayers of primary astrocytes. *J Neurosci Methods.* 150:128-137.
- Hanke ML, Kielian T (2011) Toll-like receptors in health and disease in the brain: mechanisms and therapeutic potential. *Clin Sci (Lond).* 121(9):367-87.
- Harting JK (1977) Descending pathways from the superior colliculus: an autoradiographic analysis in the rhesus monkey (*Macaca mulatta*). *J Comp Neurol* 173:583–612.
- Hengartner MO (2000) The biochemistry of apoptosis. *Nature.* 407:770-776.
- Hong J, Cho IH, Kwak KI, Suh EC, Seo J, Min HJ, Choi SY, Kim CH, Park SH, Jo EK, Lee S, Lee KE, Lee SJ (2010) Microglial toll-like receptor 2 contributes to kainic acid-induced glial activation and hippocampal neuronal cell death. *J Biol Chem.* 285:39447-39457
- Hsu JY, McKeon R, Goussev S, Werb Z, Lee JU, Trivedi A, Noble-Haeusslein LJ (2006) Matrix metalloproteinase-2 facilitates wound healing events that promote functional recovery after spinal cord injury. *J Neurosci.* 26: 9841-9850.
- Jack CS, Arbour N, Manusow J, Montgrain V, Blain M, McCrea E, Shapiro A, Antel JP (2005) TLR signaling tailors innate immune responses in human microglia and astrocytes. *J Immunol.* 175:4320-4330.
- Johnson GB, Brunn GJ, Kodaira Y, Platt JL (2002) Receptor-mediated monitoring of tissue well-being via detection of soluble heparan sulfate by Toll-like receptor 4. *J Immunol.* 168: 5233-5239.

- Jones LL, Margolis RU, Tuszynski MH (2003) The chondroitin sulfate proteoglycans neurocan, brevican, phosphacan, and versican are differentially regulated following spinal cord injury. *Exp Neurol*. 182:399-411.
- Kielian T (2009) Overview of toll-like receptors in the CNS. *Curr Top Microbiol Immunol* 2009. 336: 1-14.
- Kigerl KA, Gensel JC, Ankeny DP, Alexander JK, Donnelly DJ, Popovich PG (2009) Identification of two distinct macrophage subsets with divergent effects causing either neurotoxicity or regeneration in the injured mouse spinal cord. *J Neurosci*. 29:13435-13444.
- Kigerl KA, Lai W, Rivest S, Hart RP, Satoskar AR, Popovich PG (2007) Toll-like receptor (TLR)-2 and TLR-4 regulate inflammation, gliosis, and myelin sparing after spinal cord injury. *J Neurochem*. 102: 37-50.
- Kneisley LW, Biber MP, LaVail JH. (1978) A study of the origin of brain stem projections to monkey spinal cord using the retrograde transport method. *Exp Neurol*. 60(1):116-39.
- Knerlich-Lukoschus F, von der Ropp-Brenner B, Lucius R, Mehdorn HM, Held-Feindt J (2011) Spatiotemporal CCR1, CCL3(MIP-1alpha), CXCR4, CXCL12(SDF-1alpha) expression patterns in a rat spinal cord injury model of posttraumatic neuropathic pain. *J Neurosurg Spine*. 14:583-597.
- Kobayashi Y (2008) The role of chemokines in neutrophil biology *Front Biosci*, 2007/11/06 Edn. 2400-2407.
- Korn T (2008) Pathophysiology of multiple sclerosis. *J Neurol* 255 Suppl 6:2-6.
- Lathia JD, Okun E, Tang SC, Griffioen K, Cheng A, Mughal MR, Laryea G, Selvaraj PK, French-Constant C, Magnus T, Arumugam TV, Mattson

- MP (2008) Toll-like receptor 3 is a negative regulator of embryonic neural progenitor cell proliferation. *J Neurosci.* 28:13978-13984.
- Lehnardt S, Lachance C, Patrizi S, Lefebvre S, Follett PL, Jensen FE, Rosenberg PA, Volpe JJ, Vartanian T (2002) The toll-like receptor TLR4 is necessary for lipopolysaccharide-induced oligodendrocyte injury in the CNS. *J Neurosci.* 22:2478-2486.
- Leon S, Yin Y, Nguyen J, Irwin N, Benowitz LI (2000) Lens injury stimulates axon regeneration in the mature rat optic nerve. *J Neurosci.* 20:4615–4626.
- Li M, Carpio DF, Zheng Y, Bruzzo P, Singh V, Ouaz F, Medzhitov RM, Beg AA (2001) An essential role of the NF-kappa B/Toll-like receptor pathway in induction of inflammatory and tissue-repair gene expression by necrotic cells. *J Immunol.* 166:7128-7135.
- Li QM, Tep C, Yune TY, Zhou XZ, Uchida T, Lu KP, Yoon SO (2007) Opposite regulation of oligodendrocyte apoptosis by JNK3 and Pin1 after spinal cord injury. *J Neurosci.* 27:8395-8404.
- Li ZW, Omori SA, Labuda T, Karin M, Rickert RC (2003) IKK beta is required for peripheral B cell survival and proliferation. *J Immunol.* 170:4630-4637.
- Lin S, Liang Y, Zhang J, Bian C, Zhou H, Guo Q, Xiong Y, Li S, Su B (2012) Microglial TIR-domain-containing adapter-inducing interferon-beta (TRIF) deficiency promotes retinal ganglion cell survival and axon regeneration via nuclear factor-kappaB. *J Neuroinflammation.* 9:39
- Liu X, Zou H, Slaughter C, Wang X (1997) DFF, a heterodimeric protein that functions downstream of caspase-3 to trigger fragmentation during apoptosis. *89:175-184.*

- Liu S, Xu GY, Johnson KM, Echetebe C, Ye ZS, Hulsebosch CE, McAdoo DJ (2008) Regulation of interleukin-1 β by the interleukin-1 receptor antagonist in the glutamate-injured spinal cord: endogenous neuroprotection. *Brain Res.* 1231:63-74.
- Liu Y, Tachibana T, Dai Y, Kondo E, Fukuoka T, Yamanaka H, Noguchi K (2002) Heme oxygenase-1 expression after spinal cord injury: the induction in activated neutrophils. *J Neurotrauma.* 19:479-490.
- Livak KJ, Schmittgen TD (2001) Analysis of relative gene expression data using real-time quantitative PCR and the 2^{(-Delta Delta C(T))} Method. *Methods.* 25:402-408.
- Ma Q, Tipping RH, Boulet C (2006) Irreducible correlation functions of the S matrix in the coordinate representation: application in calculating Lorentzian half-widths and shifts. *J Chem Phys.* 124:14109.
- McGavern DB, Kang SS (2011) Illuminating viral infections in the nervous system. *Nat Rev Immunol.* 11: 318-329.
- McKeon RJ, Jurynek MJ, Buck CR (1999) The chondroitin sulfate proteoglycans neurocan and phosphacan are expressed by reactive astrocytes in the chronic CNS glial scar. *J Neurosci.* 19:10778-10788.
- Mei XP, Zhou Y, Wang W, Tang J, Zhang H, Xu LX, Li Y Q (2011) Ketamine depresses toll-like receptor 3 signaling in spinal microglia in a rat model of neuropathic pain. *Neurosignals.* 19: 44-53.
- Michel RP, Cruz-Orive LM (1998) Application of the Cavalieri principle and vertical sections method to lung: estimation of volume and pleural surface area. *J Microsc.* 150:117-136.

- Mishra BB, Mishra PK, Teale JM (2006) Expression and distribution of Toll-like receptors in the brain during murine neurocysticercosis. *J Neuroimmunol.* 181: 46-56.
- Murray LA, Knight DA, McAlonan L, Argentieri R, Joshi A, Shaheen F, Cunningham M, Alexopolou L, Flavell RA, Sarisky RT, Hogaboam CM (2008) Deleterious role of TLR3 during hyperoxia-induced acute lung injury. *Am J Respir Crit Care Med.* 178:1227-1237.
- Negishi H, Osawa T, Ogami K, Ouyang X, Sakaguchi S, Koshiba R, Yanai H, Seko Y, Shitara H, Bishop K, Yonekawa H, Tamura T, Kaisho T, Taya C, Taniguchi T, Honda K (2008) A critical link between Toll-like receptor 3 and type II interferon signaling pathways in antiviral innate immunity. *Proc Natl Acad Sci U S A.* 105:20446-20451.
- Nguyen HX, O'Barr TJ, Anderson AJ (2007) Polymorphonuclear leukocytes promote neurotoxicity through release of matrix metalloproteinases, reactive oxygen species, and TNF- α . *J Neurochem.* 102:900-912.
- Nishiyama A, Dahlin KJ, Prince JT, Johnstone SR, Stallcup WB (1991) The primary structure of NG2, a novel membrane-spanning proteoglycan. *J Cell Biol.* 114: 359-371.
- Noble LJ, Donovan F, Igarashi T, Goussev S, Werb Z (2002) Matrix metalloproteinases limit functional recovery after spinal cord injury by modulation of early vascular events. *J Neurosci* 22:7526-7535.
- Nudo RJ, Masterton RB (1989) Descending pathways to the spinal cord. II. Quantitative study of the tectospinal tract in 23 mammals. *J Comp Neurol* 286:96–119
- Nyberg-Hansen R (1964) Sites and modes of termination of reticulospinal fibres in the cat (an experimental study with silver impregnation

- methods). *J Comp Neurol.* 24:71-100.
- Ohashi K, Burkart V, Flohe S, Kolb H (2000) Cutting edge: heat shock protein 60 is a putative endogenous ligand of the toll-like receptor-4 complex. *J Immunol.* 164:558-561.
- Okamura Y, Watari M, Jerud ES, Young DW, Ishizaka ST, Rose J, Chow JC, Strauss JF (2001) 3rd, The extra domain A of fibronectin activates Toll-like receptor 4. *J Biol Chem.* 276: 10229-10233.
- Olson JK, Miller SD (2004) Microglia initiate central nervous system innate and adaptive immune responses through multiple TLRs. *J Immunol.* 173:3916-3924.
- Oorschot DE (1994) Are you using neuronal densities, synaptic densities or neurochemical densities as your definitive data? There is a better way to go. *Prog Neurobiol.* 44: 233-247.
- O'Sullivan SB, Schmitz TJ (2007) *Physical Rehabilitation*, 5th Edn, Davis Company, Philadelphia, FA.
- Overall CM, Wrana JL, Sodek, J (1991) Transcriptional and post-transcriptional regulation of 72-kDa gelatinase/type IV collagenase by transforming growth factor-beta 1 in human fibroblasts. Comparisons with collagenase and tissue inhibitor of matrix metalloproteinase gene expression. *J Biol Chem.* 266:14064-14071.
- Ogawa K, Suzuki K, Okutsu M, Yamazaki K, Shinkai S (2008) The association of elevated reactive oxygen species levels from neutrophils with low-grade inflammation in the elderly. *Immun Ageing.* 5:13-20.
- Page-McCaw A, Ewald AJ, Werb Z (2007) Matrix metalloproteinases and the regulation of tissue remodelling. *Nat Rev Mol Cell Biol.* 8: 221-233.

- Pandey S, Agrawal DK (2006) Immunobiology of Toll-like receptors: emerging trends. *Immunol Cell Biol.* 84: 333-341.
- Park C, Lee S, Cho IH, Lee HK, Kim D, Choi SY, Oh SB, Park K, Kim JS, Lee SJ (2006) TLR3-mediated signal induces proinflammatory cytokine and chemokine gene expression in astrocytes: differential signaling mechanisms of TLR3-induced IP-10 and IL-8 gene expression. *Glia.* 53:248-256.
- Parks WC (1999) Matrix metalloproteinases in repair. *Wound Repair Regen.* 7:423-432.
- Parks WC, Wilson CL, Lopez-Boado YS (2004) Matrix metalloproteinases as modulators of inflammation and innate immunity. *Nat Rev Immunol.* 4:617-629.
- Patestas MA, Gartner LP (2006) A textbook of neuroanatomy. Blackwell Pub., Malden, MA.
- Peterson BW (1979) Reticulospinal projections to spinal motor nuclei. *Annu Rev Physiol.* 41:127-40.
- Peterson BW, Maunz RA, Fukushima K. (1978) Properties of a new vestibulospinal projection, the caudal vestibulospinal tract. *Exp Brain Res.* 32(2):287-92.
- Pilcher BK, Dumin JA, Sudbeck BD, Krane SM, Welgus HG, Parks WC (1997) The activity of collagenase-1 is required for keratinocyte migration on a type I collagen matrix. *J Cell Biol.* 137: 1445-1457.
- Pompeiano O (1972) Vestibulospinal relations: vestibular influences on gamma motoneurons and primary afferents. *Prog. Brain Res.* 37:197–232.
- Popovich PG, Guan Z, Wei P, Huitinga I, van Rooijen N, Stokes BT (1999) Depletion of hematogenous macrophages promotes partial hindlimb

- recovery and neuroanatomical repair after experimental spinal cord injury. *Exp Neurol*. 158:351-365.
- Popovich PG, Wei P, Stokes BT (1997) Cellular inflammatory response after spinal cord injury in Sprague-Dawley and Lewis rats. *J Comp Neurol*. 377: 443-464.
- Prehaud C, Megret F, Lafage M, Lafon M (2005) Virus infection switches TLR-3-positive human neurons to become strong producers of beta interferon. *J Virol*. 79:12893-12904.
- Rolls A, Shechter R, London A, Segev Y, Jacob-Hirsch J, Amariglio N, Rechavi G, Schwartz M (2008) Two faces of chondroitin sulfate proteoglycan in spinal cord repair: a role in microglia/macrophage activation. *PLoS Med*. 5:1262-1277.
- Redgrave P, Mitchell IJ, Dean P (1987) Descending projections from the superior colliculus in rat: a study using orthograde transport of wheatgerm-agglutinin conjugated horseradish peroxidase. *Exp Brain Res* 68:147–167.
- Rossignol, S. and Frigon, A., Recovery of locomotion after spinal cord injury: some facts and mechanisms. *Annu Rev Neurosci* 2011. 34: 413-440.
- Rothwarf DM, Karin M (1999) The NF-kappa B activation pathway: a paradigm in information transfer from membrane to nucleus. *Sci STKE*. 1999: RE1.
- Schwab ME, Bartholdi D (1996) Degeneration and regeneration of axons in the lesioned spinal cord. *Physiol Rev* 76:319–370.
- Sen GC, Sarkar SN (2005) Transcriptional signaling by double-stranded RNA: role of TLR3. *Cytokine Growth Factor Rev*. 16:1-14.

- Sica A, Larghi P, Mancino A, Rubino L, Porta C, Totaro MG, Rimoldi M, Biswas SK, Allavena P, Mantovani A (2008) Macrophage polarization in tumour progression. *Semin Cancer Biol.* 18:349-355.
- Silver J, Miller JH (2004) Regeneration beyond the glial scar. *Nat Rev Neurosci.* 5: 146-156.
- Sims GP, Rowe DC, Rietdijk ST, Herbst R, Coyle AJ (2010) HMGB1 and RAGE in inflammation and cancer. *Annu Rev Immunol.* 28: 367-388.
- Stallcup WB, Beasley L (1987) Bipotential glial precursor cells of the optic nerve express the NG2 proteoglycan. *J Neurosci.* 7:2737-2744.
- Sternlicht MD, Werb Z (2001) How matrix metalloproteinases regulate cell behavior. *Annu Rev Cell Dev Biol.* 17:463-516.
- Stirling DP, Liu S, Kubes P, Yong VW (2009) Depletion of Ly6G/Gr-1 leukocytes after spinal cord injury in mice alters wound healing and worsens neurological outcome. *J Neurosci.* 29:753-764.
- Stoll G, Muller HW (1999) Nerve injury, axonal degeneration and neural regeneration: basic insights. *Brain Pathol.* 9:313-325.
- Susarla BT, Laing ED, Yu P, Katagiri Y, Geller HM, Symes AJ (2011) Smad proteins differentially regulate transforming growth factor- β -mediated induction of chondroitin sulfate proteoglycans. *J Neurochem.* 119:868–878.
- Taguchi T, Mitcham J L, Dower SK, Sims JE, Testa JR (1996) Chromosomal localization of TIL, a gene encoding a protein related to the Drosophila transmembrane receptor Toll, to human chromosome 4p14. *Genomics.* 32:486-488.
- Takeda K, Akira S (2004) TLR signaling pathways. *Semin Immunol.* 16: 3-9.

- Tang SC, Arumugam TV, Xu X, Cheng A, Mughal MR, Jo DG, Lathia JD, Siler DA, Chigurupati S, Ouyang X, Magnus T, Camandola S, Mattson MP (2007) Pivotal role for neuronal Toll-like receptors in ischemic brain injury and functional deficits. *Proc Natl Acad Sci U S A*. 104:13798-13803.
- Taoka Y, Okajima K, Uchiba M, Murakami K, Kushimoto S, Johnno M, Naruo M, Okabe H, Takatsuki K (1997) Role of neutrophils in spinal cord injury in the rat. *Neuroscience*. 79:1177-1182.
- Ten Donkelaar HJ (1976) Descending pathways from the brain stem to the spinal cord in some reptiles. II. Course and site of termination. *J Comp Neurol* 167:443-463.
- Termeer C, Benedix F, Sleeman J, Fieber C, Voith U, Ahrens T, Miyake K, Freudenberg M, Galanos C, Simon JC (2002) Oligosaccharides of Hyaluronan activate dendritic cells via toll-like receptor 4. *J Exp Med*. 195: 99-111.
- Tuna M, Polat S, Erman T, Ildan F, Gocer AI, Tuna N, Tamer L, Kaya M, Cetinalp E (2001) Effect of anti-rat interleukin-6 antibody after spinal cord injury in the rat: inducible nitric oxide synthase expression, sodium- and potassium-activated, magnesium-dependent adenosine-5'-triphosphatase and superoxide dismutase activation, and ultrastructural changes. *J Neurosurg*. 95:64-73.
- Venes D, Taber CW (2009) *Taber's cyclopedic medical dictionary*, Ed. 21, illustrated in full color / Edn. F. A. Davis Co., Philadelphia.
- Verma RP, Hansch C (2007) Matrix metalloproteinases (MMPs): chemical-biological functions and (Q)SARs. *Bioorg Med Chem*. 15: 2223-2268.

- Virdis A, Colucci R, Fornai M, Blandizzi C, Duranti E, Pinto S, Bernardini N, Segnani C, Antonioli L, Taddei S, Salvetti A, Del Tacca M (2005) Cyclooxygenase-2 inhibition improves vascular endothelial dysfunction in a rat model of endotoxic shock: role of inducible nitric-oxide synthase and oxidative stress. *J Pharmacol Exp Ther.* 312:945-953.
- Wang H, Katagiri Y, McCann TE, Unsworth E, Goldsmith P, Yu ZX, Tan F, Santiago L, Mills EM, Wang Y, Symes AJ, Geller HM (2008) Chondroitin-4-sulfation negatively regulates axonal guidance and growth. *J Cell Sci.* 121:3083-3091.
- Wang T, Town T, Alexopoulou L, Anderson JF, Fikrig E, Flavell RA (2004) Toll-like receptor 3 mediates West Nile virus entry into the brain causing lethal encephalitis. *Nat Med.* 10:1366-1373.
- Watson C, Paxinos G, Kayalioglu G (2008) *The Spinal Cord: A Christopher and Dana Reeve Foundation Text and Atlas*, 1st Edn. Elsevier Ltd, San Diego, CA
- Wells JE, Rice TK, Nuttall RK, Edwards DR, Zekki H, Rivest S, Yong VW (2003) An adverse role for matrix metalloproteinase 12 after spinal cord injury in mice. *J Neurosci.* 23:10107-10115.
- Willis WD, Westlund KN (1997) Neuroanatomy of the pain system and of the pathways that modulate pain. *J Clin Neurophysiol.* 14:2-31.
- Whishaw IQ, Gorny B and Sarna J (1998) Paw and limb use in skilled and spontaneous reaching after pyramidal tract, red nucleus and combined lesions in the rat: behavioral and anatomical dissociations. *Behav Brain Res* 93:167-183.
- Yamaguchi Y (2000) Lecticans: organizers of the brain extracellular matrix. *Cell Mol Life Sci.* 57:276-289.

- Yin Y, Cui Q, Li Y, Irwin N, Fischer D, Harvey AR, Benowitz LI (2003) Macrophage-derived factors stimulate optic nerve regeneration. *J Neurosci.* 23:2284–2293.
- Yiu G, Zhigang H (2006) Glial inhibition of CNS axon regeneration. *Nat Rev Neurosci.* 7:617-627.
- Yong VW, Moumdjian R, Yong FP, Ruijs TC, Freedman MS, Cashman N, Antel JP (1991) Gamma-interferon promotes proliferation of adult human astrocytes in vitro and reactive gliosis in the adult mouse brain in vivo. *Proc Natl Acad Sci U S A.* 88:7016-20
- Yu F, Kamada H, Niizuma K, Endo H, Chan PH (2008) Induction of mmp-9 expression and endothelial injury by oxidative stress after spinal cord injury. *J Neurotrauma.* 25:184-195.
- Yune TY, Lee JY, Jung GY, Kim SJ, Jiang MH, Kim YC, Oh YJ, Markelonis GJ, Oh TH (2007) Minocycline alleviates death of oligodendrocytes by inhibiting pro-nerve growth factor production in microglia after spinal cord injury. *J Neurosci.* 27: 7751-7761.
- Zayachkivska O, Gzregotsky M, Ferentc M, Yaschenko A, Urbanovych A (2008) Effects of nitrosative stress and reactive oxygen-scavenging systems in esophageal physiopathy under streptozotocin-induced experimental hyperglycemia. *J Physiol Pharmacol.* 59 Suppl 2:77-87.
- Zemans RL, Arndt PG (2009) Tec kinases regulate actin assembly and cytokine expression in LPS-stimulated human neutrophils via JNK activation. *Cell Immunol.* 258:90-97
- Zhang Z, Schluesener HJ (2006) Mammalian toll-like receptors: from endogenous ligands to tissue regeneration. *Cell Mol Life Sci.* 63:2901-2907.

Zuo J, Hernandez YJ, Muir D (1998) Chondroitin sulfate proteoglycan with neurite-inhibiting activity is upregulated after peripheral nerve injury. J Neurobiol 34:41-54

Web Pages

Spinal Cord Injury Information Pages, “Spinal Cord Injury Facts & Statistics”
at: <http://www.sci-info-pages.com/> [accessed date; 02 May 2012]

The brain from top to bottom, “The axons entering and leaving the motor cortex”
at: <http://thebrain.mdgill.ca/> [accessed date; 02 May 2012]

The Encyclopedia of Science, “spinal cord injury”
at: <http://www.daviddarling.info/encyclopedia/ET/Emain.html> [accessed date; 17 May 2012]

국문초록

척수손상은 광범위한 신경세포 사멸, 연속적인 염증 반응과 신경교상흔 (glial scar) 형성을 유발한다. 손상 받은 척수는 일반적으로 염증반응에 의해 조직 손상이 더 악화된다. 척수 손상에서 대식세포와 호중성백혈구와 같은 면역세포가 유입된다는 보고가 많이 있지만, 아직까지 이러한 세포들의 작용에 대한 역할은 명확히 규명되어 있지 않다.

1 장에서는 호중성백혈구와 대식세포에서 발현되는 IKK β 의 척수손상에서의 작용을 연구하였다. *ikk $\beta^{+/+}$* 쥐에서 척수에 측면 절반 손상을 가한 다음 척수 내로의 침윤이 호중성백혈구의 경우 6 시간부터 진행, 24 시간에 극대화되고, 대식세포의 경우 손상 후 3 일, 5 일에 관찰 되었다. 이때 침투된 대식세포는 M1 유형으로 확인되었다. 이러한 세포들의 침투가 골수 세포 특이적으로 IKK β 가 결실되어있는 *ikk β* 조건부 유전자적중생쥐 (*ikk β^{Amye}*)에서 유의성 있게 감소하였으며, 손상 후 손상 범위 감소와 행동학적 회복이 *ikk $\beta^{+/+}$* 쥐보다 *ikk β^{Amye}* 쥐에서 상당히 호전되었다. *ikk $\beta^{+/+}$* 쥐와 비교하여 *ikk β^{Amye}* 쥐에서 호중성백혈구와 대식세포의 화학유도인자수용체 발현 혹은 침투력에는 큰 차이가 없었으나 화학유도인자들의 발현이 줄어 들고, TNF- α 와 IL-1 β , IL-6 등의 염증성사이토카인과 iNOS와 COX-2 등의 활성산소종과 활성질소종을 생성하는 염증매개물질들의 발현이 감소되었다. 이상의 실험결과들은 IKK β 가 대식세포와 호중성백혈구의 활성 증가에 관여하여 척수손상 시에 나타나는 염증반응을 증대시키고 신경세포 손상을 가중시켜 기능적 손상회복을 저하시킬 가능성을 제시하고 있다.

2 장에서는 툴유사수용체 3 (TLR3) 이 척수 손상 후 기능적 회복과 축삭의 재생에 미치는 영향을 TLR3 가 결여된 유전자적중생쥐를 이용하여 연구하였다. 압축에 의한 척수손상 후, 5 일에는 두 그룹간에 신경수초화의 손상 정도와 NF-200 로 표지된 신경축삭의 손상 정도에서 차이가 없었다. 반면에, 14 일이 지난 시점부터 TLR3 유전자적중생쥐의 행동학적 점수 (BMS score)가 야생형쥐 보다 높았으며, 척수손상 35 일 후 축삭의 신경수초화가 증대되고 손상 범위가 현저히 감소하였다. 이와 더불어, 정방향 신경추적물질인 BDA 를 사용한 실험과 NF-200 면역염색 실험을 척수손상 후 24 일과 35 일에 각각 수행하여 TLR3 유전자적중생쥐에서 신경축삭의 수가 증가되었음을 관찰하였다. 척수손상 후 TLR3 는 주로 성상세포와 희소돌기 아교세포에서 증가하였으며, TLR3 유전자적중생쥐에서 성상세포에서 발현되는 신경재생 저해물질인 CSPG 의 양적 증가 정도와 성상세포 자체의 활성화가 감소하는 것을 확인하였다. 배양한 성상세포를 이용한 생체 외 실험에서, CSPG 증가 량의 차이는 CSPG 발현보다는 MMP-2 의 분해 정도에 의한 것임을 확인하였으며 또한 TLR3 효현제인 polyinosine-polycytidylic acid (poly(I:C))에 의해 MMP-2 발현이 감소함을 확인하였다. 또한, TLR3 유전자적중생쥐에서 배양한 성상세포는 야생형쥐에서 배양한 성상세포에 비해 상대적으로 많은 MMP-2 를 발현하였다. 이상의 실험결과들은, TLR3 는 성상세포의 MMP-2 발현과 활성을 억제하여 신경재생과 행동학적 회복을 저해함으로써 척수손상 시에 해로운 역할을 할 가능성을 시사하고 있다.

주요어: 척수손상, 호중성백혈구, 대식세포, 성상세포, IKK β , 툴유사수용체 3

학 번: 2007-30074